BICYCLING STABILITY

Simulations & Experiments to improve cycling safety for older cyclists

Vera Bulsink

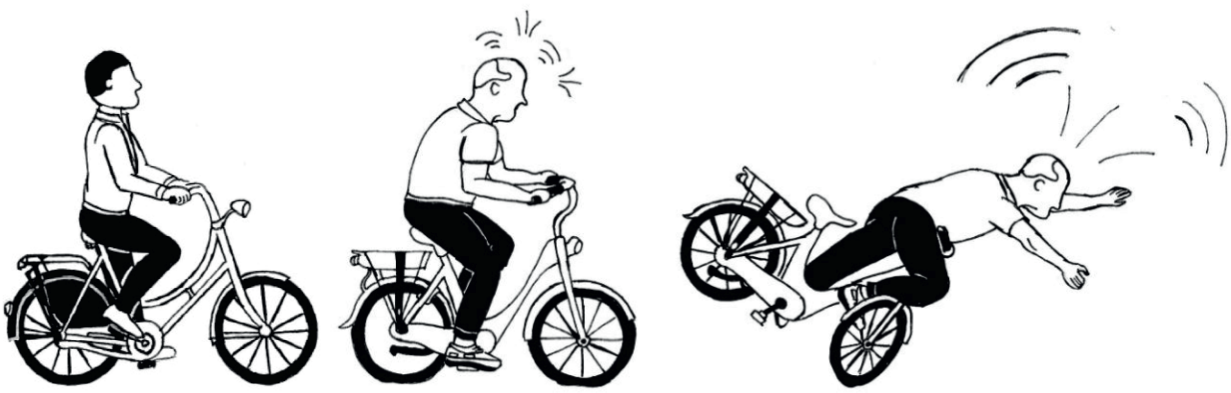

Bicycling stability

Simulations & Experiments to improve cycling safety for older cyclists

VERA BULSINK

Samenstelling promotiecommissie:

Voorzitter/secretaris

prof. dr. G.P.M.R. Dewulf	Universiteit Twente

Promotor

prof. dr. ir. H.F.J.M. Koopman	Universiteit Twente

Co-promotor

dr. ir. G.M. Bonnema	Universiteit Twente

Leden

prof. dr. ir. A. de Boer	Universiteit Twente
prof. dr. ir. S.A. van Gils	Universiteit Twente
prof. A. Doria	University of Padua
prof. dr. E. Otten	Universitair Medisch Centrum Groningen
prof. dr. J.S. Rietman	Universiteit Twente
dr. ir. A.L. Schwab	Technische Universiteit Delft

Dit onderzoek werd ondersteund door RVO NL en is uitgevoerd in het SOFIE-project bij de vakgroep Biomedische Werktuigbouwkunde van de Universiteit Twente.

Cover design:
Wim Bulsink & Inés Carvajal Gallardo

Printed by *Ipskamp Printing, Enschede*

ISBN: 978-90-365-4443-6
DOI: 10.3990/1.9789036544436

BICYCLING STABILITY

SIMULATIONS & EXPERIMENTS TO IMPROVE CYCLING SAFETY FOR OLDER CYCLISTS

PROEFSCHRIFT

ter verkrijging van
de graad van doctor aan de Universiteit Twente,
op gezag van de rector magnificus,
prof. dr. T.T.M. Palstra,
volgens besluit van het College voor Promoties
in het openbaar te verdedigen
op donderdag 7 december 2017 om 16:45 uur

door

Vera Elisabeth Bulsink

Geboren op 25 augustus 1985
te Utrecht, Nederland

Dit proefschrift is goedgekeurd door de promotor:
prof.dr.ir. H.F.J.M. Koopman

en door de co-promotor:
dr.ir. G.M. Bonnema

Contents

Samenvatting

Fietsers leveren een grote bijdrage aan het dagelijkse verkeer in Nederland, maar ook in steeds meer andere landen. Fietsen is een gezonde activiteit en de fiets is een populair transportmiddel, die met name op korte afstanden vaak sneller is dan een auto. Oudere fietsers gebruiken de fiets vooral voor winkelen, bezoekjes aan vrienden en familie en voor recreatieve doeleinden. Maar vanaf een bepaalde leeftijd beginnen ze meer moeite te krijgen met het houden van balans en het besturen van de fiets. Het verouderingsproces beïnvloedt de verwerking van sensorische informatie, zoals visuele, vestibulaire en proprioceptieve informatie. Vanaf een bepaalde leeftijd zal het verminderde vermogen om deze sensorische informatie te verwerken, leiden tot meer moeite met het balanceren en besturen van de fiets. Oudere fietsers gaan zich minder veilig voelen en zullen uiteindelijk beslissen om te stoppen met fietsen, waardoor hun mobiliteit en kwaliteit van leven (nog) verder zal afnemen. Studies hebben aangetoond dat fietsers die ouder zijn dan vijfenvijftig jaar, een verhoogd risico op fietsongevallen hebben.

Elektrische fietsen die door middel van een elektromotor pedaalondersteuning leveren, worden al vaak gebruikt om oudere fietsers te ondersteunen wanneer deze kracht of uithoudingsvermogen missen. Maar er is ook behoefte aan ondersteuning bij het houden van balans en het besturen van de fiets. Dit kan voor oudere fietsers leiden tot een hogere fietsveiligheid waardoor ze zich zekerder gaan voelen op de fiets, en ze langer kunnen blijven fietsen.

Om die redenen is het SOFIE-project (Slimme Ondersteunende Fiets) gestart. Het doel van dit project is het ontwikkelen van slimme hulpmiddelen om oudere fietsers te helpen hun veilige fietservaring te behouden. Dit proefschrift maakt deel uit van dit project en bestudeert met behulp van computermodellen en een experimentele testopstelling de dynamica van het fietsen en de fietsstabiliteit van oudere fietsers. Hieruit kunnen richtlijnen voortvloeien voor het ontwerpen en ontwikkelen van veiligere fietsen voor ouderen.

Een geavanceerd fiets-fietsermodel is ontwikkeld met de commerciële software ADAMS. Het model omvat de dynamica van de fiets zelf, een bandwegmodel, een passief biomechanisch model van de fietser en een model van het regelsysteem van de fietser (centrale zenuwstelsel). In de literatuur is de dynamica van de fiets vaak onderzocht en

gemodelleerd. Deze modellen zullen echter moeten worden opgewaardeerd met een gedetailleerder bandwegmodel en een uitgebreider model van de fietser. De modellen van de fietser zullen ook experimenteel gevalideerd moeten worden, om complexe fietssituaties goed te kunnen simuleren. Bovendien zijn de verschillen in fietsstrategieën tussen jonge en oudere fietsers nog niet bekend. Deze zullen worden bestudeerd met behulp van een experimentele fietsopstelling.

In samenwerking met de Motorcycle Dynamics Group van de Universiteit van Padova is een dataset van mechanische fietsbandeigenschappen gemaakt, die onder verschillende condities, zoals bijvoorbeeld de bandenspanning en de belasting zijn gemeten. Met behulp van deze dataset zijn de coëfficiënten van de 'Magic Formula' van Pacejka's bandmodel afgeleid en zijn bestaande fietscomputermodellen hiermee uitgebreid. De bestanden die kunnen worden gebruikt om het afgeleide fietsbandmodel in de software ADAMS te importeren, zijn beschikbaar gemaakt om te downloaden.

Dit bandwegmodel is gebruikt in een open-loop fiets-fietsermodel om de invloed van band- en fietsereigenschappen op de fietsstabiliteit te bestuderen. De waeve- en capsize-modus werden hiervoor geanalyseerd. De simulaties laten zien dat het uitbreiden van fietsmodellen met een realistisch bandmodel leiden tot een opmerkelijke afname van de weave-stabiliteit en een stabilisatie van de capsize-modus. Dit effect wordt voornamelijk veroorzaakt door de twisting torque. De verticale belasting op de fietsband heeft een groot effect op de mechanische eigenschappen van de band en daarmee ook op de fietsstabiliteit. Daarom zijn de belastingafhankelijke coëfficiënten van de Magic Formula afgeleid en gebruikt in het bandmodel. Daarentegen heeft de bandenspanning weinig invloed op de stabiliteit van de fiets, evenals het gebruik van banden van verschillende fabrikanten. Een gevoeligheidsstudie van de passieve biomechanische eigenschappen van de fietser toonde aan dat de lichaamsstijfheid en -demping slechts een klein effect op de stabiliteit hebben, maar dat de stijfheid van de armen de capsize-modus onstabiel maakt en de weave-modus stabiliseert.

Er is in het laboratorium een nieuwe en unieke experimentele fietsopstelling ontwikkeld om:

(1) de verschillen in fietsstrategieën tussen jonge en oudere fietsers te testen,

(2) fiets-fietsermodellen experimenteel te valideren en

(3) het regelsysteem van de fietser te identificeren.

In deze opstelling roteerde het voorwiel van de fiets op een lopende band, wat zorgde voor een behoud van het bandwegcontact en de mogelijkheid om stuurcorrecties te gebruiken die vergelijkbaar zijn met het fietsen op de normale weg. Het achterwiel was geplaats op een rollerbank die op een Stewart-platform stond. Met behulp van het Stewart-platform konden gecontroleerde (laterale) verstoringen worden opgelegd aan de fietser.

In totaal hebben 30 proefpersonen deelgenomen aan de fietstesten (15 jonge en 15 oudere fietsers). Zij voerden de testen uit met verschillende fietssnelheden. De kinematica van de fiets en de fietser werden gemeten met behulp van een bewegingsregistratiesysteem (Vicon) met passieve markers en inertiële sensoren. Verder werden de interactiekrachten (op de pedalen, zadel en stuur) tussen de fiets en fietser gemeten met behulp van 6-dimensionale krachtsensoren. Een aantal veiligheidsmaatregelen zorgde voor de veiligheid van de proefpersonen, zoals een veiligheidsharnas, leuningen en noodstoppen voor de lopende band en het Stewart-platform.

Drie mogelijke fietsbesturingsstrategieën van oudere fietsers (54-62 jaar) werden vergeleken met die van jongere fietsers (20-30 jaar), terwijl er laterale verstoringen werden opgelegd tijdens het fietsen op de experimentele set-up. De drie mogelijke besturingsstrategieën waren: gebruikmaken van het stuur, laterale beweging van het bovenlichaam en buitenwaartse kniebewegingen. De oudere fietsers maakten (naast sturen) meer dan de jongere proefpersonen gebruik van buitenwaartse kniebewegingen als secundair besturingsmechanisme. Verhoogde inter-individuele variatie voor de oudere fietsergroep suggereert dat deze groep gezien kan worden als een overgangsgroep in termen van lichamelijke conditie. Dit verklaart hun verhoogde risico op eenzijdige fietsongevallen. Oudere fietsers kunnen daarom profiteren van verhoogde fietsstabiliteit bij lage fietssnelheden, waardoor minder besturingsacties nodig zijn.

Deze fietsdataset is ook gebruikt voor validatie van de computermodellen. In dit geval werd het fiets- fietser interactiemodel gevalideerd met de gemeten interactiekrachten en momenten op de pedalen, op het stuur en op het zadel. De gemeten pedaalkrachten waren in overeenstemming met de literatuurgegevens. Het was een van de eerste keren dat alle kinematische en kinetische data gelijktijdig tijdens het fietsen gemeten werden. Een van de meest opvallende waarnemingen was dat de fietsers voortdurend een zijwaartse kracht uitoefenden op het stuur, die naar binnen (mediaal) gericht was. Deze kracht was hoger tijdens het fietsen bij lage snelheden, dan tijdens het fietsen met hoge snelheid. Dit zou een verband kunnen hebben met de grotere stuuruitslagen die

plaatsvinden bij lagere snelheden, maar kan ook voortkomen uit een verhoogd stressniveau van de fietser.

De gemeten fiets-fietserinteractiekrachten en kinematica werden gebruikt om het interactiemodel te valideren. De resulterende krachten van 8-19% van de maximale krachtgrootte werden gebruikt om de dynamische consistentie van het model te waarborgen. Deze resulterende krachten kunnen verbandhouden met onnauwkeurigheden van experimentele data en modelaannames. Een nauwkeurige meting van de pedaalkrachten en pedaalhoeken en meer persoonsspecifieke modellen zouden de geldigheid van het model kunnen verhogen.

Het SIMO (single-input-multiple-output) -fietserbalansregelsysteem voor jonge en oudere fietsers werd geïdentificeerd uit deze zelfde fietsdataset. Het bleek dat het sturen en de zijwaartse bovenlichaambewegingen gemodelleerd konden worden met een PD-controller met tijdsvertraging. De buitenwaartse kniebewegingen waren beperkt tot lage frequenties en daardoor lastiger te modelleren. De resultaten suggereerden dat de bovenlichaambesturingen reflexen zijn, terwijl de stuurbeweging visuele terugkoppeling gebruikt. Oudere fietsers hadden meer tijd nodig om te reageren dan jongere fietsers. De oudere fietsers leken ook vaker extra besturing te gebruiken dan jongere fietsers (naast de hoofdmanier van sturen door gebruik te maken van het stuur). Bij lage snelheden hadden de oudere proefpersonen moeite om op de vrij smalle loopband te fietsen. Dit kan verklaard worden door de verhoogde tijdsvertraging van de oudere fietsers, in combinatie met de hogere versterkingen die nodig zijn voor het fietsen op lage snelheid.

Door deze resultaten kunnen oudere fietsers profiteren van een verhoogde stabiliteit van de fiets bij lage snelheden. In dat geval hebben ze minder aanvullende besturingsacties nodig en lagere versterkingsfactoren.

Met behulp van het ontwikkelde fiets-fietser multi-bodymodel, bleek dat een achterwielmotor effectiever is dan een voorwielmotor als het gaat om de stabiliteit. Daarom is het waarschijnlijk veiliger om een achterwielmotor te gebruiken tijdens het ontwerpen en ontwikkelen van fietsen voor oudere fietsers. Remmen met de voorste motor en gelijktijdig trekkracht met de achterste motor uitoefenen, leidt tot verbeterde fietsstabiliteit en zou daarom in huidige elektrische fietsen gebruikt kunnen worden om actief meer stabiliteit aan de fiets te geven.

De computersimulaties die tijdens de ontwikkeling van het computermodel in dit proefschrift werden verricht, werden ook gebruikt bij de ontwikkeling van de SOFIETS, een fiets die door het bedrijf Indes werd ontwikkeld in samenwerking met de andere projectleden van het SOFIE-project: het Roessingh Research & Development (RRD) en de Universiteit Twente. De SOFIETS is ontworpen om de fietsveiligheid van oudere fietsers te verbeteren en is door RRD getest met oudere gebruikers. Deze testen tonen aan dat oudere fietsers minder stuurbewegingen en laterale kniebewegingen gebruiken op de SOFIE-fiets dan op een conventionele fiets. Dit is in overeenstemming met de bevindingen uit de hoofdstukken 4 en 6. Het SOFIE-project leidde tot een fietsontwerp dat voor zijn doelgroep succesvol bleek en de fietsveiligheid van oudere fietsers kan verhogen.

In dit proefschrift werd gedemonstreerd dat computersimulatiemodellen handige hulpmiddelen zijn voor het begeleiden van het fietsontwerp, zoals blijkt uit de bovengenoemde ontwerprichtlijnen. Verder is aangetoond dat het niet altijd nodig is om de meest complexe computermodellen te gebruiken om de fietsveiligheid te verbeteren. Zo bleken simulaties met een open-loop fiets-fietser-model goed te werken om de stabiliteit bij lage snelheden te verbeteren. Meer complexe modellen kunnen echter nodig zijn bij het testen van complexere situaties.

Summary

Cyclists take up a large part of the daily traffic in the Netherlands and more and more in other countries as well. Cycling is a healthy activity and the bicycle is a popular means of transportation that is often faster than car rides on short distances. Older cyclists tend to use their bicycles for shopping, visits and recreational purposes. However, from a certain age they start to encounter difficulties in balancing and controlling their bicycle. Aging influences the ability to process sensory information, like visual, auditory, vestibular and proprioceptive information. From a certain age these sensory systems degenerate, which could lead to the difficulties in bicycle balance and control that older cyclists experience. People tend to feel less safe and eventually will decide to stop cycling at all, which leads to a decrease of their mobility and quality of life. Studies have shown that cyclists over fifty-five have an increased risk of bicycling accidents.

Electric bicycles are already being used to assist older cyclists when they lack in strength or endurance, by supplying power and pedalling assistance. But, there is also a need for assistance in cyclist balance control, to increase cycling safety of older cyclists and to keep them cycling for as long as possible.

Therefore, the SOFIE (Slimme Ondersteunende Fiets/Smart Assistive Bicycle) project was started. The goal of this project was to develop smart assistive devices to help older cyclists to maintain a safe cycling experience. This thesis is part of this project and studies the bicycle dynamics and bicycling stability of older cyclists with the use of computer model simulations and a laboratory cycling set-up. The results could lead to design guidelines for the development of safer bicycles for older cyclists.

An advanced bicycle-cyclist model is developed in the commercial software ADAMS. The model includes the dynamics of the bicycle itself, a tire-road contact model, a passive biomechanical model of the cyclist and a cyclist balance control model. In literature, bicycle dynamics is examined and modelled frequently. However, these models need to be upgraded with a more detailed tire-road contact and cyclist model and experimentally validated in order to simulate complex cycling situations. Furthermore, differences in cycling strategies between young and older cyclists are yet unknown, and are therefore studied with the use of a laboratory cycling set-up.

In cooperation with the Motorcycle Dynamics Group of the University of Padova a dataset of mechanical tire properties has been created, that were measured at several operating conditions regarding tire pressure and tire load. Using this dataset, the coefficients of the Magic Formula of Pacejka's tire model were derived and used to upgrade existing bicycle dynamic models. The files that can be used to import the derived bicycle tire model in the software ADAMS are available for download.

This tire-road contact model was used in an open-loop bicycle-cyclist model to test the influence of tire and cyclist properties on bicycle stability. The weave and capsize modes were analysed. The simulations showed that extending bicycle dynamical models with a realistic tire model leads to a noticeable decrease of the weave stability and a stabilization of the capsize mode. This effect is mainly caused by the twisting torque. Tire load has a large effect on bicycle stability, therefore load-dependent coefficients of the Magic Formula were derived. On the other hand, tire pressure and different manufactured tires did not influence the bicycle's stability much. A sensitivity study of cyclist passive properties showed that body stiffness and damping have a small effect on stability, but arm stiffness noticeable destabilizes the capsize mode and arm damping destabilizes the weave mode.

A novel and unique laboratory cycling set-up was developed, in order to:

(1) test differences in cycling strategies of young and older cyclists,

(2) validate bicycle-cyclist models, and

(3) identify a cyclist control model.

The front wheel of the bicycle rotated on a treadmill, preserving the tire-road contact and the ability to use steering corrections similar to cycling on a normal road. The rear wheel was placed on a roller bench that was situated on a Stewart platform. With the use of the Stewart platform, controlled (lateral) perturbations could be applied to the bicycle-cyclist system. Thirty (fifteen young and fifteen older) participants took part in the cycling experiments at different cycling speeds. The bicycle and cyclist kinematics were measured with the use of a motion capture system and inertial sensors. Furthermore, the bicycle-cyclist interaction forces at the pedals, saddle and handlebar were measured using 6 DOF force-torque sensors. Numerous safety precautions secured the safety of the subject: a safety harness, handrails, (dis)mounting accessories, emergency stops for the treadmill and Stewart platform and safety side beams.

Three possible cycling control strategies of older cyclists (54-62 years) were compared to that of younger cyclists (20-30 years), while lateral perturbations were applied when cycling on the laboratory set-up. The three possible strategies to keep balance were: steering, lateral upper-body movements and outward knee movements. The older cyclists tend to rely more on outward knee movement as a secondary control mechanism (next to steering) than the younger subject group. Increased inter-individual variation for the older cyclist group suggests that this group can be seen as a transition group in terms of physical fitness. This explains their increased risk of single-sided bicycle accidents. Older cyclists could therefore benefit from increased bicycle stability at low cycling speeds, which will result in less need for control.

This cycling dataset is used for validation of the computer models as well. In this case, the bicycle-cyclist interaction model was validated with the measured interaction forces and torques at the pedals, handlebars and saddle. The measured pedal forces were in agreement with literature. It was one of the first times that all kinematic and kinetic data was measured during cycling. One of the most striking observations was that the cyclists constantly applied a lateral force at the handlebars that was directed inwards (medial). This force was higher during cycling at low speeds than cycling at high speeds. This can be related to the increased steering at lower speeds, but also to an increased stress-level of the cyclist.

The measured bicycle-cyclist interaction forces and kinematics were used to validate the bicycle-cyclist interaction model. Resultant forces of 8-19% of the maximum force magnitude were used to ensure dynamic consistency of the model. These resultant forces can be related to inaccuracies of the experimental data and modelling assumptions. Accurately measuring the pedal forces and increased subject-specific modelling could increase the validity of the model.

A SIMO (single-input-multiple-output) cyclist balance control model for young and older cyclists was identified from this same cycling dataset. It was found that the steering and upper-body lean control can be modelled with a PD controller with time delay, whereas the outward knee control was limited to low frequencies. The results suggest that the upper body lean control is reflex-like, while the steering control uses visual feedback loops. Older subjects needed more time to react than the younger cyclists. The older cyclists also reverted more to additional control mechanisms (next to the main control: steering) at a higher speed than younger cyclists. At low speeds, the older subjects had difficulties cycling on the rather tight treadmill. This could be explained by the increased time delay of older cyclists, together with the higher control gains that are needed when cycling at low speeds.

These results imply that older cyclists could benefit from an improvement of the bicycle's stability at low speeds. In that case they need less additional control actions and lower control gains.

Using the developed open-loop bicycle-cyclist multi-body model, it was shown that a rear hub motor is more effective than a front hub motor in maintaining bicycle stability and is therefore likely safer to use, when designing bicycles for older cyclists. Also, braking with the front motor and simultaneous traction with the rear motor leads to better bicycle stability and can therefore be used in current electric bicycles that already offer pedalling power to actively control bicycle stability as well.

The computer simulations that were performed during development of the model in this thesis were also used in the development of the SOFIETS, a bicycle that was developed by the company Indes in cooperation with the SOFIE project partners, Roessingh R&D (RRD) and the University of Twente. The SOFIETS bicycle is created to enhance cycling safety of older cyclists and was tested with older subjects by RRD. These tests showed that older cyclists used less steering actions and lateral leg movements on the SOFIE bicycle in comparison to a conventional bicycle, which is in accordance with the findings of chapters 4 and 6 of this thesis. The SOFIE-project led to a bicycle-design that was found to achieve its purposes for its targeted audience, which was to increase cycling safety for older cyclists.

In this thesis, it was shown that computer simulation models are a useful tool to guide bicycle design, as can be seen from the aforementioned design guidelines. Furthermore, it was shown that it is not always necessary to have the most complex models in order to improve cycling safety. Simulations with an open-loop bicycle-cyclist model were used to improve stability at low speeds. More complex models could be necessary, however, when testing more complex cycling situations.

Chapter 1

Introduction

As they become older, people encounter problems when riding their bicycle, including balance problems. Increasing the stability of the bicycle will prolong the ability of elderly to make use of the bicycle as a means of transportation and thereby contribute to their quality of life.

Bicycling is a healthy activity and an efficient means of transportation [1]. Furthermore, it is a social activity; people can be independent and mobile. Especially older cyclists (65 years and up) in the Netherlands use the bicycle for social activities such as shopping, visits and recreation [2]. For the quality of life of this group, it is important to remain socially and physically active for as long as possible [3, 4]. However, high injury risks have been found for older cyclists, which are in particular related to single-sided bicycle incidents (not involving other road users) [5].

Possible reasons to stop cycling reported in the literature are medical limitations, heavy traffic and insecurity of the cyclist [6]. Most problems regarding older cyclists arise in complex situations [7, 8]. Some studies also identify balance loss or steering errors as a problem [9-11].

The rise of the electric bicycle has already solved some problems for elderly cyclists; they assist the cyclists where they lack strength and physical endurance. On the other hand, new problems arise: the elderly are able to reach higher speeds than before and need to handle heavier bicycles at high & low speed. Higher injury risks were found for electric bicycles, compared to conventional bicycles [12].

Little is known about the stability problems of older cyclists, but the balance control of older adults during stance and gait is frequently examined [13-16]. These studies show that age-related deterioration of the balance control system contributes to falls and limitations in mobility [17, 18]. The same might be valid for bicycling. Therefore, improving the bicycle's stability would contribute to an increased sense of safety among older cyclists. This will in turn lead to a situation in which people are able to enjoy riding their bicycles for longer.

The sense of safety of older cyclists can be improved by increased bicycle stability, by giving longer time for the bicycle rider to react or by making the bicycle easier to control. With the use of mathematical models, the mechanical and human responses in several problem scenarios can be simulated, such as: (1) riding at low speed, (2) riding on narrow lanes, (3) during sudden change of trajectory and perturbations typically caused by uneven roads or obstacles.

The dynamics of the bicycle are frequently examined with the use of multi-body dynamic models [19-21]. Such models are used to study the effects of various design variables that can improve the stability of the bicycle. However, adding the dynamics of the cyclist to the system dramatically changes the stability: without any control, the system of a bicycle and cyclist is predominantly unstable; while a system with bicycle only seems to be intrinsically stable at higher speeds [22].

Advanced bicycle-cyclist multi-body models are required to assess and improve the stability of bicycling. Existing bicycle models need to include extended and validated tire-road contact models, biomechanical cyclist models and cyclist control models.

In this thesis newly developed advanced, validated computer simulation models will be presented, as well as a novel experimental laboratory set-up, to identify cycling strategies of young and older cyclists. The rest of this chapter provides a general description of the bicycle-cyclist system and presents the research questions and the outline of the thesis. The next chapter provides the necessary background information and the state-of-the art review of existing models and literature.

1.1. Bicycle-Cyclist System Description

In order to develop advanced bicycle-cyclist models a complete system description with its important parameters is essential. The system consists of the dynamics of the bicycle itself, the passive properties of the cyclist, the active control actions of the cyclist and its control feedback mechanisms. Furthermore, the contact and interaction of the bicycle-cyclist system with its environment plays a role. The only contact of the system with the environment is via the two contact patches of the tires with the ground. This so-called tire-road contact defines the behaviour of the rest of the system and plays therefore an important role in the system dynamics. Other influences and forces coming from the environment are: wind or aerodynamic drag or gravitational forces.

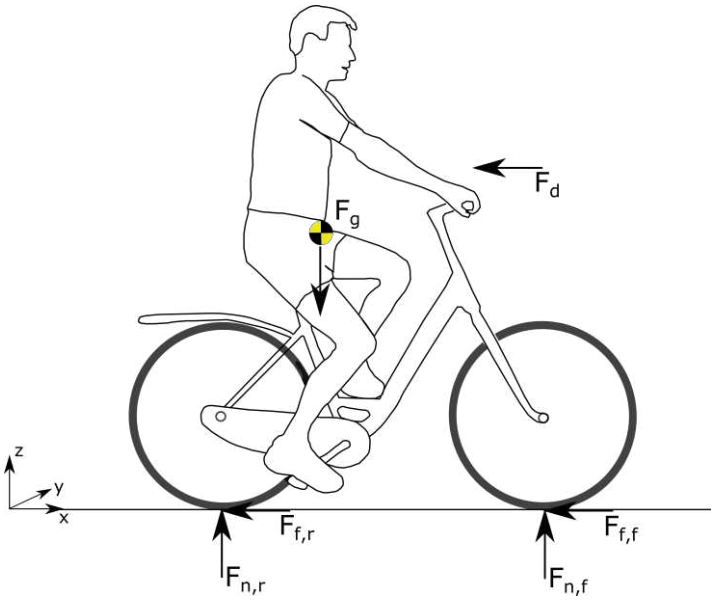

Figure 1.1. *The bicycle-cyclist system with external forces acting in the sagittal plane. F_g = gravitational force, F_d = drag force, $F_{n,f}$ and $F_{n,r}$ are the nominal ground reaction forces for respectively the front and rear tire, $F_{f,f}$ and $F_{f,r}$ are the friction forces.*

Figure 1.1 shows the external forces acting on the bicycle-cyclist system in the sagittal plane. In longitudinal direction, these forces are the friction force Fx, due to tire friction with the road, longitudinal ground reaction forces, due to longitudinal slip of the tire and an aerodynamic drag force. In lateral direction, these are the lateral component of the ground reaction forces that are a function of the camber angle of the wheel, the side-slip angle and the nominal force. Other variables are also of influence on the ground reaction forces, like for example temperature and tire pressure. The lateral dynamics are more complex and require three-dimensional multi-body simulations that need to be solved numerically. Turning forces are required for balance and for change of direction and are part of the lateral dynamics as well. Other forces that play a role are f.e. the gyroscopic force of the front wheel; a turn of the front wheel, causes a roll moment on the bicycle due to gyroscopic procession, centrifugal and gravitational forces. The tire-road contact forces are described in more detail in chapter 2.

Interaction forces between the cyclist and the bicycle play a role as well: the cyclist applies three- dimensional interaction forces at the handlebars, pedals and the saddle. These forces are partly propulsion forces, like the pedalling movement, but also contain control actions. The cyclist can control the bicycle in several ways, with applying a steering action as the most important one. The cyclist can move the handlebars directly by applying forces

on the handlebars resulting in a steering torque. Indirect steering actions can result from lateral upper-body movements or lateral knee movements. The behaviour of the bicycle-cyclist system can be influenced by moving body parts that change inertia properties or the centre of mass of the total system. Furthermore, passive properties of the human body have an effect on the system's behaviour, in particular; arm stiffness and other passive joint properties.

For the cyclist to perform these control actions, sensory information from the environment is required. The major sensory systems that are involved in balance control in humans are: vision is the system involved in planning of motion and in avoiding obstacles, the vestibular system senses linear and angular accelerations of the head, the somatosensory system is a multitude of sensors that senses the position and velocity of all body segments, their contact with the environment and the orientation of gravity (also called proprioception). The Golgi tendon organ senses muscle tension and can activate a reflex, muscle spindles sense length and velocity of muscle contraction, skin afferents sense shear and pressure forces in the skin.

The cyclist needs a combination of all the information from these sensory systems to maintain balance and to steer the bicycle in the planned direction. The sensory information is send to the CNS (central neural system) where it is processed and sent back as a motor control signal to the muscles. This feedback loop is an important part of the bicycle-cyclist system and introduces time-delays between the sensed information and the subsequent control action.

Aging can influence several properties of the cyclist that are required to perform the cycling balancing task well. Deterioration of the sensing capabilities, increase of reaction times, decrease in strength, mobility and memory could cause severe problems during performance of the cycling task. Another important aspect is the safety perception. People can perceive a situation as being particular unsafe, while this might not be necessarily the case. Anxiety can lead to dangerous behaviour of the cyclist itself, which in turn leads to complicated and unsafe situations.

Environmental properties influence the bicycle-cyclist system as well, like for example slippery roads, obstacles on the road, other traffic and the weather conditions.

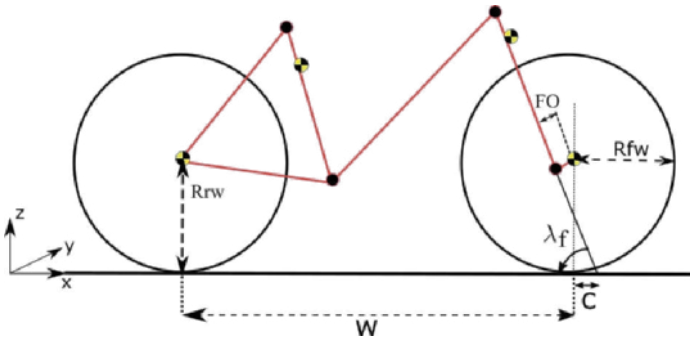

Figure 1.2. *Schematic drawing of a bicycle, with four CoM's (rear frame, front fork, rear wheel and front wheel) and important parameters: w = wheelbase, λ_f = head angle, FO = fork offset, c = trail, R_{fw} = radius of the front wheel, R_{rw} = radius of the rear wheel.*

The parameters of the bicycle itself that influence the behaviour of the system are the mass, centre of mass (CoM), moment of inertia and the bicycle's geometry. The most important geometric parameters of the bicycle are depicted in Figure 1.2: the wheelbase *w*, the head angle λ_f, the trail *c*, the fork offset *FO* and wheel dimensions. The relative positions of the contact points between the bicycle and the cyclist are of importance as well.

1.2. The SOFIE Project

The research of this PhD thesis was part of a 4-year research program, called SOFIE. The SOFIE (Slimme Ondersteunende Fiets/ Intelligent Assisted Bicycle) project was a collaboration between the design company Indes, the Roessingh Research and Development (RRD) and the laboratories of Design, Product and Management and Biomechanical Engineering of the University of Twente.

As the project name suggests, the goal of the project was to develop an intelligent assistive bicycle to improve the safety of older cyclists. The project wished to create performance and design guidelines for mechatronic appliances which improve the stability of electric bicycles, so-called Intelligent Stability Assist Devices (IAD). At the moment, there are few solutions for the problems that older and disabled people deal with on their bicycles. The end-product of this project will be used to maintain the mobility of older cyclists by increasing their sense of safety and stability on the bicycle. This will prolong their independence and maintain their social and physical levels of activity.

For the development of such a bicycle or intelligent stability assist device (IAD), extensive knowledge of the dynamics of the system of a bicycle, cyclist and their interaction with the

environment (f.e. the tire-road interaction) is required. Furthermore, the needs and feels of the user of the product are important. Therefore, important requirements that were defined before the start of the project were: the bicycle should look like a conventional bicycle, the cyclist's posture should be comfortable, the bicycle should be easy to control and not too much information to process for the cyclist should be given. These requirements provided some boundaries on the design space. For example, a tricycle would not be a suitable solution, as it notifies some stigma to the user.

The goal of the University of Twente was to develop tools and methods to measure and predict bicycle and cyclist stability and safety. One research line focused on the development of computer simulation tools, while the other research line focused on the development of an experimental laboratory set-up. Roessingh Research & Development (RRD) was responsible for defining the requirements of the user of the product: the older cyclists. With the use of workshops and cycling experiments, more insights in the behaviour of the users was required. Finally, RRD was also responsible for testing and evaluation of the developed end product with the users. The design company Indes was in charge of creating concepts and solutions for the design of the bicycle and IAD, with the use of the information provided by the other project partners.

This thesis provides the part of the SOFIE project that studies the dynamics and stability of the bicycle-cyclist system and develops computer simulation tools and experimental data to validate these models. The next paragraph explains these contributions in more detail.

1.3. Thesis Outline

The general goal of this thesis is to improve, test and validate existing multi-body models to predict the behaviour of older cyclists. This will lead to design guidelines to develop safer bicycles for older cyclists.

The research objectives to reach this goal are:

- Upgrade existing bicycle dynamic models with a more detailed tire-road contact model

- Develop an advanced integrated multi-body model of bicycle dynamics, models of cyclist dynamics (passive and active) and influences of the environment.

- Investigate and simulate differences in cycling strategies between young and older cyclists

Chapter 2

This chapter gives an overview of the state-of-the-art literature on all parts of the bicycle-cyclist system, existing computer models and experimental set-up's and data. A description of the bicycle dynamics and explanation of bicycle self-stability is given, including the important modelling aspects. Furthermore, existing bicycle model extensions, like the tire-road contact, cyclist biomechanics and control in literature are given and their importance is explained.

Chapter 3

To work towards an advanced multi-body model of the system of a bicycle, the cyclist and its environment, an open-loop bicycle-cyclist model was developed in the commercial multi-body dynamic software ADAMS. The main contribution of this paper to bicycle dynamics is the analysis of tire and rider properties that influence bicycle stability. The effect of tire properties is studied using the tire's forces and torques that have been measured in several operating conditions.

Chapter 4

A large data set has been generated on a novel experimental laboratory set-up; 15 young (20–30 year) and 15 older cyclists (54–62 year) cycled on a safe laboratory cycling set-up, while controlled lateral disturbances were applied to the rear of the bicycle. Differences in control strategies were analysed between these two groups when cycling at 4 m/s.

Chapter 5

Validation of more complex biomechanical cyclist models is needed to upgrade existing bicycle-cyclist multi-body models. The validation of bicycle-cyclist models is challenging due to the complex 3D-interactions between the bicycle and the cyclist. Therefore, this paper focuses on the measurement of 3D kinematics and bicycle-cyclist contact forces (6 DoF) and the validation of an advanced bicycle-cyclist multi-body model with the use of these measured data.

Chapter 6

The same data set of chapter 4 was used to identify a closed-loop SIMO cyclist balance control model. Young cyclists cycled at 4 different speeds, whereas older subjects cycled at

two speeds. The balance tasks performed by steering, upper-body lean and outward knee movements were modelled with the use of a PD-controller with time-delay. The identified parameters were compared between the young and older cyclists.

Chapter 7

The open-loop bicycle-cyclist model was used to study the self-stability of the system during straight cycling, by analysing the weave eigen mode of the bicycle-cyclist system. Furthermore, the behaviour during cornering was analysed.

Electrical bicycle hub motors are frequently used to assist the cyclists pedal. However, in order to ensure the further acceptance of the electric bicycle, improvement of safety is necessary. In this study, computer simulations were used to study the effect of using electric hub motors on the bicycle's stability.

Chapter 8

This final chapter summarizes the main findings of the thesis and discusses its limitations and perspectives for further research. This thesis worked towards the development of an advanced bicycle-cyclist model, with an upgraded tire-road contact model and a cyclist balance control model. We succeeded in identifying differences between control strategies of young and older cyclists and to define differences in model parameters. Older cyclists use more control actions and have more difficulties when cycling at low speeds, compared to younger cyclists. This explains their higher accident risk and shows that they can benefit from bicycles that are more stable at low speeds.

With the developed multi-body bicycle-cyclist model an optimized geometry was defined, that was used in the SOFIETS (the developed bicycle within the SOFIE project). Furthermore, a 'two-motor' system was simulated and results showed an advantage for bicycle stability.

Chapter 2

Background Information & Literature Review

2. Background Information & Literature Review

2.1. Bicycle Dynamics & Self-stability

Carvallo and Whipple [23, 24] (independently) were the first to describe the bicycle dynamics and derive the linearized equations of motion. They showed the principle of bicycle self-stability: bicycles can balance themselves when moving in a certain forward speed range. Meijaard and Schwab [25, 26] contributed to a new start of bicycle dynamics research in 2005, by publishing and benchmarking the linearized equations of the Carvallo-Whipple bicycle model (CWBM).

The CWBM consists of four rigid bodies (the rear frame plus a rigidly attached rider point mass, the front-assembly and the two wheels) and has three degrees of freedom (DOF). The front-assembly and the rear frame are interconnected by a revolute joint at the steering axis, and the wheels are connected to the rear frame and front-assembly by two hubs. The three degrees of freedom are the roll angle ϕ of the rear frame, the steering angle δ and rotation of the rear wheel with respect to the rear frame Ω_r. The linearized model restricts the motions from only small deviations from the straight-running configuration. The wheels are modelled as stiff, non-slipping knife-edge discs, and friction is not accounted for. Due to non-holonomic constraints in the lateral and longitudinal direction, there are four extra kinematic coordinates which describe the configuration of the bicycle: the x and y coordinates of the rear wheel contact point, the yaw angle of the rear frame and the rotation of the front wheel with respect to the front frame Ω_f.

The stability of a straight-running upright bicycle at constant forward speed can be investigated by calculating the eigenvalues of the system [25, 26]. Figure 2.1 shows the eigenvalues of the benchmark model plotted against the forward speed [25]. The two most significant eigen modes of a linearized bicycle model are: the capsize mode and the weave mode. The capsize mode is dominated by the roll angle of the bicycle and represents the capsizing motion of the bicycle (like a capsizing ship). The weave mode represents the oscillation of the bicycle's steering and roll angle, with the steering angle oscillation slightly lagging the oscillation of the roll angle. A third eigen mode is the castering mode, which is dominated by the steering movement and trail (also called caster). Trail is the distance that the front wheel contact point trails behind the projected steering axis contact point (see

Figure 1.2). When all eigenvalues have a negative real part, the bicycle is intrinsically stable. The benchmark bicycle model is self-stable in the forward speed range of 4.3 and 6.0 m/s [25], with v_w = 4,3 m/s (the weave speed) and v_c = 6.0 m/s (the capsize speed). Experiments showed good agreement between the weave mode of the benchmark model and the measured uncontrolled bicycle at speeds above 3 m/s [27]. At high speeds, a fourth eigen mode can appear: the wobble mode. Wobble is the oscillation of the front fork around the steering axis.

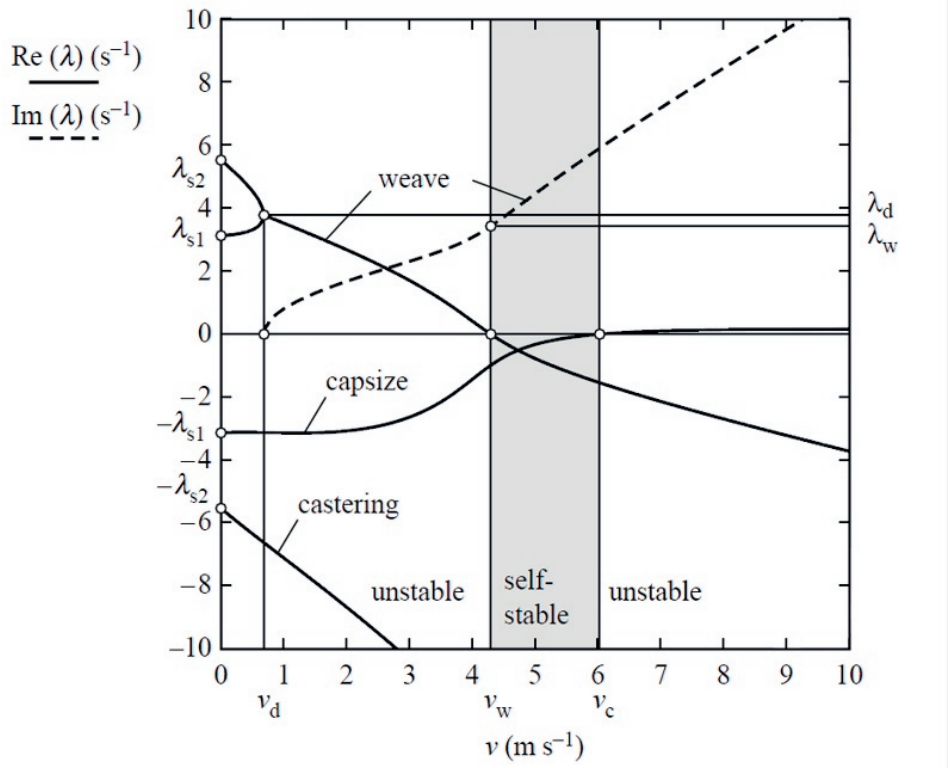

Figure 2.1. *Eigen mode plot of the benchmark model [25], with the weave, capsize and castering modes, presenting the self-stable and unstable forward speeds of the bicycle.*

The reason for this bicycle self-stability was unclear for a long time. Kooijman et al. [28] found that the reason a bicycle can balance itself is the coupling between steering and leaning: when a bicycle falls to the right, it steers to the right. When it falls to the left, it steers to the left. This is called the steer-into-the-fall mechanism. By steering in the same direction as the bicycle is falling, the bicycle brings its contact points with the ground under its centre of mass. Recall a similar mechanism when balancing a broomstick: you move your hand in the direction the broomstick is falling to move the contact point under its centre of mass.

This steer-lean coupling makes the steering of a bicycle counter-intuitive: to turn to the right, you must initially steer to the left, in order to make the bicycle lean to the right [29]. The underlying mechanisms for the self-stability of bicycles is not yet fully understood. Until recently, it was generally believed that the gyroscopic effect of the front wheel and the trail are the two mechanisms that ensure bicycle self-stability [30-32].

The gyroscopic effect of the front wheel stabilizes the bicycle in the following way: imagine a forward spinning front wheel (the first torque) that is perturbed by a second torque around the forward longitudinal axis of the bicycle (a fall to the right). Given the right-hand-rule, the third corrective torque will be around the vertical axis in the right direction, thus enabling the steer-into-the-fall principle, see Figure 2.2.

The trail of the front wheel contact point behind the projected steering axis contact point results in a steer-into-the-fall movement as well. An increased trail ensures a broader stable speed range, but also makes it more difficult to steer [30, 32].

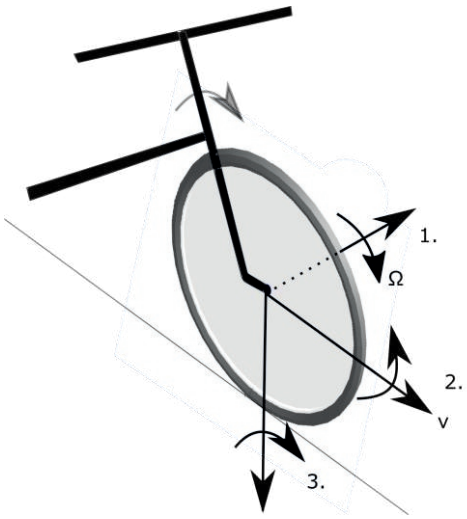

Figure 2.2. *Schematic drawing of the gyroscopic effect of the front wheel causing a steer-into-the-fall movement: 1. The front wheel rotation Ω, 2. Roll angle to the right (perturbation), 3. The resulting torque around the third axis, following the right-hand-rule: a steer-into-the fall movement.*

So, it is clear that both mechanisms are able to increase bicycle self-stability. However, Kooijman et al. [28] found that if these two mechanisms were eliminated, the bicycle still can be self-stabilizing. This implies that other design variables can also contribute to this bicycle self-stability. They found that the mass distribution of the front assembly is also an important parameter for self-stability: if the centre of mass of the front assembly is located forward of the steering axis and lower than the centre of mass of the rear frame, the front

assembly will fall faster to the side than the rear frame, causing a steer-into-the-fall motion [25].

The self-stability behaviour of uncontrolled bicycles explains why a bicycle is so easy to ride (when learned!). When riding within the optimal speed range, minimal control is necessary. However, more control is necessary when, for example riding at low speeds, compensating for high disturbances or when riding on a very narrow path. Furthermore, not only stability of the bicycle is important, but also the bicycle's handling properties influence the controllability of the bicycle. A very stable bicycle might be difficult to control.

Several studies have shown that changing the bicycle's parameters, like for example the wheelbase, the head angle and the radius of the front wheel can influence the stable speed range of an uncontrolled bicycle [21, 31, 33-35]. Multi-body dynamic models are the most frequently used tool to examine the self-stability.

2.2. Multi-Body Bicycle Models

Most multi-body dynamic bicycle models start of from the benchmarked CWBM, as described before. However, some assumptions in the CWBM could cause loss in dynamic properties. For example, the shape of the tire is not accounted for and no friction and slip in the contact point with the ground are modelled. These assumptions are sufficient when analysing the self-stability around a steady-state configuration, but it might be insufficient when studying the system over time and in more complex situations that involves the behaviour of the cyclist.

The benchmark model is further developed and used in other configurations, like steady-state cornering and acceleration. Papadopoulos [36] studied the circular motion of the benchmark model. Most of the obtained circular motions turned out to be unstable; without steering torque considered and a centred cyclist, only a few discrete lean angles are possible at each speed. Basu-Mandal [37] studied the circular motion of the benchmark model, Sharp and Limebeer [38] included acceleration and deceleration and the toroidal shape of the tires. Sharps model of a motorcycle included tire slip and tire relaxation delays. That model allows lateral displacement of the rear frame since the wheels are no longer ideal [39, 40]. Cain [41] also modelled the steady-state handling of the bicycle-cyclist system and included the cyclist lean motion into the model. McGuan [42] included a motorcyclist model in his motorcycle multi-body dynamic model in the software Adams, that was based on the benchmark model. Cossalter's model [43] of the motorcycle was more detailed and contained 7 rigid bodies and included suspension.

The model used by Popov and Meijaard contains some important extensions to the benchmark model. The motorcycle model has 11 degrees of freedom and contains 6 rigid bodies. They showed that it is possible to analyse the stability of nonlinear systems using the bifurcation theory [44]. A different approach was used by Sharma et al. [45], who used applied robotics to formulate the generalized dynamic equations of motion in Matlab-Simulink. The bicycle model consists of three rigid bodies, but is more detailed than other models. The geometry of the frame is realistic and consists of hollow cylinders; even the spooks in the wheels are modelled. The mass of all parts is calculated based on their densities and volumes. The chain is neglected and the pedalling is reduced to a circular disc. The model has only three degrees of freedom: lean, steer and rotation of the front wheel. This makes the dynamical properties of the model the same as the benchmark model.

The mass distribution of the cyclist on top of the bicycle will change this dynamic behaviour and turns it into an unstable system [22]: some form of control is required to stabilize the bicycle. This is why it is important to have a good model of the biomechanics of the rider and the human balance control.

The choices in the benchmark model could cause loss in dynamical properties, especially the non-slipping rigid-knife edge wheel model is not sufficient. Also, the tire-road model is important, which is pointed out by several authors [21, 46, 47]. These two aspects will be discussed in the next two sections.

2.3. Tire-Road Contact

The tire-road contact model is critical for the validity of the multi-body bicycle-cyclist model. The tires are the only true contact between the bicycle and the environment and therefor are very important for handling and stability. The tire-road interaction forces depend on tire properties, as well as on road properties and the motion of the bicycle with respect to the road. Acceleration and braking require longitudinal forces, whereas balancing and turning depend on lateral forces.

The limitations of a rigid-knife edge, pure-rolling, no slip tire-road contact model as is used in the CWBM, are the neglection of friction, slip, deformation and the cross-sectional shape of the tire. However, it depends highly on the application of the model which aspects of the tire behaviour should be taken into account. Some studies have shown that an extended tire model shows little difference in dynamic behaviour, compared to the CWBM and that this model predicts the behaviour of the bicycle well in the linear region [27, 48, 49]. However, it was also shown that the CWBM is sensitive to side-slip and camber

properties [46]. This means it is worthwhile to consider these properties while modelling the bicycle-cyclist system.

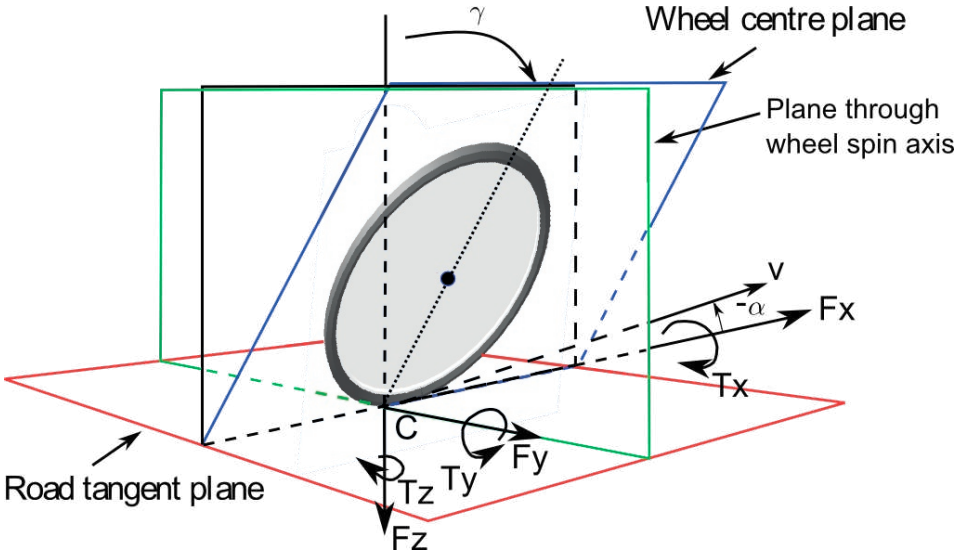

Figure 2.3. *Definitions of tire-road contact forces in the SAE coordinate system, with C the tire-road contact point, γ the camber angle of the wheel and α the side-slip angle.*

In the studies of motorcycle dynamics, it is already considered acceptable to use more sophisticated tire models that take into account side-slip and camber properties [50-53]. These tire models typically use slip quantities as input and calculate forces and torques as outputs. The forces and torques depend on the side-slip angle (angle between the heading and the wheel centre plane) and the camber angle (inclination angle of the wheel plane to the vertical), see Figure 2.3 for the definitions and Figure 2.4 for the in- and outputs typically used in tire models. The out-of-plane forces are most important for stability and handling, and are depending on the side-slip and camber angle. The lateral force *Fy* is described as immediate response to the tire side-slip α and camber γ in the linear form: $Fy = C_\alpha + C_k$, with C_α the cornering stiffness and C_k the tire camber stiffness.

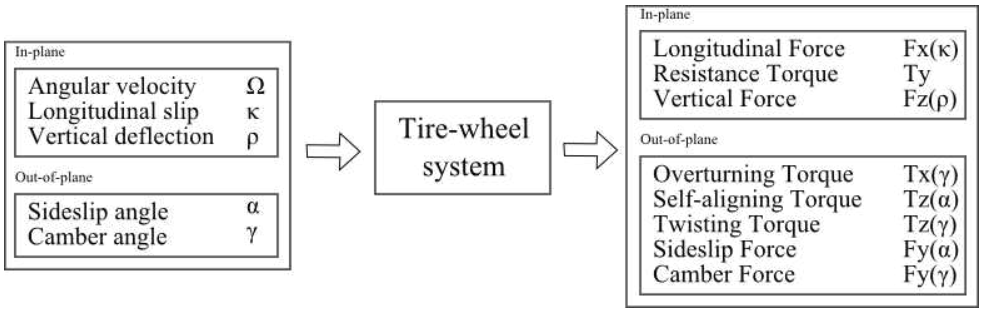

***Figure 2.4**. In- and outputs of a tire model.*

The forces and torques are applied in a contact point between the tire and the road. Modelling the finite cross-sectional shape of the tire enables the contact point to move around the outer shell of the tire during cornering, which will change the dynamic forces. An overturning torque is used to take this into account in a model which accounts for the lateral shift of the normal load when the bicycle leans [54]. $T_x = F_z \cdot r_c \cdot \gamma$ with T_x the overturning torque, F_z the vertical load, r_c the wheel-crown radius and γ the camber angle of the wheel [54].

The other two out-of-plane torques that act between the tire and the road are the self-aligning torque and the twisting torque. The self-aligning torque is a result of uneven distributed lateral shear force that is generated by the lateral slip of the tire (see Figure 2.5); the lateral force is therefore positioned at a distance from the centre of the contact patch. This distance is called the pneumatic trail t. The self-aligning torque is defined as the product of the sideslip force $T_z(\alpha)$ and the pneumatic trail $t(\alpha)$. The twisting torque is a function of the camber angle (approximately proportional) and is generated when an inclined wheel moves along a circular trajectory. When the outside part of the contact patch moves faster than the forward velocity of the wheel centre and the inside part slower, shear stresses in the contact patch generate a twisting torque that tends to move the wheel with a smaller curvature radius. The inner part has a negative longitudinal slip whereas the outer part has a positive longitudinal slip, as depicted in Figure 2.5. The self-aligning and twisting torques have opposite sign and together form the yawing torque of the tire.

The effect of these mechanical properties on the dynamics of motorcycling has been investigated by several authors. Da Lio et al. [55] found that the manoeuvrability of a motorcycle is influenced more by camber stiffness instead of cornering stiffness. Cossalter [51] published results on the study of the effect of tires on the stability of sport motorcycles, and found the tire properties of the front tire to be of significant influence.

The twisting torques increases capsize at low speeds, but has the opposite effect on the weave mode [51]. The camber force and twisting torque have a relation with the vertical load and the tire pressure which can be related to the change of the contact patch geometry [52]. He also compared simulations of a motorcycle model with experiments and found good agreement [56].

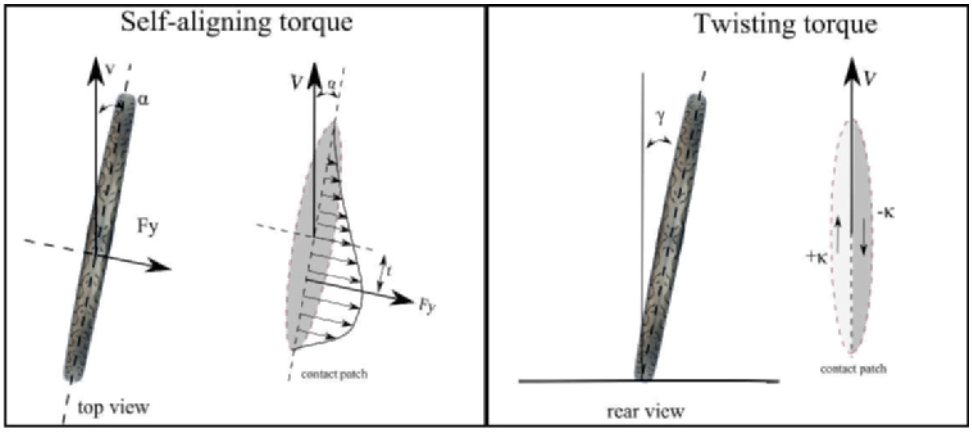

Figure 2.5. *Schematic view of the generation of self-aligning torque (left) and twisting torque (right)*

2.3.1. Non-linear tire behaviour

The steering behaviour and stability of automobiles are greatly affected by the nonlinear characteristics of tires. Before the onset of a loss of stability the tires have been working under non-linear conditions. The same could be true for bicycle tires. At large slip and camber angles, the tire no longer behaves in the linear regime. Various models of non-linear tire behaviour exist. The Magic Formula of Pacejka is the most popular and most widely used non-linear tire model [57]. The Motorcycle Magic Formula [40, 53, 58] can describe the forces and torques generated by the tire in a non-linear configuration. This approach needs an extensive data set to define the tire properties. In 1987 the first version of the Magic Formula tire model was developed [59] and defines the most important development in the literature regarding tire modelling.

Most bicycle tire models act in the linear region, but tires tend to operate in the nonlinear regime in an extreme handling situation. Baslamish et al. [60] showed that instead of the classical linear tire model, a simple rational model with validity extending beyond the linear regime of the tire may be considered. In this model, the cornering force depends on the forward velocity and the side-slip angle.

When evaluating the stability in the problem scenarios of elderly it can be expected that the tire behaves in the nonlinear region. This means that the tire model which will be used in our model should contain the nonlinear relationships between the different parameters. Measurement data is needed to define the (non-linear) relationships between the in- and outputs of the tire model shown in Figure 2.4

Recently Dressel et al. [46] developed a method to measure the camber and cornering stiffness of bicycle tires. The rotating disc machine of the Motorcycle Dynamics group of the University of Padova is developed to identify tire properties of motorcycles and scooters [61]. Data needed to develop semi-empirical models of the tire mechanics can be measured with this experimental set-up. Subsequently, the 'Magic Formula' of Pacejka can be used to fit the experimental data. To start off with a good data set of the mechanical properties of bicycle tires, a co-operation with the Motorcycle Dynamics group of the University of Padova was formed. The rotating disc machine was slightly adapted to be suitable to use for the identification of the mechanical properties of bicycle tires as well. Together, a data set was generated with this experimental set-up, that consists of the side-slip force, camber force, self-aligning torque and twisting torque data of four different bicycle tires [62]. These were tested under normal conditions and variations in inflation pressure and vertical force. The published paper on this topic can be found in [62] and the results are used in this thesis.

2.4. Cyclist Dynamics and Control

Modelling the bicycle dynamics and tire mechanics is much more straightforward than modelling the human cyclist dynamics and control. To describe human movement with the use of multi-body dynamic models many assumptions are necessary. Furthermore, no person is the same, so properties need to be scalable/changeable to people of different length, size, weight and age. Depending on the application, person-specific models could be required.

The bicycle dynamics are frequently examined, but little is known about the cyclist control. The bicycle dynamics are not even yet fully understood. Understanding and modeling the human aspects of riding a bicycle is even a bigger challenge. Adding a human on the bicycle drastically changes the dynamics of the system [63]. The cyclist also changes the dynamic behavior of the bicycle by actively applying control actions, like steering and mass shifting. In normal (steady-state) situations minimal control is necessary. More complex situations will require more tight control and faster control actions.

In this section, the biomechanics of the rider and the human balance control system needed to control a bicycle will be explained.

2.4.1. Passive properties of the cyclist

To start with, the effect of passive properties of the cyclist will be discussed. Schwab [22] studied the effect of a passive cyclist on the stability of the bicycle with the use of a linear multi-body dynamic model. From a study on observations of bicycle cyclists, two distinct cyclist postures were identified: upright configuration (arms are stretched and steering is performed by a force of the arms, no upper-body movement was considered) and the forward leaned configuration (arms are bowed, steering is performed by twisting the upper-body) [64, 65]. These two postures of the cyclist were implemented in the benchmark bicycle model without adding extra degrees of freedom. The first posture changes the stability of the open-loop system dramatically: the system is always unstable in the capsize mode, because the steer-into-the-fall mechanism is made ineffective. The second posture did not change the stability of the system much compared to a system with a rigid rider. Subsequently, the controllability of these open-loop bicycle-cyclist systems were studied by adding two control mechanisms: upper-body lean and steering. The system had a good controllability for steering torque and is controllable by lateral upper-body motions to only a limited extent [22].

Sharp [40] adopted biomechanical properties of the drivers arm's from a study that identified passive properties during a steering task from car drivers [66] for his motorcycle multi-body model. Later he tested the effect of a spring-damper restraining the upper-body lean movement of a cyclist on the bicycle stability, but did not found a significant effect [54]. In this case values were adopted from a study that identified these values for motorcyclists by laboratory testing [67].

At the Motorcycle Dynamics Group of the University of Padova the passive response of the cyclist was studied as well [68-72]. They used a laboratory set-up to identify the biomechanical properties of the (motor) cyclist. The response of the passive motorcyclist to a steer and roll perturbation were measured, to identify a simplified model of the upper-body of the motorcyclist that was interconnected with the handlebars by means of two linear spring-dampers representing the arms [72]. The passive response of the cyclist to steer excitation had a peak around 2 Hz and to the roll excitation around 1 Hz [72].

The steering impedance was identified in a different study and the effect on motorcycle stability was analysed [71]. The steering impedance caused a stabilization of the wobble

mode of the motorcycle and a destabilization of the weave mode. This effect was similar to the effect caused by a steering damper [71]. Another study presented different models of the cyclist upper-body with respectively 1, 3 and 5 degrees of freedom and fitted these biomechanical models to experimental test data [73]. Additionally, an increased grasping force was considered. One study focused particularly on biomechanical properties of cyclists and the effect on bicycle stability [68]. Torsion and lean stiffness of the upper-body in a hands-on and hands-off the handlebar configuration was considered. The extension of the CWBM with 1 extra degree of freedom (upper-body lean) and the biomechanical properties of the upper-body did not change the eigenvalues of the system much. However, the open-loop stability with hands on the handlebar had a great effect on the eigenvalues. This model was never stable, due to an instable capsize mode [68]. To include a good biomechanical cyclist model, the mass and geometrical properties of the human body need to be known as well. Moore et al. [74] estimated these properties by building up the cyclist model by using simple mathematical geometries.

Motorcyclist dynamic models are typically more advanced than cyclist models and use a higher number of rigid bodies and degrees of freedom. Keppler et al. uses for example 17 rigid bodies for his dynamic model of a motorcyclist [75] and Cossalter uses 13 rigid bodies in his motorcyclist model that studies the dynamic behaviour of a motorcycle during a fall [76]. However, the cyclist model of Cangley also uses a high number of rigid bodies (14) in his study to performance enhancement in competitive cycling [77].

2.4.2. Cyclist control actions

Cycling biomechanics and stability strategies have been studied for healthy subjects. Moore et al. [64] studied the motion of the cyclist and bicycle during normal cycling and identified pedalling, spine bending (due to hip motion in the frontal plane) and upper body lateral lean and twisting as normal behaviour during steady state cycling. Most steering behaviour takes place at or around the pedalling frequency. Upper-body motions (lean, bend and twist) are linked to the pedalling motion [64]. At lower speeds and during getting on or off the bicycle, the amount of steer, roll and yaw of the bicycle increases exponentially [64, 65].

Most control is performed by steering actions [64]. During normal cycling, these steering actions are small: about 3°, but at lower velocities higher steering angles were seen. Prior to a corner the forward speed decreases and steering angles also become larger (around 15°) [65]. Van den Ouden [78] compared the cycling behaviour of an average group with a group of elderly. He found that elderly use a quicker change of steering angle (higher

steering angle velocity) to stabilize, and that an average cyclist uses larger steering angles (during starting and stopping). Older cyclists do not decrease their speed when approaching a corner as much as average cyclists, the cause of this is yet unknown [78].

Upper-body lean is another form of control in a cycling stabilization task. During normal cycling, little upper-body motion was seen, only prior to cornering this control motion was more significant [65]. The control by leaning requires higher gains compared to the gains required by steering [79]. This means that more effort is required to stabilize the system by leaning then it is by steering. Low speed stabilization is done by lateral knee motions (only during pedalling) [65].

Doyle [63] was one of the first who investigated the human contribution to bicycle riding. He analyzed to what extent the higher functions of the cerebral cortex were needed to control the bicycle. It seems to be a rather easy task, as children can learn it very quickly. And once you learned it, you will never forget. He found that vision is not necessarily needed to maintain balance, but is only necessary for path-following. The system delay of the roll rate is very short, which means that the output of the vestibular system is almost directly connected to the controlling muscles and no higher brain functions are used in this case. Another interesting finding was that the self-stability effects of the bicycle are much faster than the reaction time of the human. This means that a broad/extended self-stability range of the bicycle can help older or disabled cyclists when they are not capable of controlling the bicycle anymore. On wide paths only every few seconds stabilization adjustments are needed, which occur at low frequencies [80].

2.4.3. Cyclist control models

Cyclist control feedback models were proposed by van Lunteren & Stassen [80] who described the bicycle-cyclist system by a model that consists of a PD-controller with time-delay, with the roll angle of the bicycle as input and the steering and upper-body movement of the cyclist as outputs. They found the behaviour of the cyclist to be time-invariant for at least 5 minutes. Weir & Zellner [81] analytically studied the control behaviour of a motorcyclist and used an inner feedback loop for the stabilization that controls the roll angle with a steering torque, and outer loops to control the path and heading of the motorcycle by means of upper-body lean. Nagai [82] developed a robot bicycle that automatically balances and steers the bicycle by applying a steering angle and upper-body lean angle, when using the roll angle and lateral deviation of a previewed point as inputs. Chen and Dao [83] developed a dynamic model of a bicycle without cyclist and

implemented a fuzzy an PID controller to stabilize the bicycle and another fuzzy controller that tracks a desired roll angle of the bicycle.

Cain et al. [41] compared experimental data with a steady-turning mathematical model. The model was based on the CWBM and did not include movements of the cyclist. The model explained a large part of the experimental data; the roll and steer angles were predicted well. However, the steering torque was not predicted well, and was greatly affected by induced lean of the cyclist. It shows that cyclist lean with respect to the bicycle plays an important role in bicycle control. Cain used several measures to quantify the skills of cyclists. In [84] he used the cross-correlation between steer and roll angular rates to quantify the skill of cyclists who learned to cycle. The results suggest that increased cycling skills can be quantified by an increased correlation between steer and roll angular rates. In another study he measured the cycling dynamic behaviour of 7 experienced and 7 unexperienced cyclists who cycled on rollers [85]. He found that the cross-correlation of the lateral position of the centre of mass to the lateral position of the centre of pressure was a good measure to quantify cycling balance. The experienced and non-experienced cyclists used similar control strategies as low speed, but at high speed the experienced cyclists performed better and used more upper-body lean compared to the non-experienced cyclists.

Moore et al. developed an instrumented bicycle with a harness to restrict movements of the cyclist in order to mimic the benchmark bicycle model with steer control. The instrumented bicycle was used in system identification experiments with the goal to identify the cyclist control system [86]. Three subjects were used in the experiments that were conducted on a treadmill and on the floor of a sports hall. Several manoeuvres were tested, like a balancing task, straight line tracking, heading tracking, lateral deviation tracking and a lane change. In a part of the tests a lateral disturbance was induced by means of an impulse force. This resulted in a large data set that was used for model validation and system identification. The validation of the open-loop bicycle model indicated that the CWBM does not explain all measured data in some cases and that an extended arm model sometimes gave better results. The control model that was used for system identification was based on the controller presented by Hess et al [87]. This model is based on a pilot control model [88] and uses a neuromuscular dynamic model, an inner-loop structure that feeds back the steering angle and roll angle and rate, an outer loop-structure that feeds back the heading and the front wheel lateral deviation. The steering torque was used as the output.

Schwab used some of this experimental data as well (cycling on a narrow treadmill with lateral perturbation impulse forces) to develop a cyclist control model for steering and stabilizing [89]. The bicycle model that was used was the CWBM extended with the cyclist inertia. The cyclist control model with steer and roll angles as input and the steering torque as output gave good fits with the experiment data. The measured steering torque did not match the model and was therefore not used in the identification process. The model feedback was performed by a PD controller on the roll angle and an ID controller on the steering angle. The proportional and derivative feedback on the bicycle roll angle represent vestibular and visual feedback, the steer angle feedback represents proprioceptive feedback and the integral of the steer angle, the heading feedback. The study concluded that the cyclist minimized the control effort at low speed and minimizes the heading error at high speeds [89].

Chapter 3

The Effect of Tire and Rider Properties on the Stability of a Bicycle

V.E Bulsink, A. Doria, D. van de Belt and H.F.J.M. Koopman

Advances in Mechanical Engineering (2015) Vol. 7(12) 1–18
DOI: 10.1177/1687814015622596

Abstract

To work towards an advanced model of the bicycle-rider-environment system, an open-loop bicycle-rider model was developed in the commercial multibody dynamics software Adams. The main contribution of this paper to bicycle dynamics is the analysis of tire and rider properties that influence bicycle stability. A system identification method is used to extract linear stability properties from time domain analysis. The weave and capsize eigenmodes of the bicycle-rider system are analysed. The effect of tire properties is studied using the tire's forces and torques that have been measured in several operating conditions. The main result is that extending simplified models with a realistic tire model leads to a notable decrease in the weave stability and a stabilization of the capsize mode. This effect is mainly caused by the twisting torque. Different tires and tire inflation pressures have little effect on the bicycle's stability, in the case of riding straight at a constant forward speed. On the other hand, the tire load does have a large effect on bicycle stability. The sensitivity study of rider properties shows that body stiffness and damping have a small effect on the weave and capsize mode, whereas arm stiffness destabilizes the capsize mode and arm damping destabilizes the weave mode.

3.1. Introduction

Bicycling is a healthy [90], effective and popular means of transportation. Furthermore, it is frequently used for social and recreational purposes. Even if the development of the bicycle was based on a trial and error process, dynamics of bicycles has drawn the interest of scientists and engineers for many years. In 1899, Carvallo and Whipple independently showed with the use of rigid-body dynamic models that some bicycles could balance themselves when riding at a certain speed [23, 24]. This linear model contained four rigid bodies, three degrees of freedom and a simplified tire-road contact model: rigid-knife edge, pure-rolling and no-slip contact. The rider is modelled as a rigid body, rigidly attached to the rear frame.

In recent years computer simulation proved to be a useful tool for studying bicycle dynamics and stability [25, 35, 54]. Major contributions were made by Meijaard and Schwab et al [25, 26], who published and benchmarked the linearized equations of the Carvallo Whipple Bicycle Model (CWBM). Their studies recently led to important insights into stability of a rider-less bicycle, that have been confirmed experimentally [28].

The CWBM is able to represent the capsize and weave modes, which play the main role in uncontrolled bicycle stability at low speed. Improvement of simulation requires extensions of the model such as the non-linearity of the bicycle dynamics, the passive rider dynamics and the interaction with the environment (i.e. tire-road contact), which increase the complexity of the system considerably. Some efforts to extend the CWBM with realistic tire-road contact models and rider models have been made. Sharp numerically demonstrated that a more realistic tire model strongly influences the weave and wobble modes of the bicycle [54]. Similarly, Dressel et al. showed the importance of upgrading existing bicycle models with the dynamic properties of tires [46] . Adding the rider's dynamics changes the properties of the system significantly and modelling of tire properties could become even more important [54]. Recently, Plöchl et al. gave details of a linear tire model that includes self-aligning and twisting torques [91]. Results showed a significant effect of tire and rider properties on the stability of the wobble mode. Schwab et al. incorporated passive properties of the rider into an open-loop bicycle model, without increasing the degrees of freedom [22]. They studied different rider postures and it was shown that an upright passive rider could destroy the stability of the system by an unstable capsize mode. Recently, Doria et al. experimentally determined the passive properties of the rider's body and integrated the derived models in the benchmark model [92]. Klinger

et al. combined a realistic tire model with a passive rider model and studied the effect of different postures of the rider on the wobble mode, in the case of a racing bicycle [93].

Even if some recent bicycle models were developed by means of multibody dynamics software that is able to generate and solve non-linear dynamics equations [22], in most researches equations were linearized and a linear stability analysis was carried out. Also in the field of motorcycle dynamics [51, 71, 94] it is a common practice to develop, by means of multibody dynamics software, models which take into account non-linear kinematics and tire properties; the full non-linear model is used for performing time domain handling simulations only, while a linearized model is used for stability analysis.

This paper is part of a research that aims to improve bicycle safety, with special emphasis on safety of elderly cyclists. To work towards an advanced model of the bicycle-rider-environment system, it was chosen to develop a non-linear model by means of a commercial multibody dynamics software. Operating in this way it is possible to model a complex 3D system and eventually simulate complex situations, for example the behaviour of elderly cyclists in critical situations. In the next section, the multibody open-loop bicycle-rider model will be described; this model was developed in the software system MSC Adams, and includes bicycle dynamics, a passive rider model and a tire-road contact model. For this last component, a specific version of the 'Magic Formula' tire model [95] was used.

Stability is the main issue of single-track vehicle dynamics and it is related to safety, because on the one hand uncontrolled unstable behaviour may lead to dangerous conditions, on the other hand a skilled rider can obtain nice and quick manoeuvres by controlling an unstable system. This paper focuses on stability analysis and the non-linear model is used for extracting linear properties in the case of riding at a constant forward speed. It appeared that for this specific modelling problem the linearization within the commercial software package yielded rather muddled results; therefore, a system identification method was used to study the stability of two eigen modes: weave and capsize. The weave mode is a combination of steer rotation and roll rotation of the whole bicycle, the capsize mode is dominated by roll rotation [26].

The main contribution of this paper to bicycle safety is the analysis of the parameters that influence stability, which can be grouped into tire and rider properties. The effect of tire properties is studied using the tire's forces and torques that have been measured in several operating conditions [62]. Regarding the rider's properties the effect of stiffness and damping properties of the limbs is dealt with. The body is represented with a lumped

element approach using inertial values found in literature [96] and recently measured stiffness and damping properties [71, 73].

3.2. Methods

3.2.1. The bicycle-rider model

The bicycle-rider model is in its entirety depicted in Figure 3.1. The bicycle's dynamics is represented by four rigid bodies (the rear frame, the front assembly and the rear and front wheel). A revolute joint at the steering axis connects the front assembly to the rear frame. Both wheels are interconnected to the frame by revolute joints.

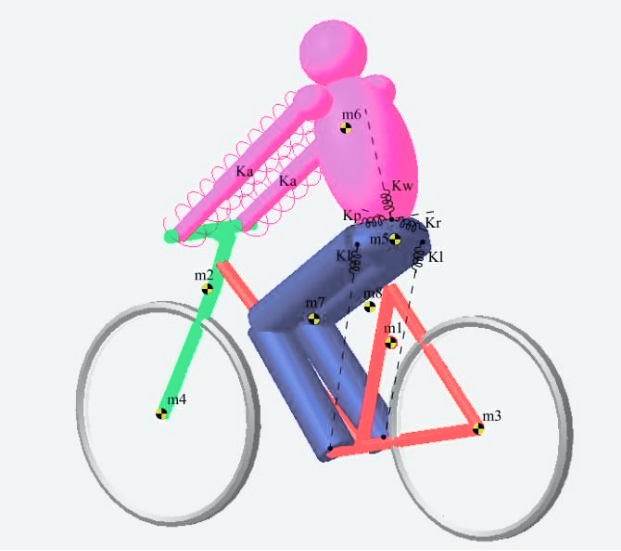

Figure 3.1. *The open-loop bicycle-rider model developed in Adams.*
m1- Rear frame *m2 - Front assembly incl. lower arm mass*
m3 - Rear wheel *m4 - Front wheel*
m5 - Pelvis *m6 - Upper body (incl. trunk, head, upper arm mass)*
m7 - Left leg *m8 - Right leg*
K_a *- linear spring-damper representing the arms*
K_w *- rotational spring-damper around the longitudinal axis of the upper body at the waist*
K_r *- rotational spring-damper around the sagittal axis of the upper body at the waist*
K_p *- rotational spring-damper around the frontal axis of the upper body at the waist*
K_l *- rotational spring-damper around the line connecting the hips and the ankles*

The rider's dynamics is also represented by four rigid bodies: the pelvis, the upper-body containing the head, trunk and mass of the upper-arms, and both legs. The pelvis is rigidly attached to the rear frame and the upper-body connects to the pelvis with a spherical joint, at the L4-L5 vertebral joint position. The arms are modelled as linear spring-dampers between the handlebars and the shoulders, similar to Cossalter et al. [71]. The linear spring-dampers generate a torsion stiffness and damping around the steering axis (coefficients Ka and Ba respectively). The mass and inertia of the lower arms are added to the front assembly. In this way, all rotational degrees of freedom of the upper-body are maintained and the passive dynamics of the rider's arms on the steering is taken into account. Passive springs and dampers are added to the rider's joints. Values are adopted from [92] and are given in Table A.1 of Appendix A.1. Each leg is modelled as one rigid part and has one degree of freedom: rotation around the line connecting the hip and the ankle. This allows for lateral knee movements; a movement which becomes interesting when rider control at low speed is considered [64].

Hence, the rider model contains five degrees of freedom (DOFs). The bicycle model has nine DOFs, due to the modelling of the tires as force and torque generators instead of constraints as being used in the CWBM. These are the positions (in all three directions) and orientations of the rear frame (roll, pitch and yaw), the spin angles of the wheels and the steering angle. Both the bicycle and rider model are fully parameterized, to enable modelling of any bicycle and any rider. Furthermore, it allows for parameter and optimization studies for improvement of the bicycle design (and possibly control) in order to increase safety. The bicycle used in this study is a regular bicycle with low entry (Twade T3001, by Flexaim, Hengelo, the Netherlands). Geometry and mass properties of the bicycle are physically measured using the methods described in [74]. The geometry and mass properties of the rider are estimated from the total weight and height of the person, using linear scaling and regression equations [96, 97]. The rider model used in this study is based on a male with a height of 1.80 m. and a mass of 80 kg. See Appendix A.1 and Figure A1 for the parameter values, as used in the model.

The tire-road contact model estimates the forces acting between the road and the tire. The actual load distribution in the contact area between the road and the tire is recalculated into a set of forces and torques in one contact point. The inputs and outputs of the tire model are given in Figure 3.2. In the radial direction, the tire is considered to behave like a linear spring-damper, with one point of contact with the ground, point C in Figure 3.3. Tire longitudinal and lateral forces and tire torques are calculated by means of the Pac MC (Pacejka motorcycle) model of the package 'Adams/tyre', which is based on the so-called

Magic Formula of Pacejka [57, 95]. In the next section, a more detailed description of the derivation of the tire model properties is given.

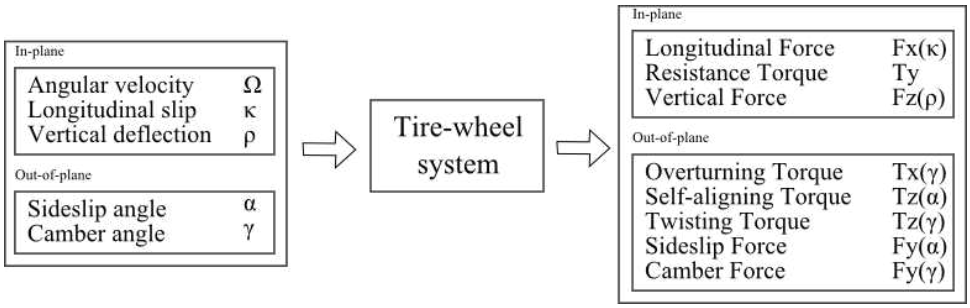

***Figure 3.2**. Definition of the in- and outputs of the tire-wheel system.*

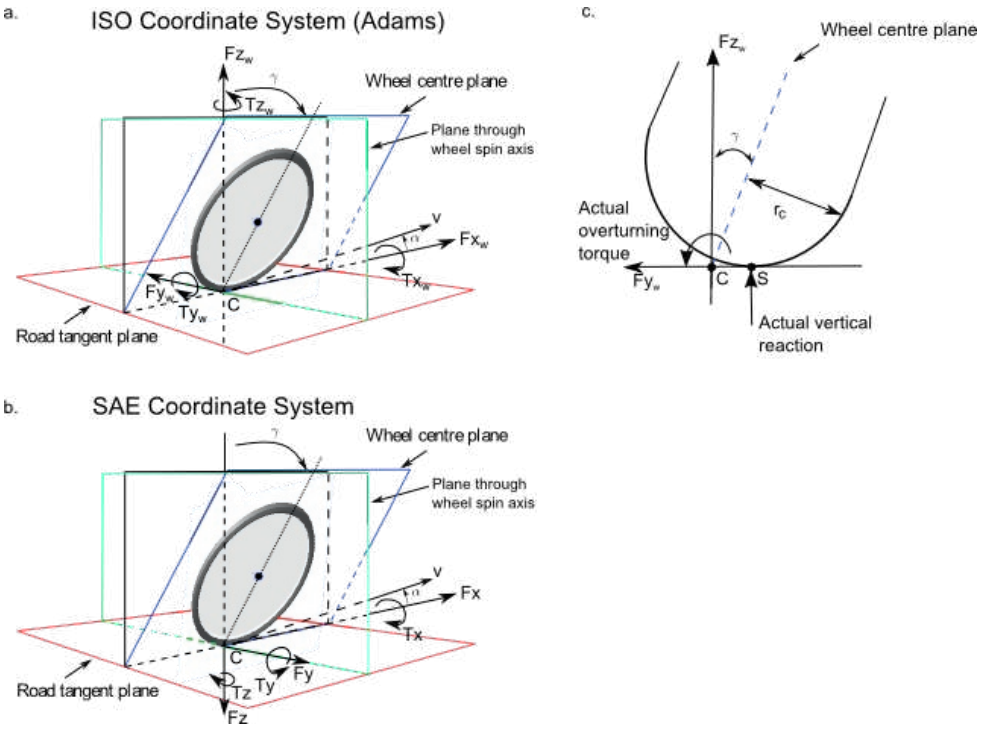

***Figure 3.3.** Coordinate systems, forces and torques exerted by the road on the tire at contact point C, which is defined as the intersection of the road plane, the wheel centre plane and the plane through the wheel spin axis. a. Coordinate system $x_w y_w z_w$ is defined in ADAMS (ISO coordinate system: x_w axis points towards the forward motion direction, z_w axis points upwards and y_w axis completes the tern). b. Coordinate system xyz is defined in agreement with SAE (x axis points towards the forward motion direction, z axis points downwards and y axis completes the tern). The forces and torques are measured in the xyz coordinate system (positive values are shown here) and given in Adams in the*

$x_w y_w z_w$ coordinate system. c. The contact point migrates to point S due to a camber angle, this effect is represented by the overturning torque.

3.2.2. Tire model properties

The tire model properties are based on the data measured by Doria et al. [62]. They measured the tire properties of 4 different bicycle tires and studied the effect of working conditions, like the inflation pressure and load, on the mechanical properties of tires. The characteristics of these tires are given in Table 3.1.

Table 3.1. *Characteristics of the tested tires in [62]. All tires originate from different manufacturers; note that tire 3 has a smaller width and tire 4 is a winter tire, especially developed for snowy/icy roads.*

Tire	Size	Type	Recommended inflation pressure	Bead
1	37-622	diagonal	4.0-6.0 bar	wire
2	37-622	diagonal	3.8-5.5 bar	wire
3	35-622	diagonal	4.0-6.5 bar	wire
4	37-622	diagonal	4.0-6.0 bar	folding

For each given tire, load and pressure, the Magic Formula coefficients are determined and used as input to the model. The nominal load on the tire, during the measurements, was set to 400 N and 600 N. The tire inflation pressure was varied between 2 and 5 bar.

The input for the model in Adams is a road property file and a tire property file. The road property file contains the friction coefficient parameter (μ_r = 1.0) and dimensions of the road. The dimensions of the tire, vertical stiffness (K_z) and damping (B_z) values and the Magic Formula coefficients are given in the tire property file. Both the road and tire property file are included as supplementary material, to make it possible for other Adams users to use the developed bicycle tire model.

It is worth highlighting that the non-linear description of the tire's behaviour, which is requested by Adams, could be useful for future handling simulations. For stability analysis, which is the focus of this paper, a linear tire model would be enough.

The vertical stiffness K_z of the tire is based on a mathematical model that is used for calculating the vertical deflection of the tire for different tire inflation pressures and nominal loads. It is assumed that the contact patch has an ellipsoidal shape and a parabolic pressure distribution [98] and that the tire radius outside the contact patch maintains the

unloaded value. The vertical deflection of the tire ρ can be calculated using half the length of the measured contact patch area *l* and the unloaded radius of the wheel r_f using the Pythagorean theorem. Subsequently, the vertical stiffness K_z can be calculated using the deflection and the known load on the wheel. The numerical value of the vertical damping B_z of the tire is chosen sufficiently large to achieve supercritical responses and is given in Table A.1 of Appendix A.1.

For the calculation of the out-of-plane forces and torques acting by the road on the tire as a function of the sideslip angle (α) or camber angle (γ), a specific version of the aforementioned Magic Formula is used, whereby the coefficient E (the curvature factor) was set to zero, see equation (2.1). Good fitting results were found using this simplified version of the Magic Formula [62].

$$y(x) = D \cdot \sin[C \cdot atan\{B \cdot x - E \cdot (B \cdot x - \arctan(B \cdot x))\}] \tag{3.1}$$

In which *y* is the output variable F_x, F_y or T_z and *x* the input variable *α, κ* or *γ*. The B-coefficient is the stiffness factor, the C-coefficient the shape factor (*>0*), the D-coefficient the peak value and the E-coefficient the curvature factor.

In the linear range Equation 3.1 becomes:

$$y(x) = B \cdot C \cdot D \cdot x \tag{3.2}$$

In which *B·C·D* is the slope of the fitting curve near the origin.

The lateral force $F_{y(\alpha,\gamma)}$ at the contact point consists of two parts, called the sideslip force and the camber force, which are functions of the sideslip angle *α* and camber angle *γ* respectively. The definitions of sideslip and camber angles are given in Figure 3.3. The self-aligning torque $T_z(\alpha)$ is a multiplication of the lateral force $F_y(\alpha)$ and pneumatic trail t(α). A cosine version of the Magic Formula is used to fit the pneumatic trail [95]. The twisting torque is also a function of the camber angle, whereby a linear relation is assumed. The fitting relations are given in Appendix A.2., together with the calculated fitting coefficients.

The in-plane forces and torques were not measured except for the rolling resistance torque Ty. This torque was measured with the tester machine of Padova University [62] on a rotating wheel, while γ and α were set to zero. The mean and standard deviations of the measured rolling resistance torques, as well as the fitting equation can be found in Appendix A.2.

The forces generated under longitudinal slip κ are not measured by the above-mentioned tester machine. Therefore, assumptions for the longitudinal force $F_x(\kappa)$ are made, which are based on motorcycle data, again see Appendix A.2. Since the lateral stiffness (K_a) of bicycle tires (about 4000 N/rad [62]) is close to the lower limit of the lateral stiffness of motorcycle tires [99], the value of longitudinal stiffness K_κ of bicycle tires is likewise chosen as the minimum value of the longitudinal stiffness of motorcycle tires (4800 N) [99] with the same vertical load.

Since bicycle wheels are relatively thin and camber angles remain small, in the model the forces are applied at one contact point. This point ('C') lies at the intersection of the wheel plane, the road tangent plane and the plane through the wheel axis (Figure 3.3c). However, in reality, due to a camber angle and the tire cross section with radius r_c, the contact point migrates and forces and torques are measured at a different point, point *S* in Figure 3.3c [62]. For this reason an overturning torque has to be added [54].

The results of the tire measurements presented in [62] show that the tire properties are load-dependent, which is also observed for motorcycle and car tires [57]. The scaling methods presented in [57] are used to scale the tire properties to the nominal load. The scaling coefficients are given in the Appendix A.2.

In the following sections, the discussion of the effect of tire properties is based on the sign conventions used for measured data (according to SAE).

3.2.3. Analysis of stability

As mentioned in the introduction the multibody dynamics software was not used for the linearization of the equations of motion. Alternatively, time domain numerical data were analysed by means of a system identification method. A lateral disturbance is given to monitor the response of the system. The disturbance is defined as a lateral force of *0.1N* lasting for *0.1s* applied at the position of the centre of mass of the bicycle rear frame.

The system identification toolbox of Matlab is used to estimate a state space model of the bicycle-rider system from time domain data generated by the Adams model for each defined forward speed. The input is the lateral disturbance signal and the outputs are the steering and roll angle. The time domain results are fitted with a state space model with four poles, corresponding to the four state variables (roll angle, roll rate, steering angle, and steering rate). The weave and capsize modes are analysed. The lowest speed at which weave oscillations of the bicycle are damped (the real part of the eigenvalue is negative),

is called the weave speed v_w (this is the lowest speed at which the weave mode of bicycle model is stable). Below this speed the oscillations increase and the bicycle will fall over. Capsize speed v_c is the highest speed at which capsize is stable. Hence, the system is stable between the weave and capsize speed.

High speed stability and the wobble mode are not analysed, since this research focuses on normal operations of bicycles ridden by common or elderly people.

3.2.4. Simulations

The Adams model and the system identification method are validated with the CWBM model, by implementing the benchmark parameter values. Next, the Magic Formula tire model is implemented and comparisons are made.

Furthermore, the effect of the following extensions of the multibody model are tested: Magic Formula tire model, rider joint properties, arm mass at the front assembly, arm damping and stiffness.

Simulations are carried out with tire properties of different manufactured tires and variations in tire pressure and load. Subsequently, the effect of single tire parameters is investigated, by changing one tire parameter at a time (*50* and *200%*) while keeping the other parameters at the nominal value.

Finally, the effect of torsional arm stiffness and damping values is investigated; both with and without the Magic Formula tire model.

3.3. Simulations results

3.3.1. Comparison tests

As indicated in the previous paragraph, the first step is taken by setting the parameters of the Adams model such that it resembles quite accurately the CWBM model with the benchmark parameters [25]. Hence, the rider is modelled as a rigid body stiffly attached to the rear frame and the rigid-knife edge, pure-rolling and no-slip contact is simulated by setting the radial and sideslip stiffness to very high values and the longitudinal force, camber force, twisting torque, self-aligning torque, rolling-resistance torque and overturning torque to zero.

a.

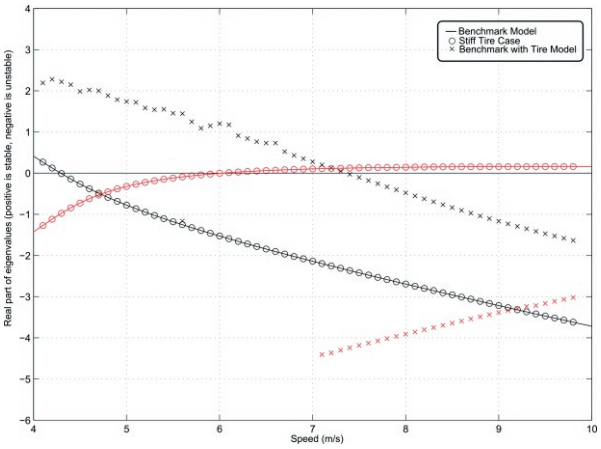

b.

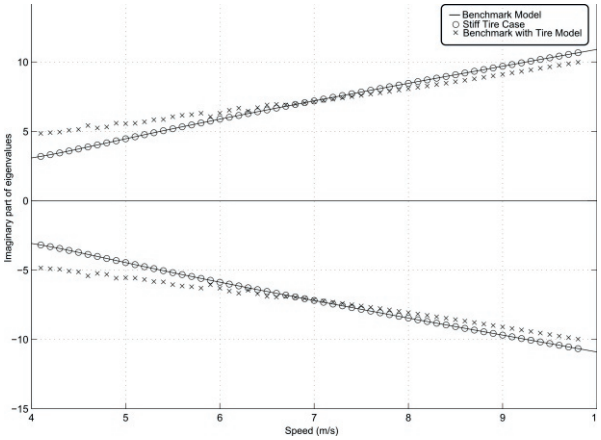

Figure 3.4. *Comparison between eigenvalues of the benchmark mode found in reference [25] and the ones calculates by means of Adams and the identification method in the stiff tire case and with the 'Magic Formula' tire model:* ***(a)*** *real parts (black: weave mode, red: capsize mode),* ***(b)*** *imaginary parts.*

Figure 3.4(a) and (b) show that the nonlinear simulation of the Adams bicycle model and the system identification method are valid between speeds of *4* and *10 m/s*. Identification at lower speeds was poor, due to the instability of the bicycle model at these speeds.

Subsequently, the 'Magic Formula' tire model is implemented in the CWBM model and comparisons are made with the stiff tire case. The tire model is based on the measurement data of tire 2, with an inflation pressure of *4 bar* and a nominal load of *400 N*. The detailed

tire model with side slip force, camber force and torques leads to an increased weave speed $v_w = 7.4\ m/s$ and a stable capsize mode in the presented speed range.

3.3.2. Effect of the extensions of the multibody model

In this section, the full Adams multibody open-loop bicycle-rider model is considered with the properties as listed in Appendix A.1 (Table A.1. Bicycle 1), which refers to the Twade bicycle and a rider of *80 kg*. The effect of several extensions of the model is studied. Table 3.3 lists the simulations that are carried out, the tested model extensions are displayed in bold.

Table 3.3. *Performed simulations, with the tested model extensions displayed in bold.*

Case	Tire Model	Rider Model	Arm Model
1	Stiff Tire, No Slip	Rigid Rider	No Arm model*
2	Stiff Tire, No Slip	***Passive Rider***	No Arm model
3	Stiff Tire, No Slip	Rigid Rider	***Added Lower Arm Mass to Front Assembly***
4	Stiff Tire, No Slip	Rigid Rider	***Arm damping***
5	Stiff Tire, No Slip	Rigid Rider	***Arm Stiffness***
6	***New tire Model***	Rigid Rider	No Arm model
7	***New tire Model***	***Passive Rider***	**Arm stiffness & damping Added Lower Arm Mass**

* the mass and inertia of the arms are lumped in the rigid rider body

Figure 3.5 deals with the effect of the model extensions on the weave mode and shows both the real (a) and imaginary (b) parts of the eigenvalues against forward speed.

a.

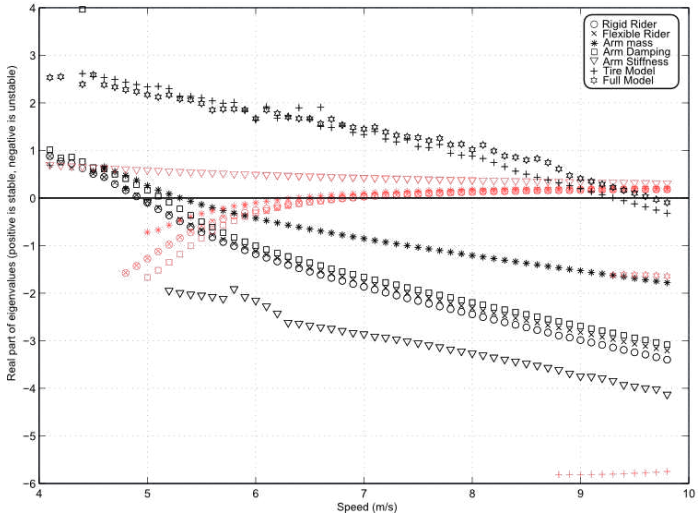

b.

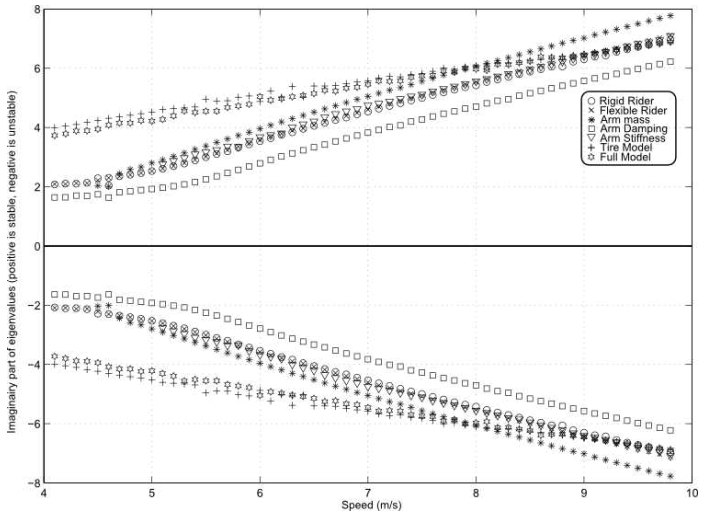

Figure 3.5. *Eigenvalues of several model extensions:* ***(a)*** *real parts (black: weave mode, red: capsize mode),* ***(b)*** *imaginary parts.*

The new bicycle rider model with stiff tire (no slip), rigid rider and arms off the handlebar (case 1) has a weave speed of 4.9 m/s, a bit higher than the one of the benchmark model. Capsize speed of the new model (6.8 m/s) is higher than the one of the benchmark model as well.

When the model is extended, the following results appear:

- Passive rider joint properties (case 2) have a very small effect on the weave mode and show no significant effect on the capsize mode.

- Arm mass (case 3) has a small effect on the weave mode, it increases weave frequency and weave speed. Furthermore, it results in a small decrease in v_c

- Arm damping (case 4) causes a small increase in v_w and a decrease in the weave frequency. No significant effect on the capsize mode was found for speeds above *6 m/s*.

- Low speed stability is not possible with arms that have realistic stiffness (values are adopted from [14], case 5), owing to the presence of an unstable capsize mode. However, arm stiffness stabilizes the weave mode.

- The 'Magic Formula' tire model (case 6) destabilizes the weave mode (weave speed increases to *9.3 m/s*), but stabilizes the capsize mode. It is worth highlighting that in reference [93], which considers a linear model of tire forces and torques, weave speed is about *9.5 m/s* and capsize mode is always stable.

- When the full model is used (which includes the new tire model, passive rider and arms), the capsize mode is always stable and weave speed increases a bit more with respect to case 6. This result means that the stabilizing effect of the tire forces and torques on the capsize motion is larger than the destabilizing effect of arm stiffness.

3.3.3. Model sensitivity to tire properties

The simulations carried out with different manufactured tires and with the same tire inflated at different pressures result in a small change in the weave speed and weave frequency. Tire 3 (which is thinner than the others) shows a small increase in the weave speed (*0.2 m/s*), and tire 4, the winter tire, is a bit more stable over the entire speed range.

However, the vertical load on the tire applied during the measurements of tire properties, influences the mechanical tire properties and therefore also the stability of the bicycle. The simulation of the open-loop bicycle-rider model with the tire model based on the measurements with a nominal load of *400N* resulted in a weave speed of *9.7 m/s*. The

simulation with the tire model based on the measurements with a higher load (*600 N*), gave a weave speed of v_w = 8.3 m/s (see Figure 3.6).

a.

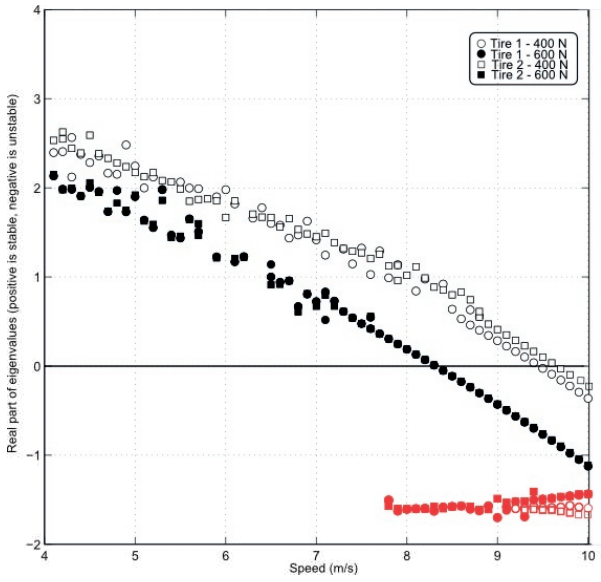

b.

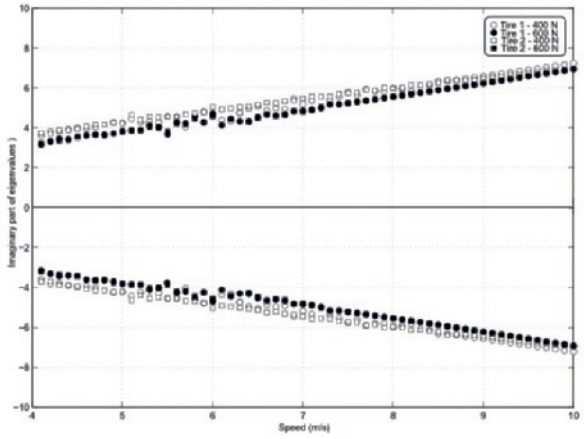

Figure 3.6. Eigenvalues for the open-loop bicycle-rider model when tire parameters are based on measurements with a vertical load of 400N and 600N, for two different tires: **a.** real parts (black: weave mode, red: capsize mode), **b.** imaginary parts.

The next step is an analysis of the sensitivity of the weave speed to the single tire properties, Figure 3.7 shows the results. Variations of 50% and 200% of the nominal value of one property at a time are considered, keeping the other parameters constant. On the one hand cornering stiffness K_α has a small effect on the weave speed: doubling of the value decreases the weave speed by less than 1%. On the other hand, camber stiffness K_γ has a remarkable effect on the weave speed; if K_γ doubles, weave speed increases by 9%.

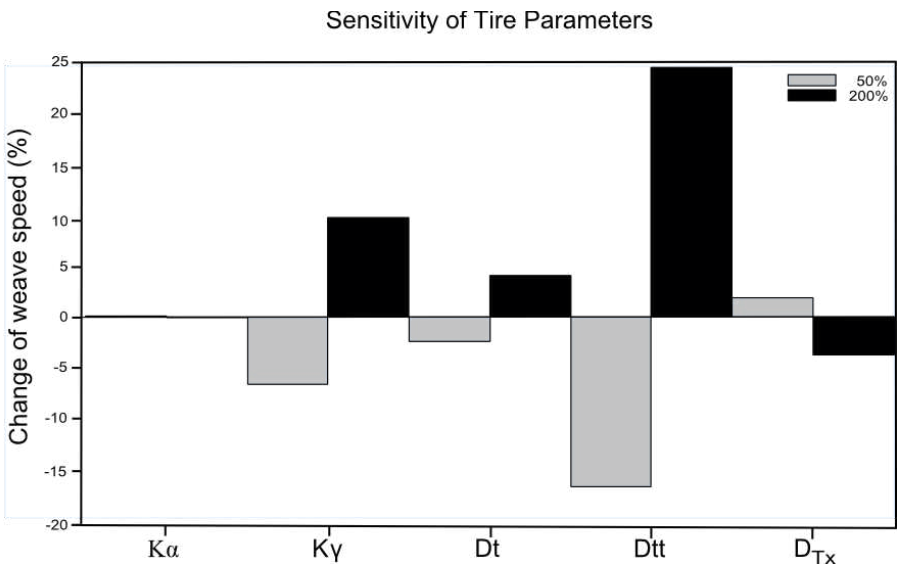

Figure 3.7. *Sensitivity of weave speed to tire parameters, it is expressed in percentage variation of the weave speed with respect to the nominal values.*

Regarding the tire torques, the twisting torque shows the largest effect on the weave stability. Parameter D_{TT} is the coefficient that determines the linear dependency of the twisting torque on the camber angle (see equation (A 2.16)); when it doubles, weave speed increases by about 25%. Self-aligning torque has a small effect on stability, when the trail factor (D_t) doubles, weave speed increases by 4%. Finally, the parameter D_{Tx}, which determines the linear dependency of the overturning torque on the camber angle, has a positive effect on weave stability, when it doubles the weave speed decreases by 3%.

Since the twisting torque strongly influences weave stability, this effect is further investigated and simulation results are presented in Figures 3.8a and b. Figure 3.8a shows the effect on the real part of the weave mode of the value of D_{TT} , which varies between 0% and 200% of the nominal value. The weave speed increases when the value of D_{TT} increases. Figure 3.8b deals with the large effect of D_{TT} on the yaw torque. The yaw torque is the summation of the twisting torque (a function of camber angle) and the self-aligning

torque (a function of sideslip angle), that are working in opposite directions. When the yaw torque is positive it generates a torque that tends to move the wheel along a trajectory with decreasing curvature.

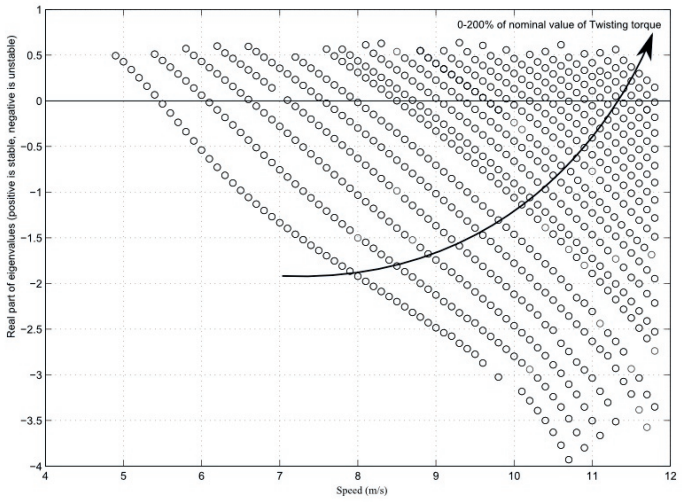

Figure 3.8(a). *Sensitivity of the eigenvalues of weave mode to the twisting torque: real parts.*

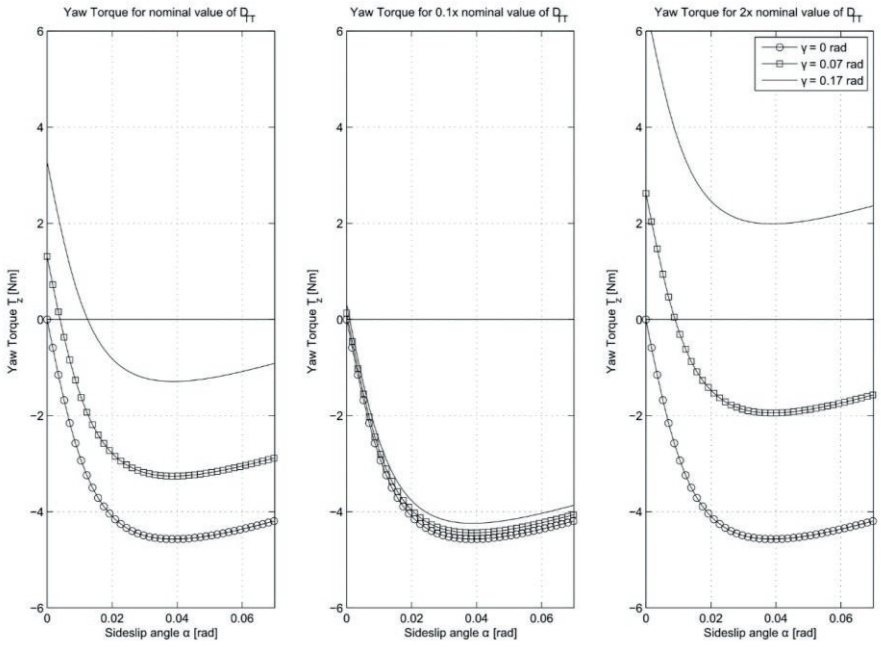

Figure 3.8(b). *Yaw torque against sideslip and camber angle, for the following three cases: 100%, 10% and 200% of the nominal value of D_{TT}.*

The plots show the yaw torque as a function of sideslip angle under three constant camber angles (0, 0.07 and 0.17 rad), for the following three cases: 100%, 10% and 200% of the nominal value of D_{TT}. A high value of D_{TT} causes a positive yaw torque for high camber and low sideslip angles. The yaw torque remains negative for a low D_{TT} value.

Up to now only the effect of tire properties on weave stability has been considered, since with the tire model (cases 6 and 7) capsize is always stable. It is worth highlighting that the simulations show that a low twisting torque (10% of the nominal value) is enough to stabilize the capsize mode.

3.3.4. Model sensitivity to rider properties

The rider's impedance around the steer influences the stability of the bicycle-rider model as was seen in Figure 3.4. Hence, it is interesting to study this effect in more depth.

In literature a large dispersion on the data of arm stiffness and damping found [66, 92], for this reason a parametric analysis is carried out.

Implementation of the realistic tire model alters the dynamics of the system, as is shown in the previous section. Therefore, first the model's sensitivity to the rider's impedance on the steer is presented considering stiff, non-slipping tires (case 4 and 5), then the combined effect of the tire model and the rider's impedance on the steer is considered (case 7).

With stiff and non-slipping tires, arm damping increases the weave speed and has no significant influence on the capsize mode (case 4). With stiff, non-slipping tires the system has a very small stability range between 3.65-4.20 m/s for a low value of arm stiffness (case 5 with Ka_t = 3.2 Nm/rad). For Ka_t > 4 Nm/rad the stability is destroyed by an unstable capsize mode.

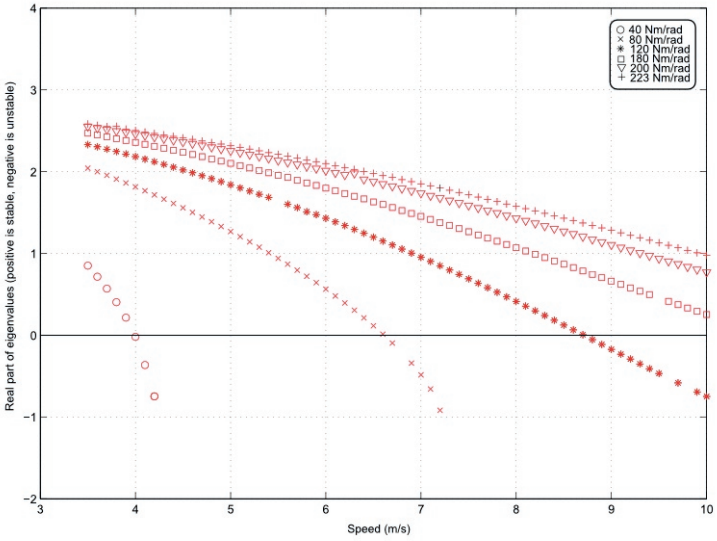

Figure 3.9. *Effect of arm stiffness on the capsize mode.*

a.

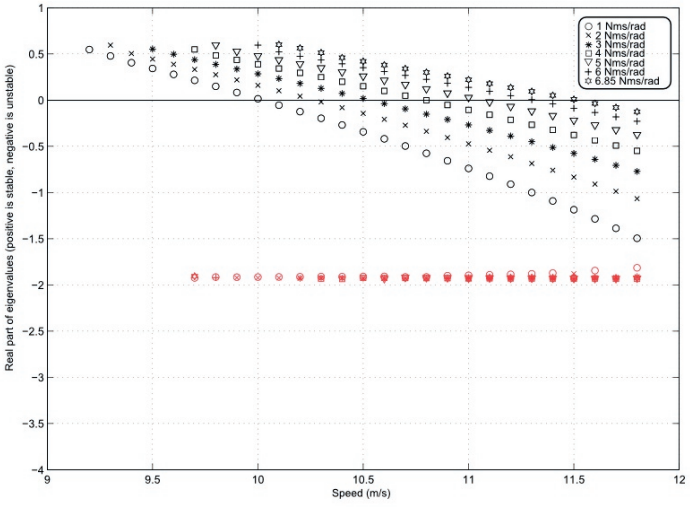

b.

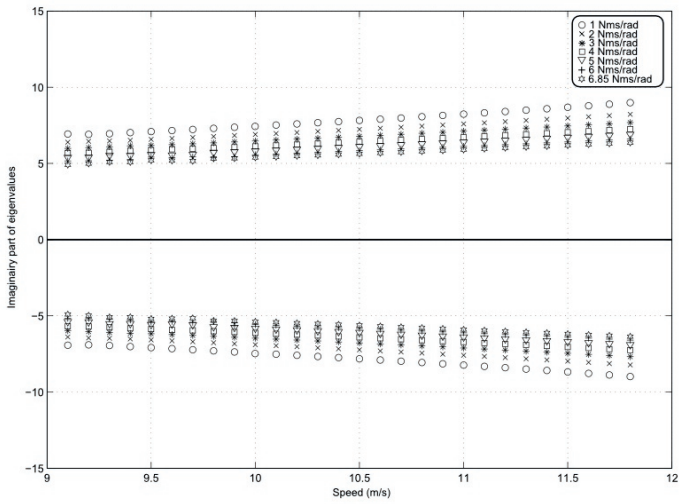

Figure 3.10. *Effect of arm damping on the weave mode:* ***a.*** *real parts,* ***b.*** *imaginary parts.*

Figure 3.9 deals with the combined effect of arm stiffness and tire dynamics, whereby arm damping is set to zero. Results indicate that the tire model causes the capsize mode to stabilize again at a certain forward speed and this speed becomes higher when arm stiffness increases. For comparison, it is worth remembering that in case 7 K_{at}*=5.0 Nm/rad*. Arm damping destabilizes the weave mode when the tire model is used (and arm stiffness is set to zero). Figure 3.10 shows that values of damping much larger than the one of case 7 (B_{at} *= 0.9 Nms/rad*) raise weave speed up to *11.5 m/s*.

3.4. Discussion

The good match of the results of the multibody dynamic simulation in Adams with the benchmark model results, points out that the time domain simulations and the system identification method are valid. A limitation of this method is that it negates the possibility of calculating the eigenvalues over the full speed range. An unstable weave or capsize mode results in a simulation time that is too short to enable fitting of the signals in the time domain. Therefore, only the identified model that fits the time domain signals well, is shown.

Destabilization of the weave mode and stabilization of the capsize mode by implementing the realistic tire model can be mainly attributed to the twisting torque. Sharp [54] showed

some effect of a linear tire model on the stability of a bicycle. Notable is that he did not incorporate the twisting torque in the tire model. In return, Plöchl et al. [91] and Klinger et al. [93] did include the twisting torque and found a significant effect of their tire model on the capsize and weave mode. In agreement with the results presented in this paper, they found that the capsize mode becomes stable and the weave mode significantly destabilizes by implementing the realistic tire model. The sensitivity study of tire parameters again confirms that the twisting torque is the main contributor. The twisting torque does not align the wheel, but it tends to move the cambered wheel along a trajectory with a decreasing curvature, due to a negative longitudinal slip at the inside of the contact patch and a positive longitudinal slip at the outside of the contact patch [99]. Together with the self-aligning torque (that works in opposite direction and tends to align the wheel) it represents the yaw torque (for each wheel). If the twisting torque coefficient (DTT) is high, the yaw torque is already positive for low sideslip and camber angles. As the weave stability is closely related to the steer-in-the-fall-mechanism, [28] the shift of the stable weave speed to higher forward speeds for an increased twisting torque, can be explained by the high positive value of the yaw torque that steers the bicycle into the fall too much. Furthermore, it was found that already a small twisting torque ensures a stable capsize mode. The capsize mode is usually a very slow motion and therefore easy to control for the rider. However, it determines the sign of the steering torque; at the capsize speed no extra steering torque is necessary for a steady forward motion (straight or during a steady turn).

The large influence of the twisting torque on stability was also found for motorcycle models [51]. It is worth highlighting that the influence is large especially at low speeds, which are the most important for bicycles.

In addition to the twisting torque, the camber stiffness has a large influence on the weave stability. Plöchl et al. [91] reported this as well. Cossalter et al. reported a high influence of the cornering stiffness for high speeds of racing motorcycles [56]. These findings cannot be extrapolated to low-speed behaviour of the bicycle. They also found that different tires and inflation pressure cause a large change in stability of a sport-touring motorcycle[100, 101]. For example using different tires may cause a change in weave damping ratio of 47% [56]. Similarly, Evangelou reported that the effect of tire inflation pressure is high for high speeds of motorcycles [100]. Contradictory, our study shows a small effect of different tires and inflation pressures on the bicycle stability. This fact can be explained considering the different properties of bicycle tires and the different ranges of variation of inflation pressure.

The effect of the vertical load on the tire properties is more prominent; when using the tire properties based on measurements with a higher nominal load, the weave mode stabilizes. This can be explained by the decrease in normalized twisting torque when increasing load, presented in [62]. This indicates that load-dependent tire properties are important and should be taken into account in dynamic bicycle models. Scaling factors are obtained from a small data set [62] and presented in the Appendix A.2.

Finally, it may be stated that tire properties change the dynamics of the bicycle to a large extent and that they should be taken into account in future dynamic bicycle models. Moore [86] performed experiments to identify the Whipple model and found some deficiencies, that might be attributed to the simplified tire-road contact model. To verify this more validation of dynamic bicycle models is needed.

Adding the passive joint properties of the bicycle's rider does not significantly change the dynamic properties, compared to the rigid rider model. This is in accordance with previous studies [54, 92]. However, modelling the rider's arms on the steer does drastically change the dynamic properties [92, 93]. In [92] it was reported that a small amount (25.7 Nm/rad) of passive arm stiffness is able to destroy the stability by making the steer-roll combination ineffective. However, in [92] tire dynamics were not considered and this significantly changes the influence of the rider's impedance on the handlebars. The tire model creates the opposite effect of the addition of arm stiffness and stabilizes the capsize mode for high speeds. This might be caused by the twisting torque that generates a yaw torque in the direction of the fall. In [93] the tire dynamics were considered, but a very small value of passive arm stiffness (3.2 Nm rad-1) was used in their basic hands-on model, therefore they did not find an unstable capsize mode.

Combining passive arm damping with the new tire model does not change the influence on the bicycle stability, compared to the addition of passive arm damping alone. In both cases a clear tendency of a decreased weave stability is seen. The capsize mode remains always stable, when the tire model is used together with passive arm damping.

3.5. Conclusion

In this paper, a new parameterized passive bicycle- rider model developed in the commercially available software package Adams is presented. This is a first step in the development of an advanced dynamic model to simulate problem scenarios of elderly cyclists. Several improvements of previous models are combined into one model: the addition of passive rider properties and tire dynamics. The simulations with this model

showed that a realistic tire model has a high influence on the stability of the system: the weave mode destabilizes and the capsize mode is always stable.

A sensitivity analysis on the influence of tire properties on the weave speed, showed that the twisting torque is the main contributor to the destabilization, followed by the camber stiffness. Tire inflation pressure has a small influence on the weave mode, in contrast to what was found for motorcycle tires. The tire properties are highly load-dependent, therefore bicycle tire models need to include load-dependent coefficients.

Extending the benchmark bicycle model with passive rider properties does not change the dynamics of the bicycle-rider system a lot when riding at a constant forward speed. Passive arm stiffness and damping however drastically change the dynamics: passive arm stiffness destabilizes the capsize mode. The tire model can however counteract this capsize instability.

Chapter 4

Cycling Strategies of Young and Older Cyclists

V. E. Bulsink, H. Kiewiet*, D. van de Belt, G.M. Bonnema, H.F.J.M. Koopman*
** these authors contributed equally to the work*

Human Movement Science (2016), Volume 46, April 2016, Pages 184–195

Abstract

This study concentrates on the cycling strategies of older cyclists (54-62 year olds) in comparison to young cyclists (20-30 year olds). While cycling in a safe laboratory set-up, controlled lateral perturbations are applied to the rear of the bicycle. Three possible strategies to keep balanced are analysed for a young and older aged group: steering, lateral trunk movement and outward knee movement. Older subjects appear to rely more on knee movement as a control mechanism than young subjects. Furthermore, the frequency domain analysis revealed that the older adults need more effort to counteract high frequency perturbations. Increased inter-individual variation for the older adults subject group suggests that this group can be seen as a transition group in terms of physical fitness. This explains their increased risk in single-sided bicycle accidents (i.e. accidents involving the cyclist only). Therefore, older cyclists could benefit from improving the self-stability of the bicycle at lower speeds.

4.1. Introduction

Bicycling is a common and popular mode of transport in the Netherlands. The Dutch citizens frequently use their bicycle for both recreational and transportation purposes; a quarter of all journeys are made by bicycle [102]. Thereby, there are more bicycles than residents in the Netherlands. A recent study reports an increase of single-sided bicycle accidents (i.e. accidents involving the cyclist only) for people aged over 55 [103]. This group has a higher risk of sustaining a bicycle fall as well as a sequential severe injury, compared to younger cyclists [12]. The increase in bicycle usage and the aging of the population partly explains the higher number of single-sided accidents amongst this group. Ormel et al. [104] showed that half of the single-sided bicycle accidents in the Netherlands are related to cycling behaviour. Despite the increased accompanying risks, continuing cycling contributes to a healthy and improved quality of life [90]. Therefore, it is important to improve the safety of older cyclists, to enable them to remain cycling for a longer time and thereby maintain their quality of life.

The study presented here, concentrates on the cycling strategies of older adult cyclists in comparison to younger adult cyclists. This possibly leads to insights in differences in control mechanisms used by older cyclists compared to young cyclists that could cause balance and control difficulties.

While bicycle dynamics is a widely studied subject [24, 28, 35] for many years, only few studies focused on the control strategies of the cyclist, and even less on those of older cyclists. The cyclist plays an important role when analysing the dynamics of the total system of the bicycle, the cyclist and the interaction with its environment. Motions of the cyclist's body relative to the bicycle in combination with the cyclist's steering actions determine the behaviour of the system.

An extensive overview of the state-of-the-art of bicycle and cyclist models and validation data is presented in the review paper by Schwab and Meijaard [105]. Several authors showed that steering is the primary control input for balancing [64, 65, 106]. However, Cain et al. found, that upper-body lean control is the dominant control strategy for balance performance for cycling on rollers [107]. Analogous to this theory, upper-body lean torque was successfully implemented in several cyclist control models [82, 108]. A third strategy was noted by Moore et al. who found that at low speeds, lateral knee movements are used as an additional control action [64, 65].

Recently, some experimental data of older cyclists was presented. Van den Ouden [78] found that the maximum value of the roll angle, the centripetal acceleration and the maximum steering angle velocity of older cyclists are larger compared to young cyclists. Dubbeldam et al. [109] investigated the coupling of cycling kinematics to physical and cognitive parameters for a large group of young (20-30 years, n=15) and older cyclists (> 65 years, n=33). They found that variation in roll angle is related to age, since the group of older cyclists showed more variation in the roll angle than the young group.

It is well-known that with aging, physiological changes take place in the human body, such as: decrease in muscle strength [110], decrease in joint velocities for knee extension and elbow flexion [111] and increased reaction times [112]. It is assumable that these factors play an important role in the increased accident risk for older cyclists. Furthermore, Vlakveld et al. reported that an increase of the accident risk of older cyclists on electric bicycles may be a result of a relatively higher mental workload for older cyclists (65+ years) compared to a middle adulthood reference group (30-45 years) [113].

The goal of this paper is to explore differences in cycling strategies, cycling kinematics and bicycle interaction forces of young and older cyclists in both time and frequency domain under unperturbed and perturbed conditions. Three balance strategies are investigated, namely steering, outward knee movement, and lateral trunk movement. To our knowledge, only one study used perturbations to assess the control mechanisms of the cyclists [89]. However, this study had a small sample size [n=2] and concentrated on the steering movement only; all other body motions with respect to the bicycle were restricted.

An extensive dataset has been generated with the use of a laboratory set-up, described in [114]. The data is collected at a cycling speed of 4 m/s to ensure active control strategies, based on the computer simulations performed by Schwab et al. They found that for a passive cyclist, the system is unstable for velocities below 4.8 m/s [22]. It is assumed that the characteristics of the instrumented bicycle used in this study are similar to the ones used by Schwab et al.

Based on the facts that additional control actions are more important at low speeds [65, 107] and that older adults have an increased delay of automatic balance-correcting muscular responses [115], the hypothesis in the present study is that older cyclists will revert more to additional balance strategies than young cyclists.

4.2. Methods

4.2.1 Experimental Set-up

The cycling tests were performed on an instrumented Trek L200 city bicycle with a straight handlebar. The laboratory setup was based on the experimental setup described in [114]. The front wheel rotated on a treadmill, preserving the tire-road contact and the ability to use steering corrections similar to cycling on a normal road. The rear wheel rotated on a roller bench, eliminating forward and backward motion of the bicycle. The roller bench was situated on a 6 D.O.F. Stewart platform, allowing controllable perturbations for identification purposes (see Figure 4.1).

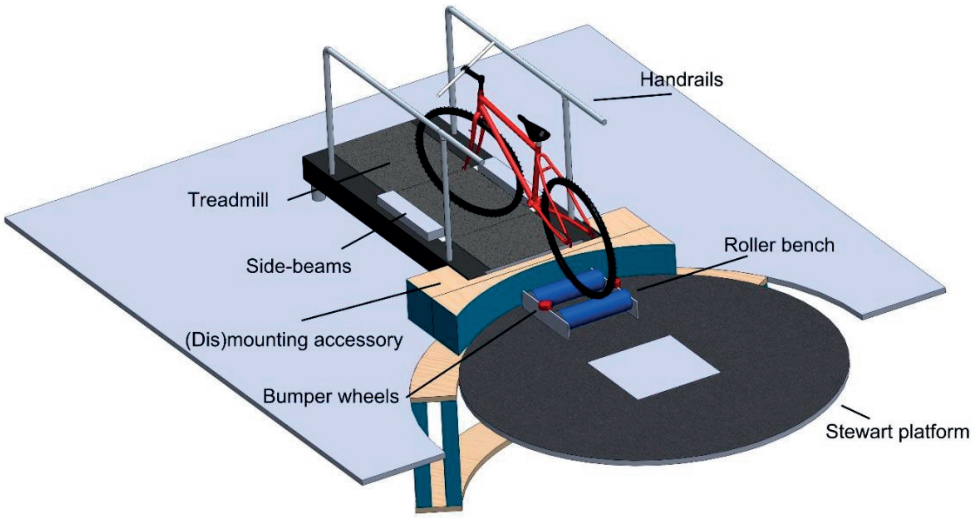

Figure 4.1. *Schematic representation of the experimental setup.*

The perturbation signal was a continuous multisine signal of 100 seconds (10 times a repetition of a signal of 10 seconds) sampled at 100 Hz. The power was distributed over a limited number of frequencies, namely: 0.4, 0.6, 0.8, 1.0, 1.2, 1.4, 1.8, 2.2, 2.6 and 3.0 Hz (see Figure 4.2). Due to the multiple sinusoids, the signal was unpredictable for the cyclists, thus preventing anticipation of the perturbation. The signal had a descending power spectrum, containing more power at the low frequencies. The maximum amplitude was set to 1.75 cm for young subjects. Pilot testing revealed difficulties for the older subject group with this amplitude. Therefore, the maximum amplitude was set to 1.25 cm for the older subject group. The results were adjusted for the magnitude of the amplitude.

Two measuring systems, an NI-USB 6218 data acquisition card (DAQ) and the marker-based Vicon motion capture system, were used to monitor the dynamics of the system. The system measured the kinematics of the complete system of bicycle, subject and Stewart platform, contact forces between subject and bicycle (handlebars and saddle), rear and front wheel velocity, pedal frequency and steering angle. The latter was measured with both systems; hence these signals were used for synchronization of the two measuring systems.

a. b.

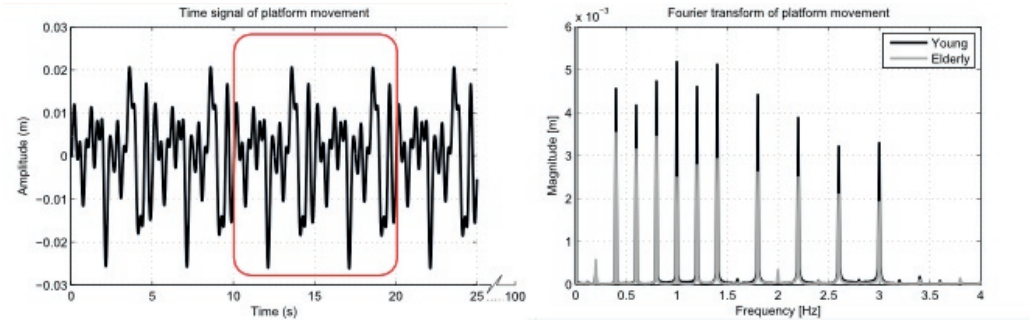

Figure 4.2. *Representation of the continuous lateral platform perturbation.* ***a.*** *Time signal of the platform movement. The perturbation signal is a continuous signal of 100 seconds (10 times a repetition of the same 10 seconds).* ***b.*** *The fourier transform of the platform movement, with power on 10 different frequencies and more power at low frequencies.*

Three 6 D.O.F. Force-Torque (FT) sensors were used to measure the contact forces between the bicycle and the cyclist. The FT sensors on the handlebar (left and right) and saddle tube were tailor made, pre-calibrated and equipped with integrated amplification (Sensix). An ambulant external power supply was connected to the FT sensors. Output was collected via the DAQ.

Numerous safety precautions secured the safety of the subject: emergency stops for the treadmill and Stewart platform, a safety harness, (dis)mounting accessory, handrails, bumper wheels on the roller bench and safety side-beams on the treadmill (see Figure 4.1 and 4.3)**.**

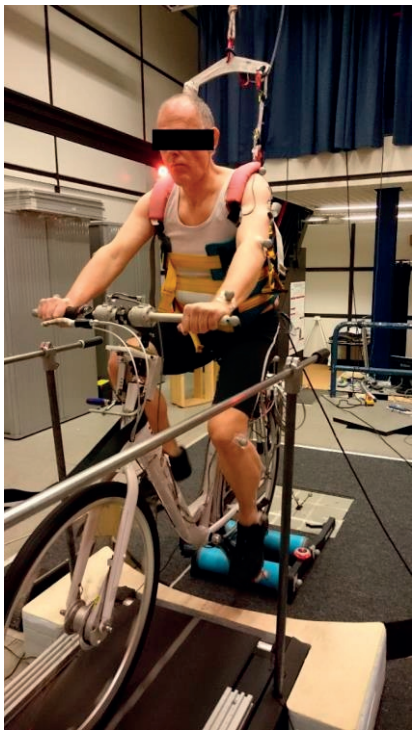

Figure 4.3. *Older subject during a cycling trial. Reflective 3D markers can be seen at bony landmarks on the leg and arm.*

4.2.2. Experiment Protocol

30 subjects participated in this study. Two groups were distinguished: one group containing 15 healthy young subjects (25.3±2.8 years, 68.4±8.5 kg, 1.75±0.17 m) and one group containing 15 healthy older subjects (58.1±2.1 years, 75.8±7.7kg, 1.79±0.07 m). Saddle height was adjusted individually to the subjects' comfort. All subjects gave their written informed consent and the study was approved by the local medical ethical committee.

The protocol started with a familiarization phase; the subjects practiced cycling on the laboratory set-up. Once they felt comfortable, the subjects were prepared for the actual experiments. Reflective markers were placed on bony landmarks to record 3D positions with the use of a motion capture system. The bony landmarks during cycling trials were defined as follows: the left -and right ulnar head, lateral humeral epicondyles, acromia, posterior superior iliac spine (psis), lateral femoral epicondyles and lateral malleoli (see Figure 4.3). Exclusively prior to the cycling trials, during a static stance trial, markers were also placed on the left and right anterior superior iliac spine (asis), medial femoral

epicondyles, medial malleoli, calcanei and first metatarsal bone. These markers were used to define segment lengths –and axes, and were removed during cycling trials.

The subjects were instructed to ride longitudinally on the treadmill without a predefined path. Since the front wheel velocity was driven by the treadmill and the rear wheel velocity by the subject, the subjects were imposed to a certain pedal frequency to ensure equal velocities of both wheels. The imposed pedal frequency was indicated with the use of a metronome. No subject experienced difficulties in hearing the metronome. The experiment was performed at different speeds. However, both groups performed the experiment at 4 m/s, so these trials were chosen to study the difference in cycling strategies between the two groups. Table 4.1. shows the imposed and mean measured pedal frequencies of both subject groups.

Table 4.1. *Imposed pedal frequency and mean measured pedal frequency of the young and elderly subject group, during unperturbed (U) and perturbed (P) cycling at 4 m/s.*

Group	Imposed PF (Hz)	Measured PF (Hz)	Offset (Hz)
Young (U)	0.87	0.89±0.03	+0.02
Young (P)	0.87	0.90±0.05	+0.03
Elderly (U)	0.87	0.93±0.07	+0.06
Elderly (P)	0.87	0.93±0.07	+0.06

4.2.3. Data Processing

The data was recorded with a sample frequency of 120 Hz. All data was pre-filtered with a second order Butterworth low pass filter with a cut-off frequency of 5 Hz. Thereafter the data was divided into two sections: unperturbed and perturbed cycling. To analyse to which extent the cyclist used the three control mechanisms (steering, trunk and knee movements), a time domain and a frequency domain analysis were performed. In sections 4.3.1.-4.3.3. the calculation of respectively the steering power, the knee power and the trunk movements will be described.

Steering Power

The steering power (P_s) is a measure that represents the amount of effort a cyclist uses to perform steering actions [107]. The steering power is defined as the steering torque multiplied by the steering angular velocity. It is therefore a convenient measure that summarizes steering kinematics and dynamics. The steering power can be positive or

negative. During positive steering power, the effort contributes to the steering movement. Negative steering power indicates that the effort counteracts the steering movement.

The steering torque (τ_s) exerted by the cyclist is defined as the torque around the steering axis (see Figure 4.4). The exerted forces and torques on the handlebars were measured with two aforementioned 6 DOF FT sensors (see Figure 4.4). Subsequently, the steering torque was calculated by rotating, translating and summating the measured forces and torques.

Figure 4.4. *3D model of the handlebars with force-torque sensors. Left and right handlebar forces and torques are measured at the origins of the coordinate systems. Subsequently, the steering torque is calculated around the steer axis.*

Knee Power

As mentioned before, the cyclist might use outward knee movements as a control mechanism. The knee power (P_k) is a measure that represents the effort which the cyclist uses to control the bicycle using knee movements. This knee movement is defined as an endo-exorotation around the axis that connects the hip with the ankle (called HA-axis), henceforth referred to as knee angle (θ_k). The HA-axis is defined from the hip joint to the midpoint between the lateral and medial malleolus (see Figure 4.5). The position of the hip joint was obtained by means of generic scaling formulas [116].

The knee power was calculated by multiplying the angular velocity around the HA-axis by the torque that is used to perform this movement. The torque was estimated as the summed moment of inertia of the upper and lower leg around the HA-axis multiplied by the angular acceleration around the HA-axis.

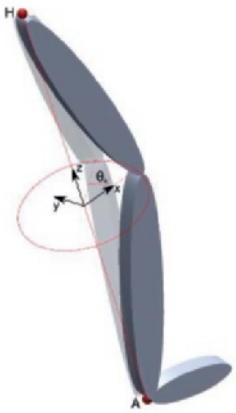

Figure 4.5. *Representation of the rotational HA-axis (Hip-Ankle axis). The axis is defined from the hip joint to the midpoint of the lateral and medial malleolus. The knee angle ϑ_k is defined as an angular displacement around the HA-axis.*

Trunk Movements

The third control mechanism is the trunk movement, which is represented by the kinematics of the upper-body and the contact forces at the saddle. 3D marker positions were expressed in the local reference frame of the bicycle, with the origin in the midpoint of the bottom bracket, the x-axis pointing forward, the z-axis upwards, and the y-axis to the left. Therefore, rotations of the body segments were with respect to the bicycle. The trunk motion is defined as three rotations of the trunk based on the marker data of the left and right psis and the acromia (lateral sway (ϑ_{ts}), flexion/extension (ϑ_{tfe}) and twist (ϑ_{tt}) respectively). The absolute forces measured by the saddle FT sensor are transformed to the bicycle reference frame and translated to the contact point between cyclist and saddle.

4.2.4. Data Analysis

Unpaired student t-tests were performed on several time-domain parameters to obtain a general insight in the difference in cycling behaviour between the two tested age groups during unperturbed cycling only. The tested parameters were: the mean and standard deviation of kinematic parameters of both the bicycle (steering, roll, yaw angles and their time derivatives) and cyclist (knee and trunk movements), and the interaction forces between the bicycle and the cyclist. Furthermore, the time delay between roll and steering angles were determined using a cross-correlation analysis. Likewise, the time delay between the exertion of a steering torque and the subsequent rotation around the steering axis has been calculated.

A test of between-subject effects has been performed on the different control strategies, age groups and cycling type (both unperturbed and perturbed) and their interactions. The variations of the angles of the balance strategies were normalized to the total summed angle. Also, a multiple comparison study has been performed to study the correlations between the normalized balance strategies.

Additionally, a frequency domain analysis was performed. The frequency content of the cyclist's control action at each perturbation frequency is given. This was calculated by dividing the Fourier transform of the particular signal by the Fourier transform of the lateral motion of the Stewart platform; for this lateral motion is representing the perturbation. In this way, the response is scaled to the actual perturbation signal, and differences in amplitude of the perturbation signal are compensated for, whereby a linear, time-invariant system is assumed. The response is given per cm lateral motion of the Stewart platform.

For statistical analysis of the response, the magnitudes were logarithmically transformed to ensure a normal distribution of the data. A repeated measures ANOVA has been conducted to test significant differences between the two groups and to test if this difference is frequency-dependent, i.e. effect of frequency and/or an interaction effect of the frequency and group. Furthermore, the interaction effect at each frequency was tested. To perform a repeated measured ANOVA, sphericity of the data was assumed and tested with Mauchly's sphericity test [117]. When the Mauchly's test was found to be significant, the assumption of sphericity was violated and the Greenhouse-Geisser method was used to test for within-subjects effects. All statistical tests were performed at the 5% significance level.

4.3. Results

4.3.1. Time domain

Statistical tests on time-domain parameters showed that most of the parameters were not significantly different between the young and older group. However, some differences were found.

The group of older adults showed a significant higher mean and standard deviation of the right knee angle ($p = 0.0054$ and $p = 0.0004$) and a significant lower mean lateral force on the right handlebar ($p = 0.0363$). Furthermore, the right knee power turned out to be significantly higher for young subjects ($p = 0.0042$).

Table 4.1 shows the imposed and measured pedal frequencies for both age groups during unperturbed and perturbed cycling. The old adult group showed an increased deviation from the imposed pedal frequency compared to the young adult subject group. Furthermore, a significant difference was found between the two age groups during unperturbed cycling (p=0.0277).

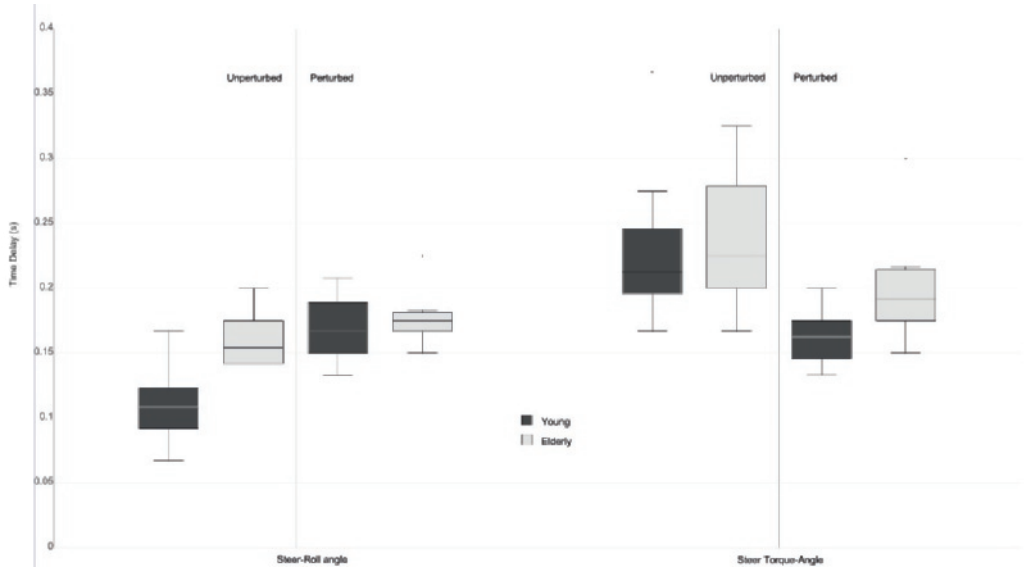

Figure 4.6. *Boxplot containing mean and standard deviations of the steer- and roll angle time delay (left) and the steer- angle and torque time delay (right) for older (dark grey) and young (light grey) subjects.*

Figure 4.6 shows the boxplots of the time delay between the steering angle and the steering torque and between the roll and steering angle respectively. The time delay between the steering angle and the steering torque was significant lower during perturbed cycling, compared to unperturbed cycling (p=0.0005) for the younger cyclists. The old adult cyclists did not show this significant change in time delay (p=0.2659). The differences between the two age groups were not significant for unperturbed and perturbed cycling (respectively p =0.5185 and p= 0.0760 p). The time delay between the roll and steering angle was significantly different between the two groups during unperturbed cycling at the 0.0012 p-level. During perturbed cycling, this difference was found not to be significant (p=0.2635).

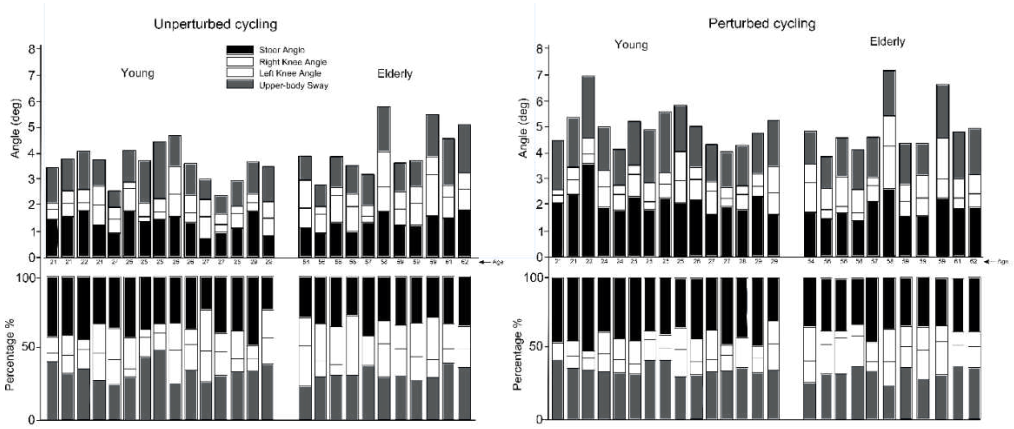

Figure 4.7. *Standard deviations of the angles of the three balance strategies during unperturbed and perturbed cycling: the steering angle, the upper-body sway and both knee angles. They are given as absolute values and as percentages of the total respective angle. On the left the young subjects are depicted and on the right the older subjects.*

Figure 4.7 presents the variation of the angles of the balance strategies for all subjects: steering angle, trunk sway and knee angles. The summation of the angles is a measure for the compensatory movement of the cyclist. The percentage of this total angle is given for each balance strategy. On the left the unperturbed cycling case is depicted, and on the right side the perturbed cycling case. The absolute variation of the angles for all balance strategies were higher during perturbed cycling, compared to the unperturbed cycling case. On the individual subject level, unperturbed and perturbed cycling showed the same pattern in balance strategies, e.g. large knee angles were used in both types of cycling. This indicates that every subject increases their balance strategies with a substantial amount when they were perturbed. The older adults made significantly more use of at least one of their knees. Remarkably, during unperturbed cycling this was mainly the right knee and during perturbed cycling this was mainly the left knee.

The test of between-subject effects on the scaled balance strategies showed a significant interaction of the cycling type and strategy at the p=0.0001 level. This indicates that the type of strategy differed when the subject was perturbed. The interaction between group and strategy was significant at the p=0.00001 level as well, pointing out that the different groups used different balance strategies. The interaction between the group, cycling type and strategy was not significant (p = 0.1039).

The multiple comparison study on the individual normalized balance strategies showed a correlation between the left and right knee balance strategy (Bonferroni test: p =0.87). No correlations were found between other balance strategies. Old adult cyclists showed an

increase in outward knee movement during perturbed cycling, compared cycling, whereas young adult cyclists showed a decrease.

4.3.2. Frequency domain

The transfers of the perturbation to the control mechanisms in the frequency domain are shown in Figure 4.8. Table 4.2 gives the results of the associated statistical tests. A significant difference between the two groups was found for all parameters in the frequency domain, except for the trunk sway. For all parameters there was a significant effect of the frequency on the response. A significant interaction effect between the frequency and the group was found for the response of the steering angle, the steering power, the trunk sway and the left knee angle. The results of Figure 4.8 illustrate that older adults showed more response in all control mechanisms per cm movement of the platform, except for the trunk sway (see Figure 4.8e).

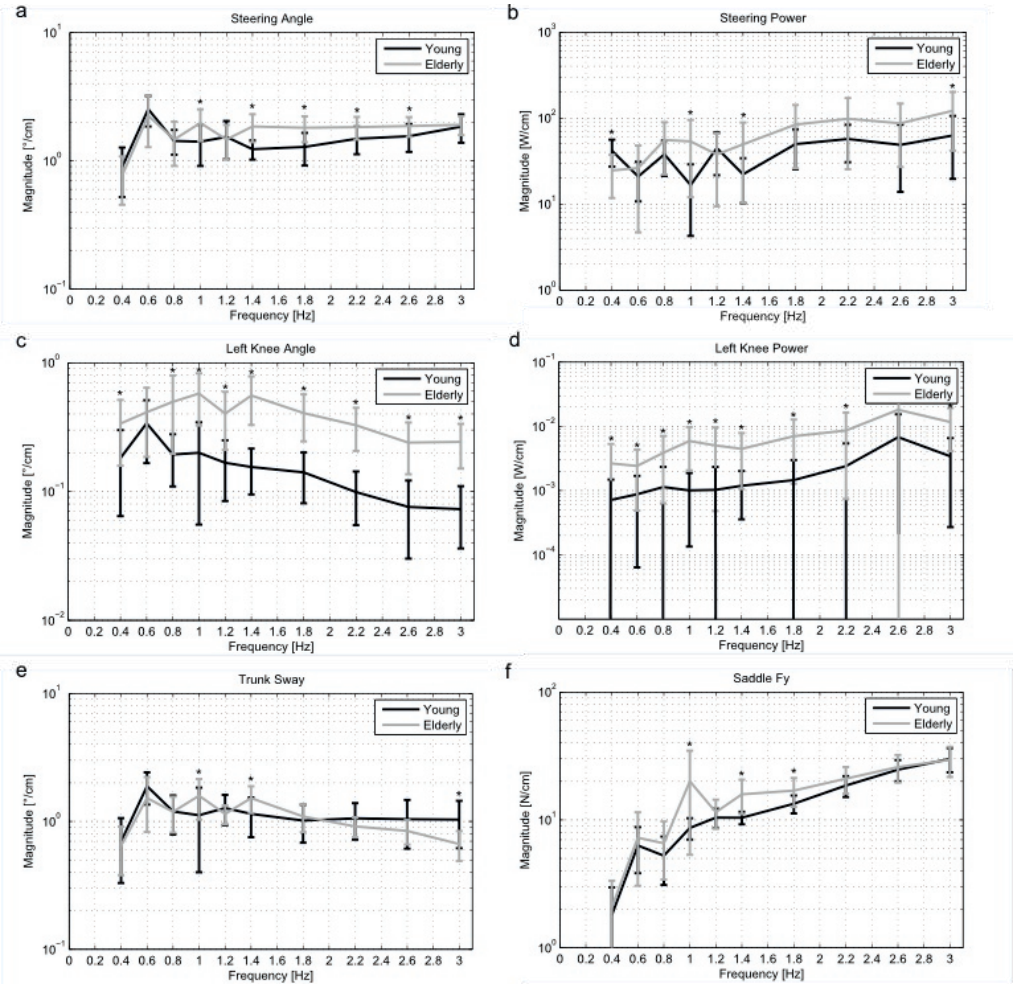

Figure 4.8. *Mean and standard deviation of the frequency response per cm movement of the platform at the perturbed frequencies of* ***(a)*** *the steering angle* ***(b)*** *the exerted steer power,* ***(c)*** *the left knee angle,* ***(d)*** *the left knee power,* ***(e)*** *the trunk sway and* ***(f)*** *the lateral saddle force. The black lines represent the younger subjects and the grey lines the older subjects. The asterisk marks a significant difference between the two groups at the specific frequency.*

On average older subjects showed a rather flat frequency response for the steering angle, compared to the young subjects. The frequency response was significantly different for higher frequencies (see Figure 4.8a). Looking at the frequency response of the steering power (see Figure 4.8b), it can be observed that the response increased at higher frequencies and that the difference between the groups was only significant at a few frequencies.

Table 4.2. *Results of the repeated measures ANOVA test, with frequency as within subject factor and age group as between subject factor. Significant outcomes are indicated with an asterix.*

Parameter	**Mauchly's test**	**Effect of frequency**		**Interaction effect frequency*group**		**Pairwise comparison**
	p-value	F(10,9)	p-value	F(10,9)	p-value	p-value
Steering Angle	0.000*	279.635	0.000*	3.134	0.026*	0.036*
Steering Power	0.000*	100.852	0.000*	5.823	0.000*	0.066*
Trunk Sway	0.000*	307.180	0.000*	3.826	0.010*	0.483
Left Knee Angle	0.000*	309.916	0.000*	3.663	0.006*	0.000*
Left Knee Power	0.503	128.383	0.000*	1.257	0.257	0.001*
Saddle Fy	0.000*	267.710	0.000*	0.800	0.512	0.038*

The outward left knee movement was applied in a limited frequency range (see Figure 4.8c). The older adults showed a significant higher response over the entire tested frequency range. Likewise, the frequency response of the left knee power was significantly higher for the older adult group for all tested frequencies (see Figure 4.8d). Moreover, high standard deviations were observed, and an increase of the response for higher frequencies.

Figure 4.8.e shows the frequency response of the trunk sway. A significant difference between the two groups was observed at a few frequencies only (1.0, 1.4 and 3 Hz). However, the graph shows that young subjects had a rather flat frequency response, whereas older subjects applied their control in a more limited frequency range.

The lateral saddle force frequency response graph has a similar shape for both groups. They applied this force in the higher frequency range. The older adult group showed a significant higher response at 1.0, 1.4 and 1.8 Hz, compared to the younger subjects. The

high standard deviation of the response of the older adult group at 1 Hz can be related to some subjects deviating from the imposed pedal frequency.

4.4. Discussion

Older subjects seemed to have more difficulties while cycling in the laboratory set-up than the younger subjects; they needed more time to familiarize themselves and they experienced more challenges when cycling at low speeds (< 3 m/s). Therefore, the protocol was adjusted for the older adult group, resulting in less cycling trials, exclusion of low speed trials and a decrease in the amplitude of the perturbation signal.

Older subjects deviated significantly more from the imposed pedal frequency than the younger subjects during unperturbed cycling. This suggests that older adults experience more difficulty in performing the cycling task together with an additional task ("use the imposed pedal frequency"). Studies involving dual-tasks also show that young adults show less decline in performance under dual motor and cognitive tasks than older adults [118]. Since participating in traffic demands dual motor and cognitive tasks, this will result in more difficulties for older cyclists.

Due to the narrow treadmill, the cycling experiment demanded higher concentration levels than cycling on a normal road. However, the cycling action itself is similar to normal cycling, as was shown by Kiewiet et al. They compared both cases with the use of computer simulations [114]. In general, cyclists under stationary conditions might experience visual distortion since the environment is motionless. However, no subject in this experiment indicated to experience difficulties with this phenomenon.

4.4.1. Time Domain

Statistical analysis of kinematic cycling parameters and control strategies did not show major age-related differences. Significant increase of the variation in roll, steering and sway angles and angular velocities found by Dubbeldam et al. for cyclists older than 65 years [109], were not observed for the older adult subject group tested in this study. This could be explained by the fact that the older adults were younger in this study (54-62 years) and therefore possibly physically more fit. However, during the experiments it stood out that they experienced some difficulties with riding on the experimental set-up at low speeds and that they needed more time to familiarize themselves. Furthermore, it was noticed that the older adult group had to put in more effort than the younger cyclists. Vlakveld et al. [113] found an increased mental workload for older cyclists. It is therefore reasonable

to belief that the higher mental workload might contribute to the increase of difficulties which the older adult cyclists experienced. It is also expected that larger/more differences between the two groups will be found when subjects are tested and analysed at cycling speeds below 4 m/s.

The two main age-related differences at 4 m/s were the increased usage of the outward knee movement and the increased time delay between roll and steering angles for the older cyclists. The time delays were determined using a cross-correlation analysis. Since bicycling is a closed loop system, it is difficult to add value to the magnitude of this time delay using this method because no distinction between the cause and effect can be made [15]. However, it showed a difference between the two groups. The increased usage of the outward knee movement for control purposes indicates that older adults already switch to additional control strategies at a speed of 4 m/s, while it is expected that young subjects tend to use more knee movements at lower speeds.

The between-subjects test on the scaled balance strategies again did not reveal major differences between the two age groups. The group, strategy, cycling type-interaction-effect was not statistically significant. However, the low p-value give reason to belief that differences were likely to be present. Larger group samples might reveal significant differences. The group-strategy interaction effect was significant and can be explained by the different outward knee strategies found for each group.

4.4.2. Frequency Domain

The frequency domain analysis proved to be a useful addition to the time domain analysis. While in the time domain few differences between the two age groups were found, the frequency domain analysis revealed significant differences between the young and older cyclists. For instance, the standard deviation of the steering angle was similar for both groups in the time domain, while the frequency response of the steering angle was not. This highlights the contribution of this dataset and the inclusion of continuous perturbations.

The older cyclists showed higher steering angles and steering power response than young cyclists, especially in the higher frequency range (1.4-3 Hz). High-frequent disturbances need quick responses to prevent an unbalanced situation. Whereas young cyclists showed a decreased steering torque to steering angle time delay when imposed to perturbed circumstances, the older adult cyclists did not. A decrease in this aforementioned time delay may indicate a more intense response to the perturbation, allowing only smaller

steering corrections. Finally, the increased time delay between the roll and steering angle could explain the higher steering angles and steering power of older cyclists as well. Klitgaard et al. observed a decrease in elbow flexion velocity to be age related [111]. As flexion and extension are the prime movers for active steering this could explain the increased time delay for older cyclists.

Regarding the outward knee movement, the results from the present study confirm that under perturbed conditions the knee movement is used as a control strategy. Previously, it was already suggested by Moore et al. that outward knee movement is used for bicycle control at low speed [119]. High frequency movements require more effort (knee power) than low frequency movements. This might explain why high frequency knee movements are not beneficial for bicycle control and that outward knee movements are applied within a limited frequency range. Furthermore, it appears that the outward knee movement is used more actively by older cyclists at the perturbed frequencies. This suggests that older cyclists rely more on outward knee movements than young cyclists at a speed of 4 m/s.

Previous studies showed that steering is the primary control input conducted by the cyclist, and trunk sway was only observed in the pedalling frequency [105, 119]. However, in the present study the experiments with perturbations show that the trunk sway is used at all perturbed frequencies by young cyclists. Older cyclists, on the other hand, seem to apply their trunk sway control within a limited frequency range only. Extrapolating these results for higher frequencies may lead to an increased difference between the two groups. This could imply an increase of trunk stiffness with age. This is consistent with Allum et al., who showed that the trunk stiffness in lateral motion is age-related [115]. Although, the results suggest that the trunk sway is used as an active control strategy, this could only be confirmed by measuring muscle activities of trunk muscles.

The reduced ability of the lateral trunk movement may play an important role in the additional use of the outward knee movement and increased steering control as balance strategies found for the older cyclists.

Cain et al. found that trunk sway is the dominant control strategy for balance performance for riding on rollers [107]. He also reported that experienced cyclists use more trunk sway than steering and less steering power to maintain balance, compared to less experienced cyclists (especially at higher speeds). The same relation is found for younger cyclists with respect to older cyclists: younger cyclists use less steering power, but seem to use more trunk sway.

4.4.3. Cyclist Behavioural Perspective

With the time domain analysis, we showed that in the present study the older adult group (54-62 years) does not decline much in their bicycling performance. As long as they are able to cycle well, they perform the same as younger cyclists. It was observed that in general the inter-subject variability was higher for the older adult group. This suggests that from the age of 55 some people show a decline in cycling performance, while others do not. A previous study showed indeed an increased risk in single-sided bicycle accidents for people of the age 55 and over in the Netherlands [103] .

The addition of the continuous multisine perturbation provided valuable insight into the extent of balance strategies under perturbed conditions. Whereas outward knee and trunk movement are identified as secondary balance strategies during unperturbed cycling, they seem to become active contributors to bicycle balance during perturbed cycling. Unexpected perturbations are an important factor for single-sided bicycle accidents, since half of single-sided bicycle accidents are cycling behaviour related [104]. If unbalanced, often high frequent corrections are desired to restore balance. The results suggest that older adults need more effort to counteract the perturbations (especially at high frequencies) and that they rely on different balance strategies compared to young adults. They use more additional knee movements at low speeds than younger cyclists. Young cyclist eventually revert to more additional knee movement for control as well, as shown by Moore et al [119], but at lower speeds (lower than 4 m/s).

Design of safer bicycles could be a solution to counteract the increased risk of cyclists aged over 55. Especially, a bicycle with improved intrinsic stability at low speed could lead to a reduction of the need of additional balance strategies of older cyclists. Such a bicycle, with an optimized frame geometry and the subsequent low forward speed to accomplish self-stability, proved to be safer and more supportive for older cyclists [120] .

4.5. Conclusion

We presented an extensive dataset of a comparison of the cycling strategies between young and older cyclists. For the first time continuous, controlled perturbations were used to assess the balance control of cyclists.

Older subjects appear to revert more to additional outward knee movement as a control mechanism than younger subjects, confirming the initial hypothesis. The increased inter-individual variation for the older adult group suggests that this group can be seen as a

transition group in terms of physical fitness, which possibly explains their increased risk in single-sided bicycle accidents. Subsequently, older cyclists are likely to need more effort to restore from perturbations.

These results contribute to the insights of balance and control difficulties of older cyclists. Since old adults need more effort to restore from perturbations, the design of a bicycle with a higher intrinsic stability will be beneficial for elderly cyclists.

Chapter 5

Validation of a Bicycle-Cyclist Interaction Model

Using measured kinematics and contact forces

V.E. Bulsink, D. van de Belt, G.M. Bonnema, H.F.J.M. Koopman

Submitted to Transactions of Biomedical Engineering

Abstract

Validation of more complex biomechanical cyclist models is needed to upgrade existing bicycle-cyclist multi-body models. The validation of bicycle-cyclist models is challenging due to the complex 3D-interactions between the bicycle and the cyclist. Therefore, this paper focuses on the measurement of 3D kinematics and bicycle-cyclist contact forces (6 DoF) and the validation of an advanced bicycle-cyclist multi-body model with the use of these measured data. The cycling experiments were performed on a laboratory set-up at four different speeds.

Measured pedal forces were in agreement with previous published data. The presented forces on the handlebars and saddle can lead to improved bicycle-cyclist interaction models.

During the validation process, resultant forces of 8-19% of the maximum force magnitude were used to ensure dynamic consistency of the model. Accurately measuring the pedal forces and increased subject-specific modelling could increase the validity of the model.

5.1. Introduction

Development of accurate and realistic bicycle-cyclist mathematical models is important to understand and predict the behaviour and stability of the bicycle-cyclist system but also as a useful tool for designing and developing safer bicycles [35]. Existing bicycle dynamical models have been upgraded with realistic tire-road contact models [54, 93, 121] and have been experimentally verified [27, 62], in contrast to models that also include a cyclist. The validation of these models is challenging due to the complex 3D interactions between cyclist and bicycle, the large number of mechanical degrees of freedom and the possibility for the cyclist to actively influence the system by steering. In other words, the mechanical properties of the cyclist are not constant. This paper focuses on the measurement of 3D kinematics and bicycle-cyclist contact forces and torques and the validation of an advanced bicycle-cyclist multi-body model with the use of this measured data.

Several cyclist/motorcyclist models exist in literature, varying from simple to very complex models, depending on the application of the model. Cangley [122] developed a detailed multi-body model of a cyclist on a racing bicycle and validated it against experiments, however this was related to the performance in competitive cycling. Doria and Tognazzo [92] experimentally studied the passive response of the body of the cyclist and developed biomechanical models of the cyclist coupled with the bicycle to perform open-loop stability analysis. A similar approach was used by Schwab et al. [22] who studied different poses of the cyclist with an open-loop passive cyclist model, without adding extra degrees of freedom (DOF) for the cyclist with respect to the bicycle model. Moore developed a bicycle model including a cyclist control model using four DOF and steering torque as the input [86]. Wang et al. recently experimentally validated their dynamical bicycle and cyclist control model with steering angle and upper-body lean torque as inputs [123]. Another validated bicycle model was presented by Cain and Perkins who compared a steady turning model with experiments [124]. They showed that the cyclist position on the saddle influences the steering torque, which highlights the importance of including body movements in bicycle-cyclist multi-body models.

In general, motorcyclist multi-body models are more complex than cyclist multi-body models. Consequently, few validated biomechanical motorcyclist models appear in literature. Capitani [125] compared a multi-body model with experimental data during several motorcycle manoeuvres and reported that differences between the model and experiment were due to the fact that the movements of the driver were not taken into

account. Cossalter et al. as well as Schmitt et al. developed a complex motorcyclist multi-body model, but did not experimentally validate it [126, 127].

Validation of more complex biomechanical cyclist models is needed to upgrade existing bicycle-cyclist multi-body models. Therefore, a large data set is generated from laboratory cycling experiments with a total of 30 participants [114, 128]. Bicycle and cyclist kinematics and contact forces and torques were measured during cycling trials at different cycling speeds. The measured contact forces and torques give insight in the complex 3D interaction between the bicycle and the cyclist and are used to validate a multi-body model of the bicycle dynamics and biomechanics of the cyclist developed in the commercially available software Adams [121].

The biomechanical cyclist model presented in [121] is adapted and used in this study. The model consists of six rigid bodies, enabling modelling of the pedalling movement, outward knee movements and trunk movements with respect to the bicycle. Connors and Hubbard found that the pedalling movement of the legs significantly change the steering control effort of a recumbent bicycle [129], a similar effect is expected for the control of a 'regular' bicycle. Therefore, the pedalling movement is included in the model, in contrast to the previous version of the model [121].

Furthermore, three balance control strategies are assumed, namely the steering action, the outward knee movement and trunk movements. These body movements are for the first time combined in a multi-body bicycle-cyclist model and compared to experimental data of cyclists of different age and physique.

The inputs for the validation process are the multi-body model of the cyclist, measured kinematics and contact forces. To ensure dynamical consistency of the model and the experimental data, a 6 DoF residual force is applied to the centre of mass (CoM) of the cyclist model. The magnitude of the residual force is used as the outcome measure of the validation process.

The goal of this paper is firstly to present measured bicycle-cyclist 3D interaction forces, to increase the understanding of the complex 3D interactions between the bicycle and the cyclist. Furthermore, the goal is to validate the bicycle-cyclist interaction model with measured 3D kinematics and interaction forces.

5.2. Methods

5.2.1. Experiments

The cycling experiments were performed in a laboratory set-up, described in [128] and [114]. The front wheel rotated on a treadmill, while the rear wheel was situated on rollers. The treadmill was set at a pre-defined speed, while the subject was instructed to keep a certain pedal frequency to ensure equal rotational speeds of both wheels. A large data set of kinematic data and measured contact forces and torques was generated, with a total of 30 participants for various research purposes. Contact forces were measured for a subset of 10 participants. The kinematic data and contact forces are made available as supplementary material to this paper.

For the validation process a subset of the kinematic data and the measured bicycle-cyclist contact forces of three subjects were extensively analyzed. The three subjects were all in their mid-twenties, but differed in physique. Subject 1 was a male of 1.97m length and weighted 78 kg, subject 2 was also a male of 1.81m length and weighted 71 kg. Subject 3 was a female of 1.64m length and had a weight of 63 kg.

Kinematics of the cyclist and bicycle were measured using reflective markers and a 3D motion capture system (Vicon). In addition, the steering angle was measured with a rotary potentiometer and the rotational speeds of the wheels and the pedals were measured with Hall sensors. Contact forces and torques between the bicycle and the cyclist were measured by five force-torque sensors in six DOF. The force-torque sensors on the handlebars and saddle tube (Sensix) and the pedals (AMti) were tailor-made, amplified and pre-calibrated.

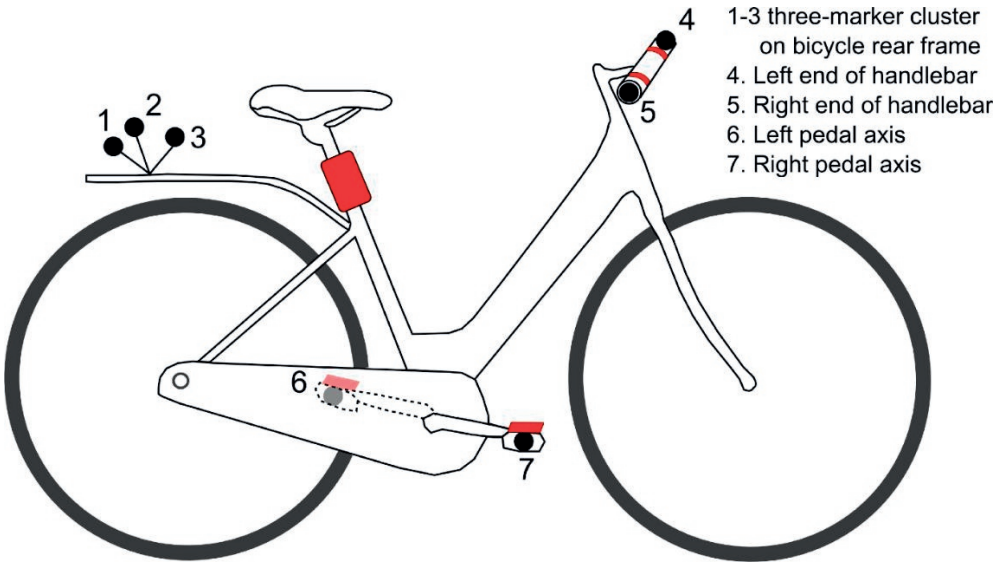

Figure 5.1. *Marker positions on the bicycle and position of the contact force-torque sensors on the left and right pedal, the saddle tube and the left and right handlebar (in red).*

Figure 5.1 shows the instrumented bicycle (a Trek L200 city bicycle) with the positions of the reflective markers and the contact force-torque sensors (in red). The roll, yaw and pitch angles of the bicycle were calculated using the three-marker cluster on the rear frame of the bicycle. From the 3D positions of the three markers a quaternion was estimated, that represents rotation information as a four-component vector q = (q0; q1; q2; q3). Horn's method for absolute orientation estimation using quaternions [130] was used to estimate a rotation matrix from the three marker positions.

Table 5.1. *The trials that were performed during the experiment*

Trials	Description
Static bicycle trial	A measurement of the bicycle standing static in a bicycle stance to define the offsets of the force-torque sensors and to calibrate the bicycle angles.
Static human stance trial	A static stance measurement of the human subject. The marker positions of this trial were used to scale the computer model of the cyclist.
Static human-bicycle trial	A measurement of the human subject sitting on the bicycle on a bicycle stance to define the positions of the force sensors relative to the cyclist model.
Cycling trials at 2, 3, 4 and 7 m/s	The subject cycles on the laboratory set-up at a pre-defined speed. The imposed pedal frequency was presented to the subject by a metronome.

Prior to the cycling trials a static bicycle trial, a static human stance trial and a static human-bicycle trial were performed, see Table 5.1. Figure 5.2 shows the positions of the markers on the human subject during the static stance measurement. These positions were used to scale the mechanical properties (dimensions and mass distribution estimates) of the cyclist computer model. Next, a static human-bicycle trial was performed, whereby the cyclist was sitting on the bicycle (on a bicycle stance) in a static position.

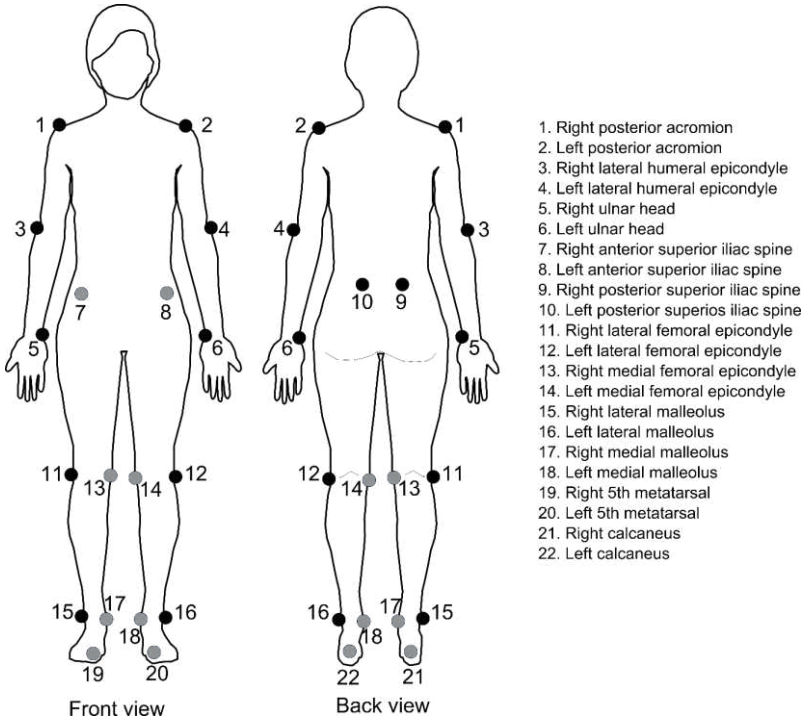

Figure 5.2. *Marker positions on the human subjects during the static stance measurement. Markers 7, 8, 13, 14, 17, 18, 19, 20, 21 and 22 (displayed in grey) were removed during cycling trials.*

5.2.2. Model Description

The multi-body model of the bicycle and cyclist was developed with the commercial software package Adams and is based on the model described in [121]. The bicycle model contains five parts: the rear frame, the front frame, the two wheels and the crank system. A revolute joint connects the rear frame and front frame at the steering axis. Both wheels are interconnected to the frame at the wheel axis by a revolute joint as well. The crank system is likewise connected to the rear frame at the bottom bracket position. The geometry and mass properties of the instrumented bicycle were measured using techniques described in [74, 131] and are given in the Appendix A1 (Bicycle 2). The tire-

road contact was modeled with the Pacejka motorcycle tire model, see [121] for a detailed description.

The cyclist model contains six rigid parts; the HAT-segment (combining the head, arms and trunk), the pelvis, the left and right upper leg and the left and right lower leg. The mass of the feet is added to the crank system. The HAT-segment has three rotational DOF and is connected to the pelvis with a spherical joint at the L4L5 vertebral joint position. The upper legs are connected to the pelvis at the position of the hip joint with a spherical joint. The knee joints have one rotational DOF. The HAT-segment is interconnected at the shoulder positions with the handlebars by two linear spring-dampers that simulate the arms.

Table 5.2. *Definition of the local reference frames of the cyclist multi-body model*

Body part	Location of LRF	Direction of LRF
Left Upper Leg	Mid of knee markers	z upwards to Left Hip, y to Lateral Epicondyle
Right Upper Leg	Mid of knee markers	z upwards to Right Hip, y to Medial Epicondyle
Left Lower Leg	Mid of ankle markers	z upwards to Left Knee, y to Lateral Malleolus
Right Lower Leg	Mid of ankle markers	z upwards to Left Knee, y to Lateral Malleolus
Pelvis	Mid between hip joint centers (HJC)	x in direction of Mid-ASIS to Mid-PSIS, y to right hip
HAT	L4L5 vertebral joint	z upwards, orientation same as pelvis LRF

Local reference frames for each modeled body part were based on the marker positions of the static stance measurement, see Table 5.2 for the positions and directions. The position of the hip joint centers and the L4L5 vertebral joint were estimated using scaling techniques [116], see the Appendix A.3. for the definitions. The dimensions of the body parts were also obtained from the marker positions of the static stance measurement. Center of Mass (CoM) positions and mass properties of the body parts were scaled to the dimensions of the body parts using linear regression formula's [96], see the Appendix A3.

5.2.3. Model validation

The cyclist computer model was validated with the measured kinematics and bicycle-cyclist contact forces and torques. A tracking agent in the CoM of the cyclist model was added to compensate for model inaccuracies and measurement errors. The tracking agent applied 6

DoF guiding forces based on the motion of the CoM. The magnitude of the guiding forces was used as a measure for the agreement between the model and the experiments.

Data Preparation

The motion capture data and measured contact forces and torques data were prepared in Matlab to be suitable for loading into the Adams software with the use of splines. The data were recorded with a sample frequency of 120 Hz and filtered with a second-order Butterworth low-pass filter with a cut-off frequency of 5 Hz.

Motion agents were created, that consist of a marker point rigidly attached to the cyclist model, a massless part (representing the model marker) driven by the motion capture trajectory data and a bushing that connects these two points. The distance between the marker points and the model markers were minimized by the bushings. Scaling factors were used to change the stiffness and damping values of the bushings to make some markers more important than other. The scaling factors of the bushings were set in such a way that the distance between the marker points and the model markers were within 1 cm.

Step 1: Scaling of the cyclist model - the LRF's of the body parts were based on the 3D positions of the markers of the static human stance trial. The lengths and CoM positions of the body parts were updated according to the locations and orientations of the LRF's. The masses and moments of inertia of the body parts were calculated using scaling formulae's based on the total height and mass of the subject [96].

Step 2: Positioning of the cyclist model on the bicycle model – The position of the cyclist and bicycle model were based on the static human-bicycle measurement using motion agents. The positions and orientations of the force sensors were known in the bicycle LRF and were created on the cyclist model on the same positions.

Step 3: Inverse kinematics – The human model was driven by the model markers to match the positions of the cycling trial, using the motion agents. The joint angles and locations and orientations of the contact points and CoM of the cyclist model were captured and saved.

Step 4: Model simulation – Measured contact forces and torques were given as inputs at the saved locations and orientations of the contact points in the cyclist model. PD-controllers were used to produce joint torques to ensure that the previously saved joint angles were reproduced at the human model joints. A tracking agent in the CoM ($F_{residual}$ in 6 DOF) of the human model was applied to achieve dynamic consistency between motion and applied forces.

A tool was built in Adams to automatically run the validation process step by step.

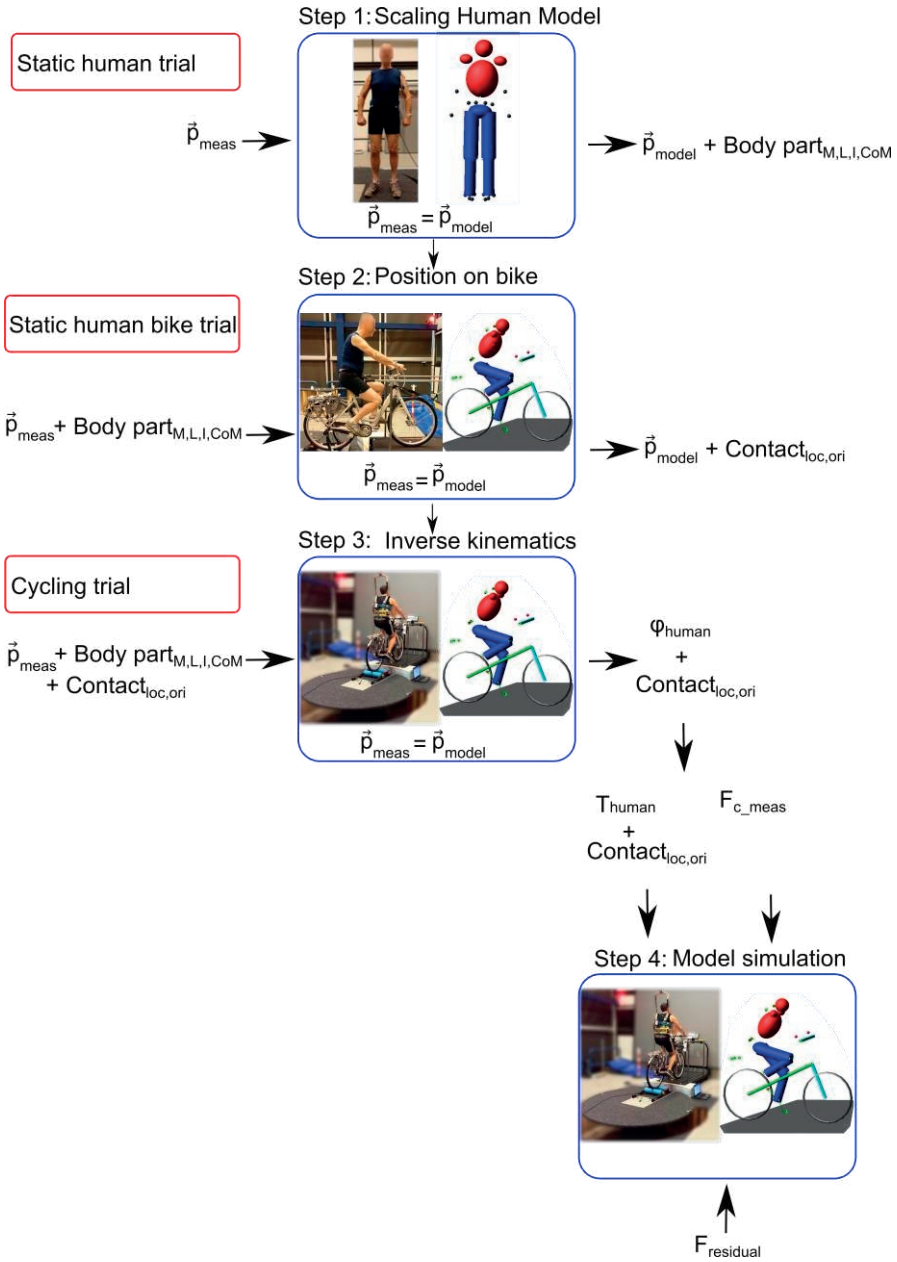

Figure 5.3. *Validation steps. Step 1: scaling of the human model, input: positions of the measured markers of the static human trial and subject mass and length, output: positions of the model markers and mass, length, inertia, CoM of the body parts. Step 2: positioning of the human model on the bicycle model, input: positions of the measured markers of the static human-bicycle trial and properties of the body parts (from step 1), output: positions of the model markers and the contact points. Step 3: Inverse kinematics, Step 4: Model simulation with the measured contact forces applied on the contact points of the human model, human joint torques and a residual force in the CoM.*

5.2.4. Pedal angle estimation

The angle of the pedals relative to the bicycle coordinate system was not measured, and therefore unknown. Large errors can appear when these angles are ignored and the pedal forces are applied in the local reference frame of the bicycle. Hence, it is important to estimate the actual LRF's of the pedals, to calculate the actual pedal forces in the LRF of the bicycle.

The pedal angles were estimated with a sinus function based on data from literature [132]. The estimated left and right pedal angle were represented with seven parameters: the frequency *f* equals the pedal frequency, the amplitudes *A* (A_1 for the left and A_2 for the right pedal angle), the time shifts B_1 and B_2 and the offsets C_1 and C_2. Figure 5.4 shows an example of the estimated pedal angles for one pedal cycle during a cycling trial and presents the parameters describing it.

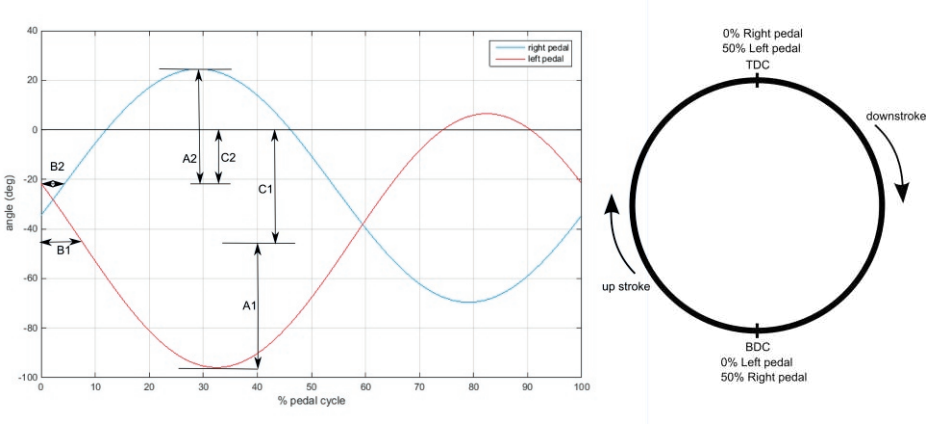

Figure 5.4. *Left: An example of an estimated right and left pedal angle, with A1 – the amplitude of the left pedal, B1- the time shift of the left pedal and C1 – the offset of the left pedal. A2, B2 and C2 represent the same parameters for the right pedal. Right: The pedal cycle with TDC – Top Dead Centre and BDC – Bottom Dead Centre.*

To estimate the pedal forces in the LRF of the bicycle, the following objective function was solved in Matlab for each pedal cycle, using the optimisation method *lsqnonlin*.

$$F = MIN\left(\sqrt{(Fx_r)^2 + (Fz_r)^2}\right) \quad (5.1)$$

Fx_r and Fz_r represent the residual forces in respectively the x and z direction that equals the summation of the forces on the seat, the left handlebar (LHB) and right handlebar (RHB) in these directions:

$$Fx_r = Fx_{seat} + Fx_{LHB} + Fx_{RHB} + Fx_{rp\_b} \pm Fx_{lp\_b} \tag{5.2}$$

$$Fz_r = Fz_{seat} + Fz_{LHB} + Fz_{RHB} + Fz_{rp\_b} + Fz_{lp\_b} - mg \tag{5.3}$$

Fx_{rp_b}, Fx_{lp_b}, Fz_{rp_b} and Fz_{lp_b} represent the right and left pedal forces in the x and z direction, given in the LRF of the bicycle. These are related to the measured pedal forces, which were measured in the LRF of the pedal, in the following way:

$$\begin{matrix} Fx_b \\ Fz_b \end{matrix} = \begin{matrix} Fx_p \\ Fz_p \end{matrix} \cdot \begin{bmatrix} \cos\varphi & -\sin\varphi \\ \sin\varphi & \cos\varphi \end{bmatrix} \tag{5.4}$$

φ is the pedal angle that is assumed to be a sinusoidal function: $\varphi = A\sin(2\pi ft + B) + C$

5.3. Results

The measured contact forces between the bicycle and cyclist are shown in section 5.3.1, the estimated pedal angles in section 5.3.2, and section 5.3.3 presents the model validation results.

5.3.1. Measured contact forces

The mean measured contact forces between the bicycle and the cyclist of 10 subjects are displayed in Figure 5.5, to provide insight in the 3D interaction between the cyclist and the bicycle. The mean and standard deviation of the longitudinal (*Fx*), lateral (*Fy*) and vertical (*Fz*) contact forces scaled to the subject's mass are given as a function of the pedal cycle for four different cycling speeds. The pedal cycle is given in percentages based on the right pedal, starting from the TDC (see Figure 5.4). The displayed forces represent the forces that the cyclist applied to the bicycle. The subjects were 24±2.0 year old, 66.5±7.0 kg and 1.72±0.20 m.

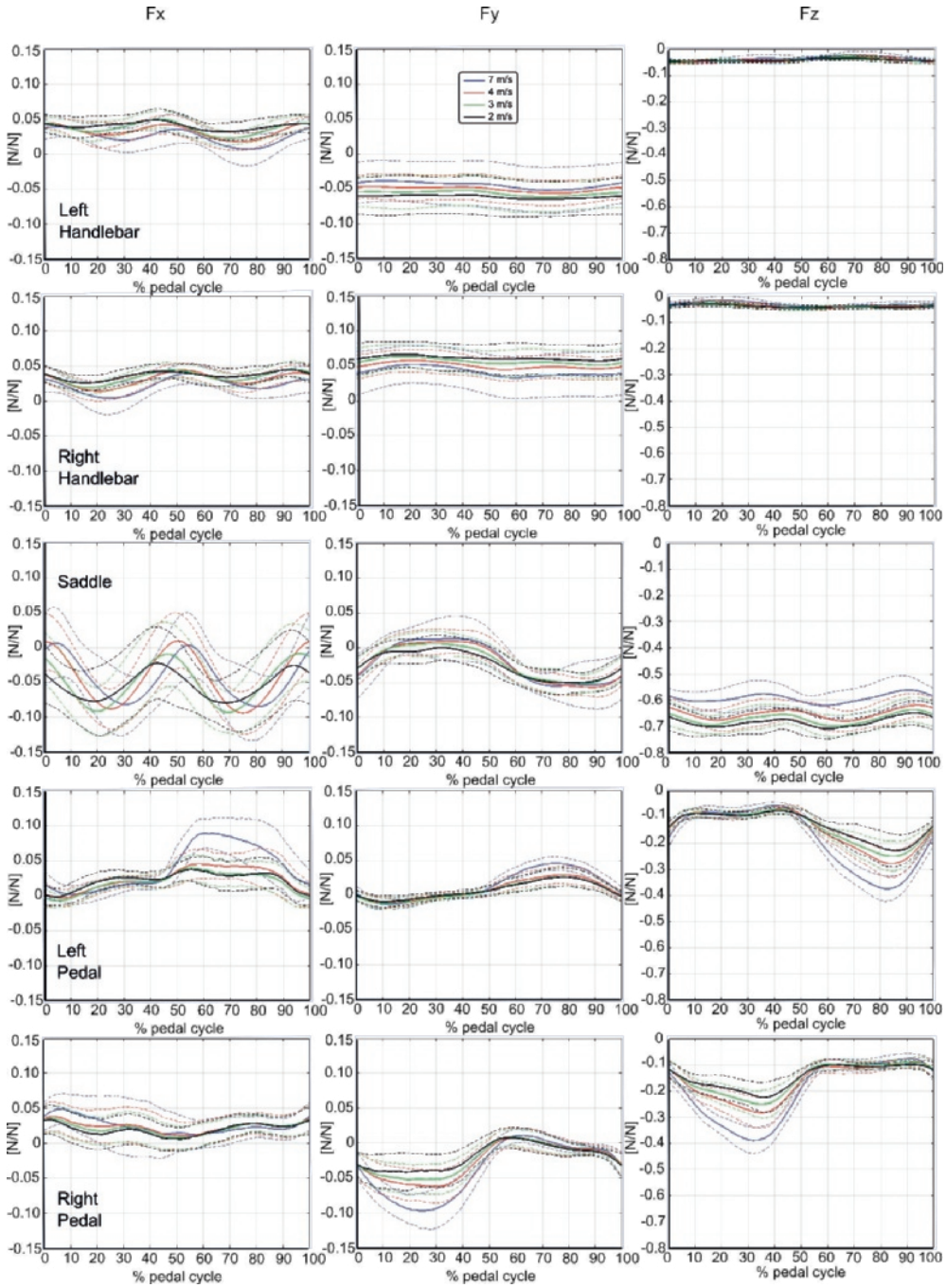

Figure 5.5. *Mean and standard deviation of the longitudinal (Fx), lateral (Fy) and vertical (Fz) contact forces of 10 subjects scaled to subject mass, for the left and right handlebar, the saddle and the left and right pedal. The results of 4 different cycling speeds are presented: 7 m/s (in blue), 4 m/s (red), 3 m/s (green) and 2 m/s (black). Note the change in y-axis for the vertical forces.*

The longitudinal force on the handlebars decreased with increasing cycling speed and had mostly positive values. The lateral force on the handlebars was negative for the left handlebar and positive for the right handlebar; both of them were applied inwards. The lateral force was lower for higher cycling speeds.

The longitudinal and vertical force on the saddle had a frequency of twice the pedal frequency, while the lateral saddle force had a frequency of one time the pedal frequency. The amplitude of the longitudinal and lateral forces on the saddle increased for higher cycling speeds. The vertical saddle force was lower for higher cycling speeds.

The pedal forces were applied in particular during the down stroke phase of the pedal cycle. The vertical forces were quite similar between the left and right pedal, however differences appeared in the longitudinal and lateral directions. The mean scaled lateral force exerted on the right pedal was higher than the mean scaled lateral force that was exerted on the left pedal. Both were directed outwards. The longitudinal force was directed in positive direction and starts at the TDC position. It was higher for the left pedal compared to the right pedal. The pedal forces were higher for higher cycling speeds.

5.3.2. Pedal Angle Estimation

The pedal angles were estimated using an error reduction method, explained in section 5.2.4. The pedal angles of the static-human-bicycle trial were also estimated. In this case the φ had a constant value in the optimisation function.

Table 5.3. *RMSE values of the rest forces in longitudinal (Fx_{rest}) and vertical direction (Fz_{rest}) before and after correction of the pedal angle, for the static human bicycle trials. The improvement as percentage of the original value.*

Subject	Fxz_r [N]		
	RMSE	RMSE after correction	Improvement (%)
1	57	57	0
2	23	17	28
3	21	21	0

The results of the static human-bicycle trials are shown in Table 5.3 and the results of the cycling trials in Table 5.4. The RMSE (Root Mean Squared Error) of the rest force vector in the longitudinal and vertical direction (Fxz_r) is given and the improvement in percentages after the correction of the pedal forces in the LRF of the bicycle.

In Table 5.3 it can be seen that the estimation of the pedal angle of the static human-bicycle trial only gave an improvement for subject 2. For the other two subjects no improvement was found, which means that the pedal angle was estimated to be close to zero. A small rest force remained after the pedal angle correction was performed.

Table 5.4. *RMSE values of the rest forces in longitudinal and vertical direction (Fxz_r) before and after correction of the pedal angle, for the static human bicycle trials. The improvement as percentage of the original value.*

Subject	Body weight	Cycling Speed	Fxz_r [N]		
			RMSE	**RMSE after correction**	**Improvement (%)**
1	765 N	7	121	84	31
		4	77	28	64
		3	80	40	50
		2	91	34	63
2	697 N	7	69	30	57
		4	64	30	53
		3	66	43	35
		2	59	22	63
3	618 N	7	62	25	60
		4	51	26	49
		3	48	28	42
		2	41	22	46

The RMSE of the rest forces of the cycling trials were reduced between 31 and 64%, as is shown in Table 5.4. The improvement in the longitudinal direction was in most cases higher than the improvement in vertical direction. Figure 5.4 shows an example of the estimated pedal angles during a cycling trial and the six parameters describing it. All estimated parameters of the pedal angles of the cycling trials are tabled in Appendix A4.

5.3.3. Model Validation Results

The results of the cyclist model validation were represented with the use of the RMSE of the resultant forces and torques in the CoM of the model that were used during the model simulation in step 4 of the validation process.

Table 5.5. *Resultant forces and torques of the static human-bicycle model simulation of 3 subjects.*

Subject	Resultant Forces/Torques	
	F [N]	**T [Nm]**
1	35	30
2	18	34
3	20	16

Table 5.6. *RMSE of resultant forces and torques of the cycling simulations of the human-bicycle model of 3 subjects and the maximum measured net forces and torques.*

Subject	Body weight	Cycling Speed	RMSE of Resultant Forces/Torques		Maximum Measured Net Forces/Torques	
			F [N]	**T [Nm]**	**Max F [N]**	**Max F·d [Nm]**
1	765 N	7	71	88	492	226
		4	98	59	525	242
		3	62	52	567	261
		2	59	39	579	266
2	697 N	7	60	92	493	222
		4	60	71	541	243
		3	48	41	572	257
		2	66	54	557	251
3	618 N	7	59	69	458	202
		4	56	49	481	212
		3	40	36	492	216
		2	41	40	493	217

The cyclist model validation results are shown in Table 5.5 and 5.6. Table 5.5 shows the resultant forces and torques in the CoM of the simulation of the static human-bicycle trial. Table 5.6 shows the RMSE of the resultant forces and torques in the CoM of the model simulations of cycling trials at resp. 7 m/s, 4 m/s, 3 m/s and 2 m/s.

The resultant forces of the static human-bicycle model simulation differ between the three subjects. Subject 2 and 3 showed a smaller resultant force, compared to subject 1. The resultant torque was smallest for subject 3; approximately half the value of the resultant torque of the other two subjects.

The RMSE of the resultant forces and torques of the cycling trials were higher than the rest forces and torques of the static human-bicycle simulations, approximately twice as high. The RMSE of the resultant force, that represents the 3D force vector in the CoM, varies between 41 and 98N. The RMSE of the resultant torque, that represents the 3D torque

vector in the CoM, varies between 36 and 92Nm. Furthermore, Table 5.6 shows the maximum measured net forces and torques. The maximum measured force vector was in all cases the force measured on the saddle. This force increased when cycling speed decreased. The maximum torque was calculated as the maximum measured net force multiplied by the distance between the CoM and the application point of this force.

The RMSE of the resultant forces of subject 1 are between 10-19% of the maximum measured net force, while those of subject 2 and 3 are between 8-13% of the maximum measured net force. The RMSE of the resultant torques were highest for the simulations with a cycling speed of 7 m/s, around 35-40% of the Max *F·d*. For the other cycling speeds, this value was between 15 and 30%.

Figure 5.6a-d show the mean resultant forces and torques of subject 3 over a pedal cycle during the simulation of the cycling trials, given separately for each direction. It can be seen that the Fy, Tx and Tz have a sinusoidal shape with the same frequency as the pedal frequency, while the frequency of the Fx, Fz and Ty is twice the pedal frequency. The amplitude of the signals decreases with lower cycling speeds. The above tables showed that the RMSE values also decreased with lower cycling speeds.

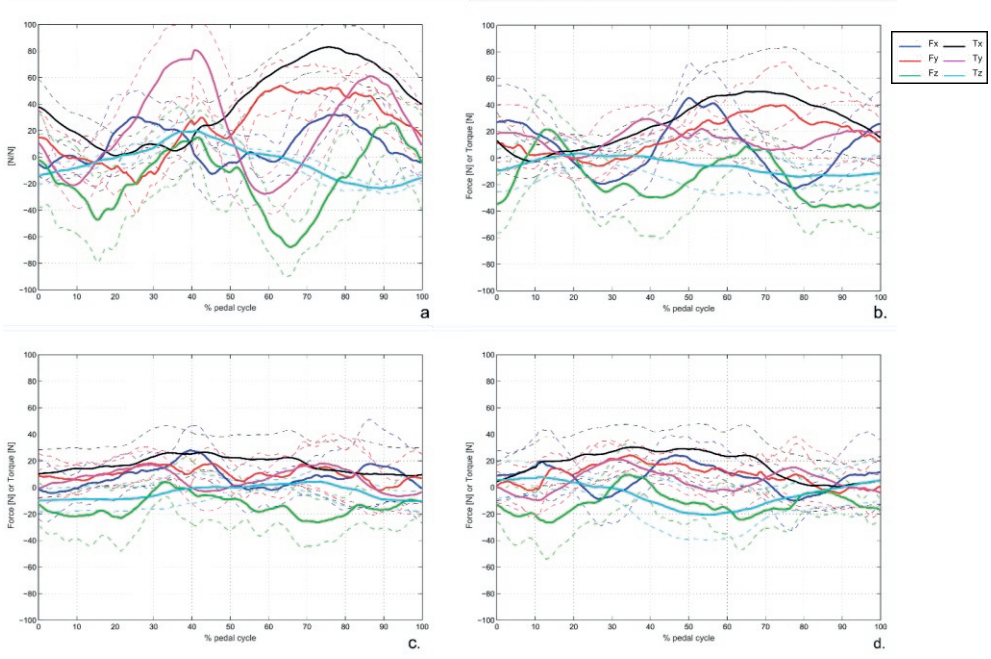

Figure 5.6. *Mean and standard deviations of the resultant forces and torques of the cyclist model validation of subject 3 of the cycling trials with speeds: a. 7 m/s, b. 4 m/s, c. 3 m/s, d. 2 m/s.*

5.4. Discussion

This paper presented six DoF bicycle-cyclist contact forces of 10 healthy, young subjects, while cycling at 4 different speeds. The forces were scaled to the subject mass and averaged over the pedal cycle. Clear patterns were visible, giving insight in the complex 3D contact between the cyclist and the bicycle.

It was shown that the cyclist constantly applied a lateral force at the handlebars that is directed inwards. This means that the cyclist pushed at the handlebars instead of pulled. The lateral force was higher during cycling at lower speeds than cycling at high speed. This can be related to the increased steer control actions at lower speeds. Furthermore, it can be linked to an increased stress-level of the cyclist while riding on the narrow treadmill (50 cm width) at low speeds, causing more co-contraction of upper-arm muscles [133]. The longitudinal forces applied at the handlebars were positive. Again, this implies that the cyclist pushed the handlebar instead of pulled. These findings have implications when developing bicycle-cyclist interaction models. It implies that a linear spring-damper [121] or rotational spring-damper [92] does not realistically represent the forces applied by the cyclist on the handlebars. To include the lateral force that the cyclist applies on the handlebar, in a bicycle-cyclist interaction model, a lumped arm model with active elbow flexors-extensors could be necessary.

The scaled vertical forces on the saddle increased when cycling speeds decreased. This can be related to the higher pedal forces that were applied during cycling at higher cycling speeds. This relationship is linear; the mean vertical saddle forces increase with 0.10 times the body weight and the mean pedal forces each decrease with 0.06 times the body weight when the cycling speed decreases from 7m/s to 2 m/s.

The frequency of the longitudinal saddle force is twice the pedal frequency and can be related to the reaction forces due to the pedalling movement. The lateral force on the saddle is also a reaction force of the pedal forces. The net lateral force should be close to zero. This means that the lateral forces on the pedals should be compensated by the lateral force on the saddle. When the pedalling movement is included in the multi-body model it is therefore important to also include the movement of the pelvis with respect to the saddle.

The profile and magnitudes of the vertical pedal force corresponds quite well to the data presented by Hull and Jorge [134]. The vertical load reaches a maximum at around 100° (30%) and decreases to a value of 0.1 times the body weight in the upstroke. The two

maxima during the upstroke, described by Davis and Hull [132] were not clearly visible in our data. Davis and Hull reported data that is typical for cycling with cleats, while the cycling task of the experiments of Hull and Jorge were more similar to the cycling trials of our experiment, as their subjects also cycled on rollers. That is why also the measured longitudinal forces match better with the data of Hull and Jorge. The measured left pedal forces are closer to this value than the right pedal forces. The same is true for the left lateral pedal forces that are similar as presented in literature [132], while the right lateral pedal forces are higher.

The measured pedal forces were, as expected, larger for higher cycling speeds. The difference between the left and right pedal forces can be explained by the fact that the cyclists were urged to maintain a certain pedal frequency. Each of them used a certain method to accomplish this. It is therefore likely that they kept track of one leg to match a certain position at the tick of the metronome. It is possible most subjects used their left leg for this, which could explain the different forces measured at the right pedal. The high lateral pedal force measured at the right pedal indicates an ineffective pedalling technique. This could be caused by sitting askew on the bicycle, because it causes a net lateral force that deviates from zero

Note also that the force sensors used in our study were several centimetres thick and were placed on the normal surface of the pedal. This caused a slightly different pedal technique.

The pedal angles were estimated by an optimisation procedure to obtain minimal net forces in the longitudinal and vertical direction. The net force should be minimal, as the net movement between the bicycle and cyclist can be neglected. The inclusion of the estimated pedal angles decreased the net forces to 15-25N in the longitudinal and vertical direction. This error, that still remains, could be caused firstly by the optimisation method, but also by misalignment of the force sensors on the bicycle. Furthermore, discrepancies in the vertical direction could be caused by an askew position of the cyclist on the bicycle or asymmetries of the bicycle frame itself. The forces measured on the handlebars are assumed to act in the bicycle LRF. However, this is not the case, due to the rotation of the handlebars with respect to the bicycle rear frame. The steering angles are small and the forces on the handlebar are also quite small compared to the other forces, therefore this only caused a small error that can be neglected.

In general, the offset of the estimated left pedal angle is larger compared to the offset of the estimated right pedal angle. The difference between the estimated left and right pedal angle can be related to the difference in measured pedal force at both pedals. Davis and

Hull measured pedal angles while cycling on rollers and found amplitudes of 30° with an offset of 30° [132]. These values are quite similar as the ones found in this study. However, smaller values were reported by Kautz and Hull: amplitudes around 15° with an offset of 15° [135]. This last study was performed on elite cyclists cycling on a bicycle ergometer, which could explain the difference. Differences in pedal angles could also be due to different cycling styles. In our study, sometimes unrealistic pedal angles were found. For example, angles less than -90° or more than 20°. A deviation of the estimated pedal angle in the upstroke of the pedal cycle has a very small influence on the forces that were used in the validation process. However, a deviation of the estimated pedal angle in the down stroke could lead to errors in the range of 20N.

As mentioned above, rest forces were still present after the error reduction method, whereby the pedal angle was estimated. This means that the validation process is performed with data that is not perfect. The kinematic data is dependent on the accuracy of the marker-based motion capture system. These have system errors of 1-5 mm [136]. Errors due to soft tissue artefacts could go up to 1 cm for human movement [137] and then marker placement errors add up to this [138]. In particular, errors in estimating the hip joint centre influence the accuracy of biomechanical cycling models [139]. In this study only the PSIS markers were used to estimate the hip joint position, during cycling trials.

The measurement of contact force data is also prone to errors: misalignment of force sensors on the bicycle and measurement errors of the force sensor positions play a role. As highlighted by Hicks et al., is a model as good as the accuracy of the experimental data [140]. Therefore, in our case, it needs to be taken into account that some discrepancies in the experimental data are present due to the reasons described above. These have an influence on the validation results.

The recommended RMS of resultant forces applied at the CoM, to achieve dynamic consistency between motion and applied force is 5% of the maximum force magnitude [140]. This accuracy is not achieved in this study; however, they were between 8 and 19% of the maximum force magnitude. The resultant forces were related to the pedal forces. Accurately measuring the pedal angles could therefore improve the results.

The geometry and the positions of the CoM of the body parts of the multi-body cyclist model were based on a static stance trial. However, more subject-specific modelling might be needed to improve the cyclist model. The cyclist biomechanical model depends on a lot of assumptions and is therefore more difficult to validate than the bicycle model.

With these results, we show that accurately measuring the 3D kinematics and interaction forces is necessary to generate accurately the cyclist part of bicycle-cyclist models.

5.5. Conclusion

This study presented measured bicycle-cyclist 3D interaction forces, during cycling on a laboratory set-up at four different cycling speeds. The measured pedal forces were in agreement with previous published data. The presented forces on the handlebars and saddle can lead to improved bicycle-cyclist interaction models.

The measured bicycle-cyclist interaction forces and measured 3D kinematics were used to validate a bicycle-cyclist interaction computer model. Resultant forces of 8-19% of the maximum force magnitude were used to ensure dynamic consistency of the model. These resultant forces can be related to inaccuracies of the experimental data and modelling assumptions. Accurately measuring the pedal forces and increased subject-specific modelling could increase the validity of the model.

Chapter 6

Identification of a Cyclist Balance Control Model

V.E. Bulsink, R.G.K.M. Aarts, G.M. Bonnema, H.F.J.M. Koopman

Submitted to Journal of Biomechanics

Abstract

In this paper, we focus on identifying the cyclist balance control model and the differences between younger and older cyclists. An extensive dataset of cycling experiments on a laboratory set-up with young and older subjects is used to identify a Single-Input-Multi-Output (SIMO) cyclist balance control model. The subjects cycled at different speeds while a perturbation was applied to the rear of the bicycle with the use of a Stewart platform. The three outputs of the control model are steering, upper-body lean and outward knee movements, while the roll angle is the input. All three control mechanisms are represented as PD-controllers with time delay.

From this study, we can conclude that the cyclist balance control can be modelled with a PD controller with time delay in the case of steering and upper body lean control. The outward knee control was mostly limited to low frequencies and more difficult to model with linear time-invariant models. The results suggest that the knee control and upper body lean control are reflex-like, while the steering control uses visual feedback loops. We found differences in the time delays between younger and older cyclists. Higher time delays were seen in older cyclists and they also seem to use more knee control.

6.1. Introduction

Cycling safety as a research topic is growing in popularity. The topic can be approached from different angles, such as infrastructural aspects [141], mobile phone use during cycling [142], mounting and dismounting the bicycle [143, 144] and interaction with other traffic [145]. One of the most important aspects of cycling safety is cyclist behaviour and the role it plays in events leading to traffic accidents [11, 146]. Cyclist behavioural aspects mostly influences single-sided accidents. In particular, older cyclists tend to cause more accidents and are more vulnerable to injuries [12, 103]. Balance issues, faults of judgment or overestimation of cycling performance by elderly cyclists may contribute to accidents.

Computer simulations can be used to predict and analyse behaviour of the bicycle-cyclist system. Parameter studies with the use of these simulation models could lead to improved bicycle designs and more insight in the factors leading to unstable situations. Multibody dynamic bicycle models are already being used frequently to analyse bicycle stability [25, 54]. These models are continuously expanded upon, for instance with tire-road contact models or passive and active models of the cyclist [22, 93, 121, 124]. In order to accurately simulate the behaviour of the entire system and to incorporate age-dependent differences in the model, accurate and validated models of the cyclist control are necessary.

Schwab and Meijaard [105] presented an overview of bicycle dynamics, cyclist control models and experimental studies. Several other authors compared the Carvallo-Whipple bicycle model with experimental data of a bicycle without a cyclist [27, 34, 147]. Moore and Kooijman et al. [65, 119, 148] performed cycling tests during normal cycling and on a treadmill, while measuring bicycle kinematics and movements of the cyclists with respect to the bicycle. Their experiments showed that the cyclist can exercise most control on the bicycle by steering and that lateral knee movements are used at low speeds. Upper-body motions are found to be relatively small [64]. However, Cain et al. [149] showed these are used for balance control during cycling on rollers. Computer simulations show that control by upper-body lean requires high gains compared to steering [22, 54, 150].

Recent examples in literature of bicycling control models showed the development of a linear feedback controller representing the visual, vestibular and proprioceptive feedback gains [89] and the development of PD-controllers with a time-delay for upper-body lean control and steering control, focusing on the balance task [123].

In this paper, we focus on identifying the cyclist balance control model and the differences between younger and older cyclists, using an extensive dataset of cycling experiments on

a laboratory set-up. In [114] it was already demonstrated that the experimental set-up was useful to apply controlled perturbations to the bicycle-cyclist system. In [128] we showed a comparison between the control strategies used by younger and older cyclists using the aforementioned dataset. However, the study was limited to only one cycling speed (4 m/s). Therefore, in the present study, data of cycling trials at various speeds will be analysed. A time-invariant and linear behaviour of the cyclist control is assumed, similarly as in previous human postural balance control studies [16, 151].

The assumed cyclist balance control model will use steering, upper-body lean and outward knee movements as control strategies [128]. The cyclist balance control model that we identify in this study is assumed to be a PD-controller with time-delay. We expect to see differences in balance control parameters between younger and older cyclists, such as a different time-delay or feedback gains. This will lead to insights regarding balance control that can be used to design safer bicycles for older cyclists.

6.2. Methods

6.2.1. Cyclist Balance Control Model

Figure 6.1. represents the cyclist balance control model with its input and outputs. Roll stabilization is performed by feedback on the roll angle φ and roll rate $\dot{\varphi}$ representing visual and vestibular feedback. The transfer functions $H_{\varphi T_S}$, $H_{\varphi Y_u}$ and $H_{\varphi\theta_k}$ are therefore assumed to resemble PD-controllers. Each output has a different time delay (resp. τ_s, τ_u and τ_k) that is given by the transfer function:

$$H_{TD} = e^{-\tau_d s} \tag{6.6}$$

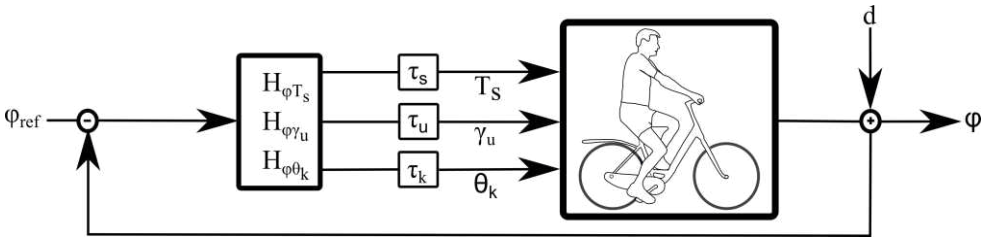

Figure 6.1. *Cyclist Balance Control model, with d the disturbance of the Stewart Platform, ϕ the roll angle of the bicycle, the three control mechanisms used by the cyclist: T_s the steering torque, Y_u the upper body lean angle and θ_k the knee angle. The transfer functions from the input (φ) to the three outputs of the controller are respectively $H_{\varphi Ts}$, $H_{\varphi Yu}$ and $H_{\varphi\theta k}$, with τ_s, τ_u and τ_k the corresponding time delays.*

6.2.2. Experiments

15 healthy young (25.3±2.8 years) and 15 older (58.1±2.1 years) cyclists participated in the cycling experiments in a laboratory set-up [114, 128]. The rear wheel of the bicycle was situated on rollers and the front wheel on a treadmill. The treadmill was set at a predefined speed, while the cyclist was instructed to maintain a certain pedal frequency to assure equal rotational speeds of the wheels. The pedal frequency was different for all trials and was presented to the subject by a metronome. The younger subjects performed the cycling experiment at 2, 3, 4 and 7 m/s and the older cyclists at 4 and 6 m/s.

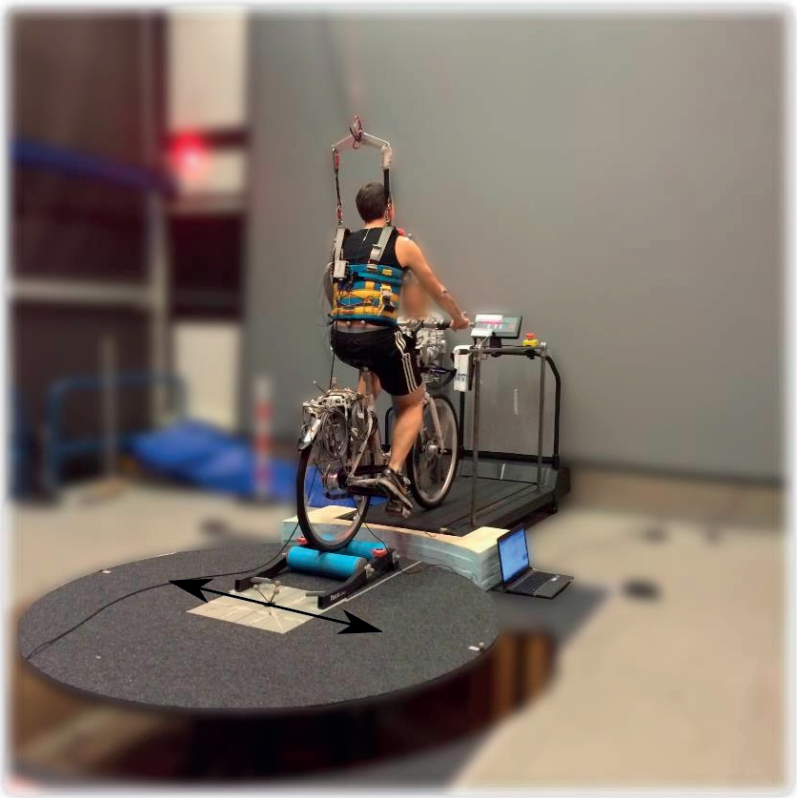

Figure 6.2. *The experimental laboratory cycling set-up. The front wheel rotates on the treadmill and the rear wheel is situated on rollers that are placed on a Stewart platform. Lateral movements of the Stewart platform perturb the bicycle.*

During the cycling trials, the rear wheel of the bicycle was laterally perturbed by a Stewart platform (see Figure 6.2). The disturbance signal used (Figure 6.3) was a continuous multisine containing 10 different frequencies. The maximum amplitude was set at 1.75 cm

for the young subjects and at 1.25 cm for the older subjects. The signal had a descending power spectrum.

a. b.

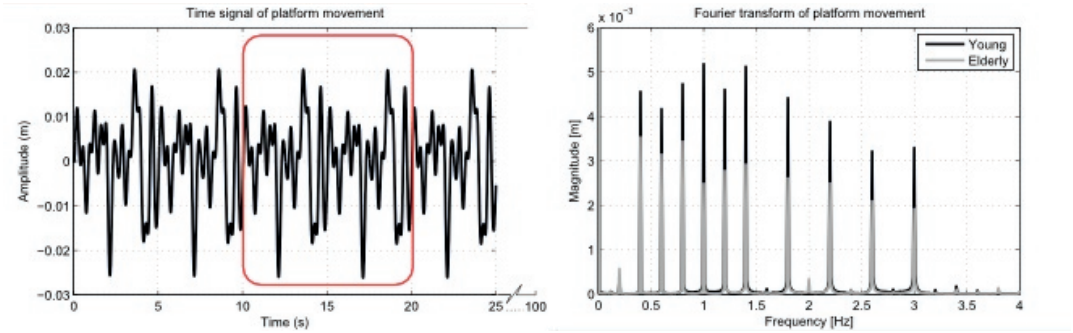

Figure 6.3. *Representation of the continuous lateral platform disturbance signal.* ***(a)*** *Time signal of the platform movement. The disturbance signal is a continuous signal of 100 s (10 times a repetition of the same 10 s).* ***(b)*** *The Fourier transform of the Stewart platform movement with power on 10 different frequencies and more power at low frequencies.*

6.2.3. The measurement system

The bicycle used in the experiments was a city bicycle with straight handlebars (Trek L200). The bicycle was instrumented with several sensors to measure the kinematics and steering torque. The roll angle of the bicycle was measured using a reflective marker-based motion-capture system (Vicon), the steering angle was measured by a potentiometer and the steering torque was obtained from two 6-DOF Force-Torque sensors (Sensix) placed on the left and right handlebars.

Reflective markers were also placed on the cyclist to measure his/her motions with respect to the bicycle. The outward knee movement is defined as an endo-exorotation around the axis that connects the hip and ankle and is averaged between the movements of both legs. See [128] for a more detailed description.

6.2.4. Data processing

The data were recorded at a sample frequency of 120 Hz, with two measuring systems, i.e. the Vicon motion data and all other signals respectively. All data were pre-filtered with a second-order Butterworth low-pass filter with a cut-off frequency of 5 Hz and subsequently detrended. The measured data were synchronized by calculating the correlation and time-shift between the steering angle signal that was measured with both systems.

The data were divided into the 10 periods of 10 seconds. Measurement errors due to invisibility of reflective markers were removed and corrected by interpolating the gaps. When correction was not possible the specific period was removed from the data.

6.2.5. Frequency Response Functions

The closed-loop cyclist balance controller $\widehat{H}_C(\omega)$ is identified in the frequency domain using the joint-input-output method [15] at the exited frequencies ω for each period of 10s.:

$$\widehat{H}_C = -\hat{S}_{dy}(\omega) \cdot \hat{S}_{du}{}^{-1}(\omega) \tag{6.1}$$

with $\hat{S}_{dy}(\omega)$ the estimated cross spectral density (CSD) of the disturbance and controller output signals and $\hat{S}_{du}(\omega)$ the estimated CSD of the disturbance and controller input signal. The estimate from the disturbance signal to the input and outputs is given by:

$$\hat{S}_{du} = D(\omega) \cdot U(\omega) \tag{6.2}$$

$$\hat{S}_{dy} = D(\omega) \cdot Y(\omega) \tag{6.3}$$

where $D(\omega)$, $U(\omega)$ and $Y(\omega)$ represent the Fourier coefficients at the excited frequencies of the disturbance, controller input and controller outputs, respectively.

The frequency response functions (FRF) of the balance controller for the 10 periods of each trial were averaged to obtain the averaged FRF per subject. The FRF's give the magnitude and phase shift of each output as a function of frequency in comparison to the input and give a characterization of the dynamics of the balance control system.

6.2.6. Coherence

The coherence value between the disturbance signal $d(t)$ and the input and output signals is calculated and reflects a quality measure of how well the system was perturbed. Additionally, it represents the linearity and time-invariance of the system. The coherence function between the disturbance signal $d(t)$ and an input or output signal $u(t)$ or $y(t)$ is defined as

$$\gamma_{du}^2 = \frac{|S_{du(\omega)}|^2}{S_{dd}(\omega) \cdot S_{uu}(\omega)} \tag{6.4}$$

and $\gamma_{dy}^2(\omega) = \frac{|S_{dy}(\omega)|^2}{S_{dd}(\omega) \cdot S_{yy}(\omega)}$ (6.5)

where $S_{du(\omega)}$ and $S_{dy(\omega)}$ denote the cross-spectral density functions as before and $S_{dd}(\omega)$, $S_{uu}(\omega)$ and $S_{uu}(\omega)$ are the power spectral density functions of $d(t)$, $u(t)$ and $y(t)$. The coherence values lie in the interval $0 \leq \gamma_{du}^2(\omega) \leq 1$ and $0 \leq \gamma_{dy}^2(\omega) \leq 1$. A coherence of 1 indicates a perfect correlation or linear dependency of the signals. Measurement noise or non-linearities and time-variant behaviour lead to low coherence values.

Similarly, the coherence between the controller input and an output is computed as

$$\gamma_{uy}^2(\omega) = \frac{|S_{uy}(\omega)|^2}{S_{uu}(\omega) \cdot S_{yy}(\omega)} \quad (6.6)$$

where the cross-spectral density function $S_{uy}(\omega)$ of controller input and output follows from a similar expression as in Eq. (6.4).

6.2.7. Parameter estimation

The cyclist balance control model is assumed to be a linear, time-invariant system with one input and three outputs, i.e. Single-Input-Multiple-Output (SIMO). The parametrized control model contains 9 parameters, three for each control mechanism that is fitted with a PD-controller with time-delay. This PD-controller with time-delay is fitted on the mean FRF of each subject, using the *lsqnonlin* function in Matlab. The following object function is minimized in a least-squares sense, to obtain an estimate of the P gain, D gain and time delay τ:

$$F = \sum_{j=1}^{n} \gamma_{uy}^2 \omega_j \cdot ((P \cdot \cos(\tau \cdot \omega_j)) - Re(\hat{H}_j)) + (D \cdot i\omega_j \cdot i \cdot (-\sin(\tau \cdot \omega_j) - Im(\hat{H}_j))) \quad (6.7)$$

Where index j counts the frequencies ω_j at which the system is excited and the balance controller FRF $\hat{H}_j$ is estimated. The function is weighted with the coherence between the input and output, γ_{uy}^2. The VAF (Variance Accounted For) is computed to give a performance measure of the model fit (a PD-controller with time delay) to the FRF, in the following way:

$$VAF = 1 - \frac{\sum_{j=1}^{n} \left(\hat{H}_j - (P + D \cdot jw) e^{-j\omega\tau}\right)^2}{\sum_{j=1}^{n} (\hat{H}_j)^2} \cdot 100\% \quad (6.8)$$

It shows how much the estimates can be explained by the model. The VAF is 100% when the PD-controller with time delay fits perfectly the estimated FRF. When they differ the VAF will be less. Model fits with a low VAF will be disregarded from the results.

Unpaired Student t-tests are used to test whether differences between the estimated parameters of young and older cyclist are significant when cycling at the same speed (4 m/s). A p-value of 0.05 was used.

6.3. Results

All cyclists in both age groups managed to successfully cycle on the experimental setup during the perturbations of the Stewart platform. The experimental protocol was adapted for older cyclists, as was described in [128].

6.3.1. Coherence

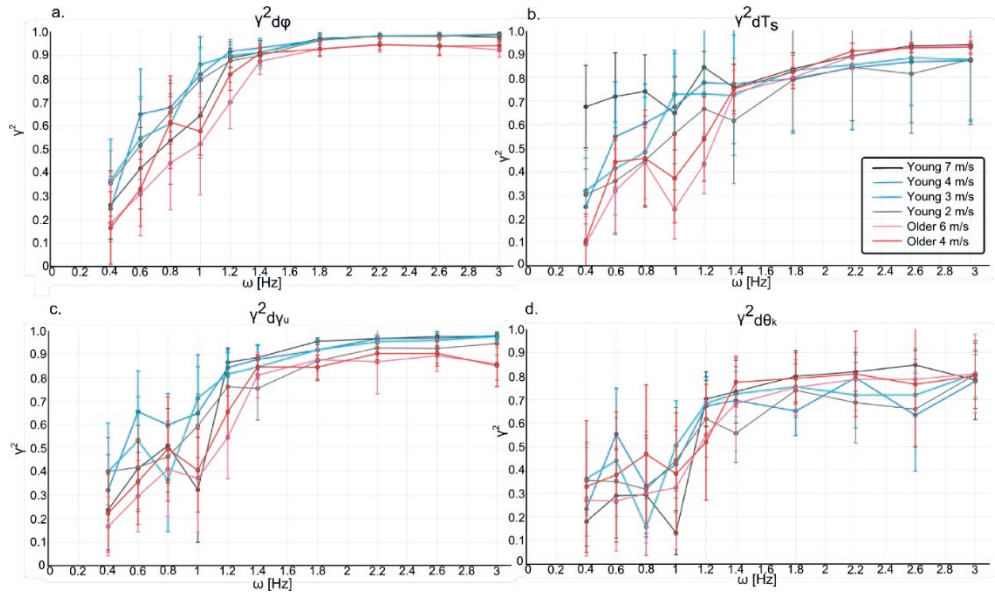

Figure 6.4. *Coherence γ^2 of the disturbance signal d(t) and the in- and output signals averaged for all subjects of the different trials. The vertical bars indicate the standard deviation.*

Figure 6.4 depicts the coherence of the disturbance signal and the controller input and output signals averaged over the subject groups for different speeds. Here, $\gamma^2_{d\varphi}$, $\gamma^2_{dT_s}$,

$\gamma^2_{dY_U}$ and $\gamma^2_{d\theta_k}$ signify the coherence between the disturbance signal and respectively the roll angle, the steering torque, the upper body lean and the knee angle.

Clearly the coherence between the disturbance signal and all input and output signals increases from low values at the lower frequencies to a higher, more constant value in the range of 1.2 to 3 Hz. The plot for $\gamma^2_{d\varphi}$ represents the coherence between the disturbance signal and the roll angle $\varphi(t)$ and is higher for the younger cyclist group. The plot for $\gamma^2_{dT_s}$ shows high standard deviations for cyclists in the young age group and a better coherence at high frequencies for the older age group. The plot for $\gamma^2_{dY_U}$ shows higher values for cyclists in the younger age group. The coherence for younger subjects is almost equal to 1 at high frequencies. Finally, the plot for $\gamma^2_{d\theta_k}$ shows high standard deviations for all groups and speeds and shows the lowest coherence values of all signals.

6.3.2. Frequency Response Functions

In general, the frequency response functions (FRF) show similar trends for all experimental subjects, as depicted in Figure 6.5. For most subjects, the values lie close together and follow the same pattern, though individual values may differ slightly. Incidentally, a subject shows deviant behaviour, as will be detailed next.

a. b.

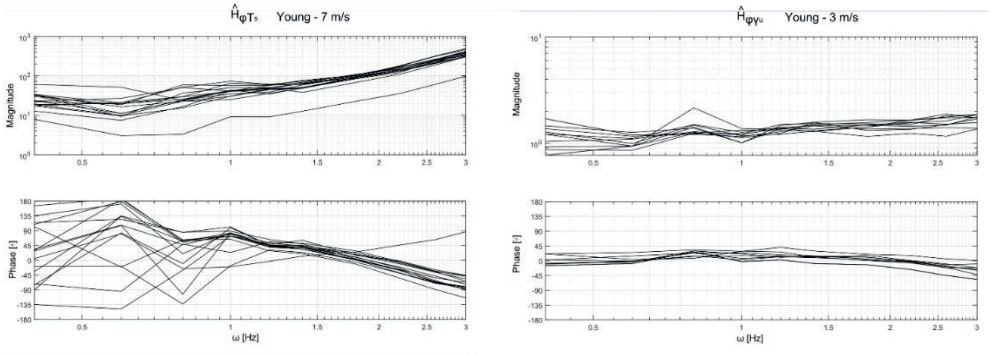

Figure 6.5.a. *shows $\hat{H}_{\varphi T_s}$, the estimated FRF of the roll angle to the steering torque, for all young subjects when cycling at 7 m/s.* ***b.*** *shows$\hat{H}_{\varphi Y_u}$, the estimated FRF of the roll angle to the upper-body lean, for all young subjects when cycling at 3 m/s.*

Figure 6.5.a. shows the FRF of the roll angle to the steering torque of all young subjects when cycling at 7 m/s. The magnitude values are all in a similar range, except for one

subject. The phase plots also show deviant behaviour for one subject. The VAF of the model fit will be low in these cases and therefor these results will be disregarded.

Figure 6.5.b. shows the FRF of the roll angle to the upper body lean (UBL) of all young subjects when cycling at 3 m/s. This example shows that all subjects performed in a similar way in this cycling test.

To visualise similarities and differences for both age groups and all cycling speeds, the FRF data for all subjects as in the examples of Figure 6.5 are averaged. Figure 6.6 shows the mean and standard deviation of the three controller FRFs obtained in this way.

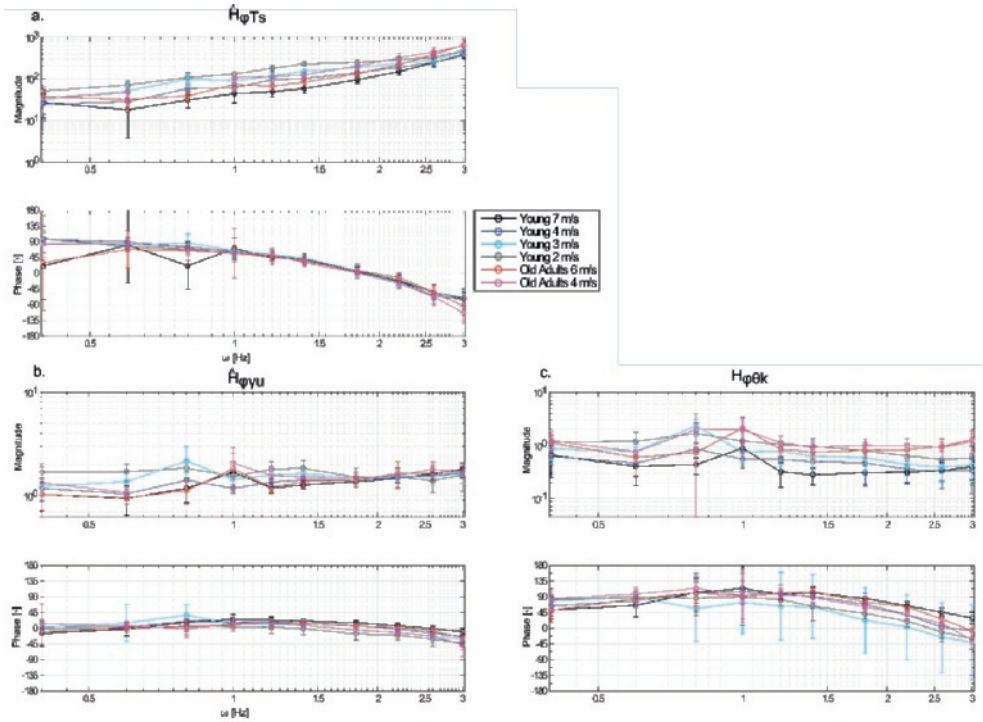

Figure 6.6. *Shows the magnitude and the phase plot of the mean and standard deviation of the FRF of* ***a****. the roll angle to the steering torque,* ***b.*** *the roll angle to the upper-body lean angle,* ***c.*** *the roll angle to the knee angle. The different colours represent the different cycling trials: for the younger subjects at the cycling speeds 7, 4, 3 and 2 m/s and for the older subjects at the cyling speeds 6 and 4 m/s.*

Figure 6.6.a. represents the averaged FRF of the roll angle to the steering torque of all subjects, for different speeds and age groups. The magnitude values do not show a clear trend, apart from the lowest speed showing highest value and the highest speed showing

the lowest values. Few differences can be seen in the phase plot, except for values at high frequencies where the phase shift is higher for older subjects. The behaviour of the FRF seems to mimic a PD controller with time-delay.

Figure 6.6.b. represents the averaged FRF of the roll angle to the UBL. Compared to the values in Figure 6.6.a., the magnitude is much lower and the phase shift is much less. However, the behaviour could still resemble a PD controller with time-delay.

Figure 6.6.c. represents the averaged FRF of the roll angle to the knee. The magnitude plot shows a difference in values between subjects in different age groups. Values for older subjects are higher than those of younger subjects. Also, the magnitude values for younger subjects are higher for lower cycling speeds. The phase shift values show higher values for higher cycling speeds in both age groups.

6.3.3. Identified Parameters

The following tables give an overview of the average identified parameters per cycling speed and age group and the VAF of the estimated model. The asterix (*) indicates a significant difference between the two age groups at a speed of 4 m/s.

Tables 6.1 and 6.2 give the parameters (mean and standard deviation) of the estimated steering torque and steering angle control mechanism respectively. Both control mechanisms show a clear trend of increasing P-values for decreasing cycling speeds. The same trend appears in the D-value of the steering angle control. Note also the statistical difference in the value for τ_δ between the two age groups. The VAF values for the steering angle controller are higher than for the steering torque controller, and therefore more accurate.

Table 6.2. *The mean and standard deviation of the estimated parameters of the steering torque control mechanism. The horizontal bars represent the value of the parameter.*

Steering Torque												
	$P_{Ts\,[-]}$			$D_{Ts\,[-]}$			$\tau_{Ts\,[s]}$			VAF [%]		
	Mean	SD		Mean	SD		Mean	SD		Mean	SD	
Young 7 m/s	-5.73	2.87		-17.59	4.88		0.16	0.03		67	12	
Young 4 m/s	-14.99	7.48		-14.41	7.63	*	0.12	0.06		81	11	
Young 3 m/s	-21.88	9.84		-18.73	7.78		0.12	0.06		78	13	
Young 2 m/s	-30.51	12.24		-22.17	5.72		0.14	0.04		83	10	
Older 6 m/s	-14.06	6.29		-33.33	13.74		0.16	0.05		76	11	
Older 4 m/s	-30.24	22.1		-30.27	14.63	*	0.21	0.13		73	15	

Table 6.3. *The mean and standard deviation of the estimated parameters of the steering angle control mechanism. The horizontal bars represent the value of the parameter.*

Steering Angle												
	$P_{s\,[-]}$			$D_{s\,[-]}$			$\tau_{s\,[s]}$			VAF [%]		
	Mean	SD		Mean	SD		Mean	SD		Mean	SD	
Young 7 m/s	-0.62	0.27		-0.10	0.03		0.22	0.02		92	5	
Young 4 m/s	-1.69	0.34	*	-0.11	0.05	*	0.22	0.02	*	95	3	
Young 3 m/s	-2.68	0.47		-0.13	0.06		0.21	0.02		92	7	
Young 2 m/s	-3.98	0.67		-0.19	0.08		0.20	0.05		92	5	
Older 6 m/s	-0.61	0.28		-0.19	0.07		0.24	0.01		93	5	
Older 4 m/s	-1.14	0.29	*	-0.21	0.05	*	0.27	0.02	*	79	15	

The P-value for the upper-body lean controller increases when cycling speed decreases. The time delay is much lower compared to the steering control action. Values of the VAF are around 60%.

Table 6.4. *The mean and standard deviation of the estimated parameters of the upper-body lean angle control mechanism. The horizontal bars represent the value of the parameter.*

Upper Body Lean Angle												
	$P_{Yu\,[-]}$			$D_{Yu\,[-]}$			$\tau_{Yu\,[s]}$			VAF [%]		
Young 7 m/s	-0.91	0.22		-0.07	0.03		0.06	0.02		60	3	
Young 4 m/s	-1.16	0.17		-0.05	0.03		0.05	0.02		57	2	
Young 3 m/s	-1.27	0.19		-0.04	0.04		0.05	0.03		67	6	
Young 2 m/s	-1.62	0.14		-0.05	0.03		0.06	0.03		59	3	
Older 6 m/s	-0.95	0.27		-0.08	0.03		0.07	0.04		60	7	
Older 4 m/s	-1.22	0.25		-0.05	0.03		0.06	0.04		65	8	

The results of the estimation of the knee control mechanism have been disregarded, as the VAF values were too low, they did not represent accurate results.

6.4. Discussion

The experimental setup contained a narrow treadmill for cycling, which necessitated a more focused manner of cycling than on the road. This could influence the results.

In this study, we only considered the balance control of the cyclists by modelling their behaviour with a SIMO (Single Input Multiple Output) model. In reality, heading control also plays a role, which means that the cyclist control system is a MIMO (Multiple Input Multiple Output) model. For this study, we decided to simplify this control system in order to reliably model the balance control. For future research, an additional perturbation could be applied in order to identify this MIMO model [152, 153].

The perturbations at high frequencies resulted in higher coherence, which means that subjects always respond in a similar way to this disturbance. Therefore, the reaction to the perturbation can be modelled with a linear and time-invariant model. However, at lower frequencies, the subjects behaved in different ways to the perturbations, possibly because at lower frequencies, subjects have more time to react. The results at lower frequencies are therefore less reliable.

The knee control mechanism is difficult to model due to the fact that subjects do not always use knee control in a similar way. This can be seen from the lower coherence values for the knee angle and the identification that resulted in low VAF values. Furthermore, the outward knee movement signal is small and subjected to noise and calculation errors. The FRF's did not resemble the structure of a PD-controller with time-delay. At a higher frequency, the knee control mechanism is not used as much, which seem to indicate that the knee control mechanism could be modelled by inserting a low-pass filter. Above a frequency of 1.5 Hz, younger subjects no longer used the knee as a control mechanism.

Moore et al. [119] previously showed that lateral knee movements are used by cyclists at low cycling speeds. This study and our previous study [128] confirm that the knee control mechanism is used more at lower speeds than at higher speeds. Furthermore, the older subjects seem to use more knee control [128], as is also visible when comparing the graph with the FRF's of young and older subjects in figure 6.6.c.

In general, subjects tend to use the same strategies for balance control. However, some individuals deviated from the general strategies. This means that different cycling strategies are always possible, but there was a clear general trend in the subjects' behaviour indicating that a general model of the cyclist balance control system is possible.

Some difference in performance during the cycling tasks was noted between the two age groups. The most striking difference was the higher time delay needed for steering control for the older age group. The differences between control models of the two age groups were relatively small, which may be since the subjects in the older age group were relatively young. Furthermore, the cycling trials of the older age groups were less taxing than those of the younger age group, which may have influenced the results. Due to safety precautions, we did not stretch the cycling abilities of the subjects in the older age group, but for future research a different setup could be used in which the subjects can perform more difficult cycling tasks.

The highest speed of 7 m/s was too physically taxing for the older cyclists, whereas the lowest cycling speeds were more difficult with respect to bicycle control. This difficulty could be explained by the higher reaction times for steering seen in older subjects and the fact that at lower cycling speeds, higher control gains are necessary. The combination of these two results in higher steering amplitude, which is limited by the edge of the treadmill.

The identified time delays suggest that steering is influenced by visual information and that UBL control behaves like neural reflexes. These time delays are in the same range as values found in other studies [80, 123, 153]. The gains for the steering controller are in the same range as found by Wang et al. [123]. The gains for the steering torque controller are lower compared to the values found by Schwab et al. [89].

6.5. Conclusion

From this study, we can conclude that the cyclist balance control can be modelled with a PD controller with time delay in the case of steering and UBL control. The knee control was mostly limited to low frequencies and more difficult to model with linear time-invariant models. The results suggest that the UBL control is reflex-like, while the steering control uses visual feedback loops. These insights can be used to further develop bicycle-cyclist models.

We found differences in the time delays between younger and older cyclists. Higher time delays were seen in older cyclists.

The model we identified was a SIMO model, using the roll angle as an input. In future studies MIMO models could be used in order to include the heading as an input.

Chapter 7

Electrical Bicycle Hub Motors & Stability

Why a rear motor is better than a front motor & Two motors are better than One

V.E. Bulsink, G.M. Bonnema, D. van de Belt, H.F.J.M. Koopman
International Cycling Safety Conference 2016 3-4 November 2016, Bologna, Italy

Abstract

Electrical bicycle hub motors are frequently used to assist the cyclists pedal. However, in order to ensure the further acceptance of the electric bicycle, improvement of safety is necessary. In this study, computer simulations were used to study the effect of using electric hub motors on the bicycle's stability.

The two goals of the study were to show that using a rear wheel hub motor is better than using a front wheel hub motor, and to show that with using two hub motors simultaneously the bicycle self-stability can be improved.

An open-loop bicycle-cyclist model was used to study the self-stability of the system during straight cycling, by analysing the weave eigen mode of the bicycle-cyclist system. Furthermore, the behaviour during cornering was analysed.

The difference in self-stability of the bicycle-cyclist system with a front or rear hub motor was small in the straight cycling case; the weave speeds were quite similar. However, with the simulation of a cornering movement it was shown that using a rear motor is better than using a front motor; traction with the rear motor stabilizes the system more than traction with the front motor did.

Additionally, the computer simulations showed a decrease in the weave speed during straight cycling, when a sufficiently high traction torque was applied on the rear wheel and an equally high braking torque on the front wheel. Using two motors as an electric bicycle add-on, not only provides the benefits of the current electric bicycle, like assistance in pedalling power. It also assists in active bicycle stability control and can therefor improve the safety of electric bicycles, especially when considering older cyclists who experience more difficulties with active bicycle stability control.

7.1. Introduction

The emergence of the electric bicycle has enhanced the mobility of cyclists, in particular less mobile cyclists such as older cyclists or persons with disabilities. Furthermore, the cycling range has been extended without fatiguing the cyclist, with the support of a battery and electric motor. The electric bicycle has become a popular means of transportation, it promotes health and wellbeing and replaces short car rides. However, some barriers of purchasing an electric bicycle have been reported by Jones et al.: the increased weight of the bicycle, the battery life, the increased price, social stigmas and limitations of the infrastructure [154]. The use of the electric bicycles is also associated with an increased risk of injury due to a crash [12]. In order to ensure the further acceptance of the electric bicycle as a replacement for the conventional bicycle and short car rides, improvement of safety is necessary.

Findings of recent studies indicate that older cyclists may encounter difficulties in controlling the bicycle in situations that require active stabilisation control. These studies showed that older cyclists (>65) showed larger steering movements and lateral movements of the bicycle, compared to a younger control group [109, 155]. Furthermore, another study showed that cyclists from the age of 55 can be seen as a transition group, as they showed difficulties in bicycle control at low speeds and used different control mechanisms compared to younger cyclists [128]. Therefore, safety of especially older cyclists can be improved by using assisting add-ons that not only assist in pedalling power, but also assist in active bicycle stability control.

The electric bicycle goes through constant technical development. These developments are focused on comfort [156], model-based assistance control design [157], improvement of battery life and lighter batteries. Some recent studies focus on the safety aspects as well. For example, Maier et al. aims to develop an active braking dynamics assistance system for electric bicycles [158]. However, the effect of electric bicycle hub motors on the bicycle's lateral stability have not been scientifically examined yet.

In recent years, computer simulation proved to be a useful tool for studying bicycle self-stability [21, 28, 54, 105], but also for development of stabilization systems on bicycles [159, 160]. Different stabilisation systems have been tested, for example Liu et al. used a parallel mechanism that adjusts stability [161], while Lee et al. developed a bicycle that self-stabilizes with mass balancing [162]. In this paper the effect of electrical hub motors on the bicycles stability is investigated, using an advanced multi-body model of the bicycle dynamics, passive cyclist dynamics and the tire dynamics developed in the commercial

software ADAMS [121]. The computer model and the used system-identification method to obtain the stability parameters have been validated against the Carvallo-Whipple model [23, 24] with the benchmark [25] parameters. Good comparison has been found [121], therefore the model is suitable to use for testing the effect of add-ons, such as electrical hub motors, on the bicycle's stability.

Different configurations exist that are used to mount the electric motor onto the bicycle; one can choose between a front wheel drive, rear wheel drive and chain drive. Each of these choices has its advantages and disadvantages. It can be expected that there will be differences regarding its effect on stability. Furthermore, using electric hub motors could provide opportunities for improving stability, as was shown by Karagol et al. with four-wheeled vehicles [163]. They showed that an active torque distribution system in cars achieves vehicle stability control. From previous studies [38, 164], it can be expected that the use of traction and braking and different wheel driving methods on electric bicycle hub motors can improve the stability of electric bicycles.

Therefore, the goal of this study is twofold: the first one is to scientifically prove that using a rear wheel hub motor is better than using a front wheel hub motor. The second goal is to show that two hub motors that work simultaneously can improve the bicycle stability.

7.2. Methods

7.2.1. Model description

In this study an open-loop bicycle-cyclist model, which was developed in the commercial multi-body software ADAMS was used [121]. The parameters of the bicycle model were based on a city bicycle with low entry (Twade) and are given in the Appendix A.1 (Bicycle 1 in Table A1). Figure 7.1 shows the bicycle-cyclist model, containing 8 rigid bodies in total: the rear frame and front frame of the bicycle, the two wheels and the pelvis, two legs and the upper-body (containing the trunk, head and arms) of the cyclist. The tire-road contacts were modelled as force-torque generating systems, using Pacejka's Magic Formula [57], see [121] for a detailed description. The tire model parameters were based on measurements performed on a rotating disk machine [62], and are presented in Appendix A.2. The bicycle-cyclist model contains the following degrees of freedom: a rotation around the steering axis, rotation of the two wheels around their wheel axes, three rotational degrees of freedom of the upper-body with respect to the pelvis of the cyclist and one rotational degree of freedom of each leg, around the hip-ankle axis. The movements of the cyclist were restricted with passive spring/dampers to represent a passive cyclist.

The electric bicycle hub motors were simulated in the model by applying torques that act between the bicycle frame and the wheel axis, see Figure 7.2.

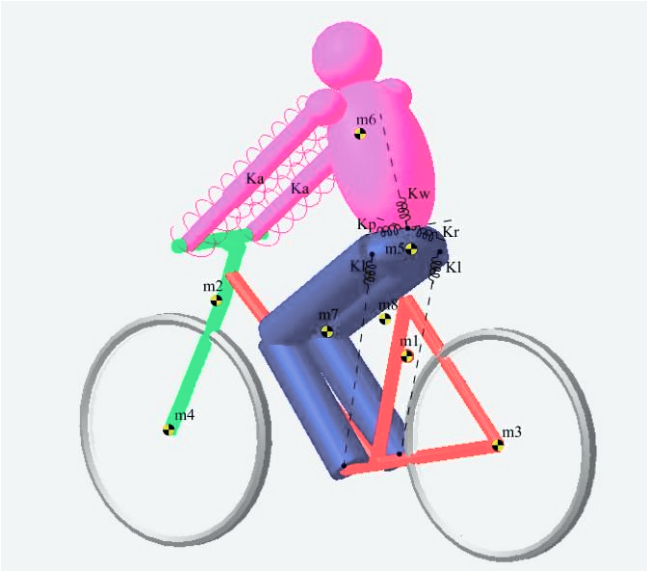

Figure 7.1. *Open-loop bicycle-cyclist model [121] developed in the commercial multi-body dynamic software Adams.* m1*= rear frame,* m2 *= front frame,* m3 *= rear wheel,* m4 *= front wheel,* m5 *= pelvis,* m6 *= upper body,* m7 *= left leg,* m8 *= right leg.* Ka *= arm linear spring/damper,* Kl *= leg rotational spring/damper,* Kp, Kw, Kr *rotational spring/dampers at the L4L5 joint position in respectively the lateral, anterior/posterior and vertical direction.*

7.2.1 Simulations

The effect of using electric hub motors on the stability and behaviour of the bicycle-cyclist system was analysed during straight cycling and during a cornering movement. First, the difference in self-stability of the bicycle-cyclist system when using a front and a rear motor was analysed, using the linearization method described in 7.2.2.1. Next, the difference in behaviour of the system when using a front or rear motor was shown with the example of a cornering movement (described in section 7.2.2.2).

Furthermore, simulations were performed using two motors simultaneously, that show improvement of the bicycle self-stability. The bicycle stability can be increased by applying an additional traction force on the rear wheel and a braking force on the front wheel at the same time, see Figure 7.2. These are applied as torques around the wheel centers and are of equal value, so no change in the net longitudinal force occurs (hence the forward speed does not change). The weave speed was analysed for different values of the motor torque.

7.2.2 Analysis

7.2.2.1 Stability during straight cycling

Time domain signals were recorded during the simulation of a straight running bicycle that was driven by either a torque around the rear wheel axis or around the front wheel axis (simulating the rear wheel drive and front wheel drive electric motors). A PD-controller was used to get up to the desired forward speed. When the bicycle-cyclist system was moving forward at the required speed, a lateral disturbance was applied to the rear frame at the position of the centre of mass (CoM). The time signals that were saved for each run were: the roll angle, the steering angle and the forward speed. These signals were exported to Matlab and a system identification method was used to estimate a state-space model with four poles. The input to the state-space model was the disturbance signal and the roll and steering angle were the two outputs. With this method the weave and capsize mode can be analysed, as was shown in [121]. The open-loop bicycle-cyclist model in ADAMS as well as the system identification method were previously validated with the Carvallo-Whipple Bicycle model. The lowest speed at which the weave oscillations are damped, is called the weave speed. This speed is used in this paper as an indication of the stability of the open-loop bicycle-cyclist model, which has been done before in several other studies [35, 165, 166]. The bicycle can be considered unstable when moving forward at a speed lower than the weave speed.

7.2.2.2. Cornering movement

To analyse the behaviour of the bicycle-cyclist system during a cornering movement a steering controller was used that steered the bicycle into a corner. An initial small steering movement was applied to initiate the cornering movement (a steering angle of 1.5 degrees during 0.2 sec.). Next, a steering controller kept the bicycle roll angle on an approximate constant value. After the steering controller stopped, the behaviour of the system was analysed by looking at the time domain signals of the steering angle, the roll angle, the yaw angle and the forward velocity.

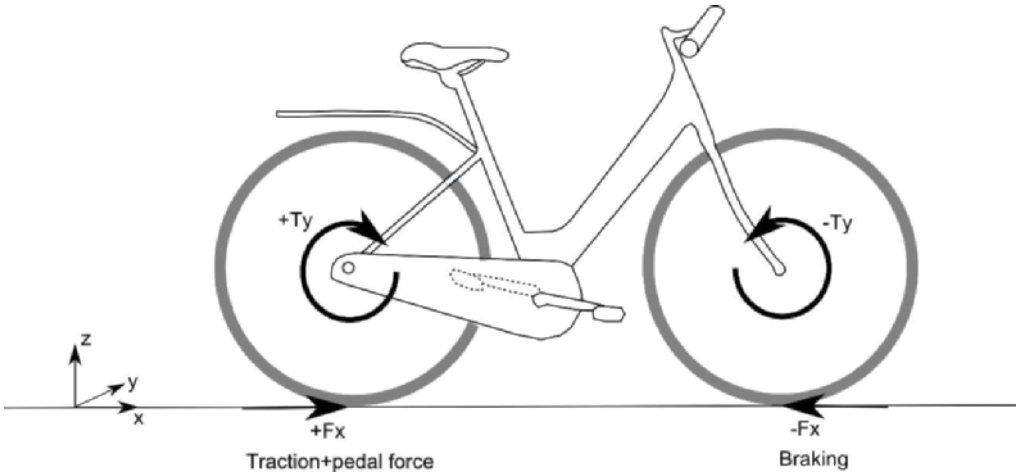

Figure 7.2. *The two-motor system to improve bicycle stability: the front motor generates a braking force, while at the same time the rear motor generates an equal traction force.*

7.3. Results

7.3.1. One motor

The stability of the open-loop bicycle-cyclist system with a rear wheel hub motor and a front wheel hub motor was analysed using the system identification method described above. The weave speeds were found to be quite similar, the one of the rear wheel motor being a bit lower: 8.34 m/s against 8.39 m/s for the front wheel motor case. This is an insignificant difference.

This result indicates that the position of the hub motor did not influence the stability much during straight cycling. However, more effect on the behaviour of the cyclist-bicycle system was shown with the simulation of an example cornering movement. Figure 7.3 shows the in- and output time signals of this simulation for the following three cases: a. no extra hub motor torque was added, b. a (positive) front motor torque was added, c. a (positive) rear motor torque was added.

The cornering movement was initiated by a short steering movement at t=3 s, then the steering torque controller steers and keeps the bicycle in the corner. At t=7.5 s the steering torque controller was switched off.

Figure 7.3.a shows that the system becomes unstable when the steering torque was switched off and no other control was considered. Figure 7.3.b shows the effect on the behaviour of the system when a front wheel torque of 80 Nm was added after the steering

torque controller was switched off. The front wheel torque caused an increase in speed and a small increase in stability, but the system is still unstable. Figure 6.3.c shows the response of the system in case a rear wheel torque of 80 Nm was added. The same increase in forward speed was observed, and in addition a stabilization of the cyclist-bicycle system occurred (the amplitude of the steering and roll angle decreased over time).

a.

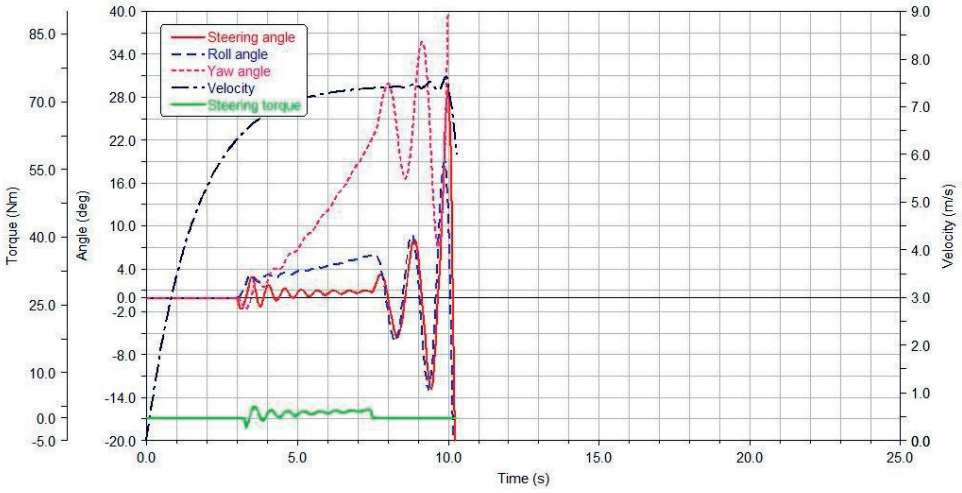

b.

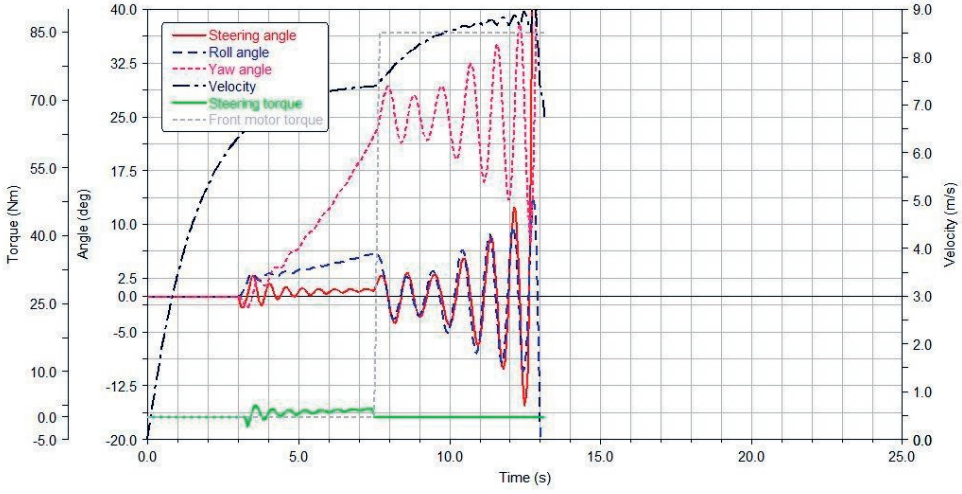

c.

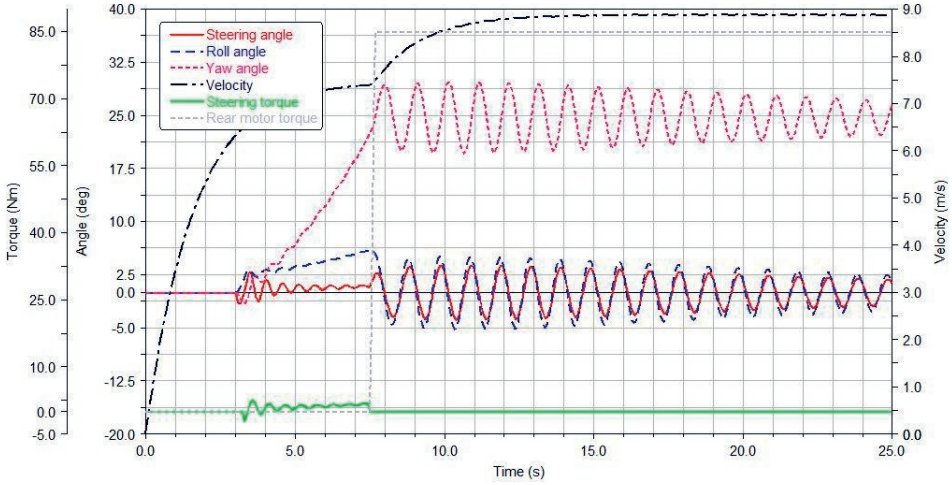

Figure 7.3. *Time signals of a cornering simulation of the bicycle-cyclist system, with input: steering torque and outputs: steering angle, roll angle, yaw angle, velocity.* ***a.*** *no extra hub motor torque was added,* ***b****. a (positive) front motor torque was added,* ***c.*** *a (positive) rear motor torque was added.*

7.3.2. Two motors

With the previous simulations with one motor it was shown that traction of the rear motor could lead to increased stability. The following figures show the results of using a constant braking torque of the front motor while simultaneously applying a constant traction torque with the rear motor. In this way, the forward speed is not influenced, as the braking and traction force had the same value.

Figure 7.4.a shows the roll and steering angle of a straight riding passive bicycle-cyclist system riding at 7 m/s, after a lateral disturbance at t = 15 s. The oscillations with increasing amplitude indicates that the (weave mode of the) system was unstable. Figure 7.4.b shows that a torque of 80 Nm applied simultaneously by the two motors was able to stabilize the system. The constant motor torques were turned on right after the disturbance at t = 15 s and turned off again at t = 20 s. Figure 7.4.c shows the same result, however here the 2 motors were working during the whole simulation.

a. b. c.

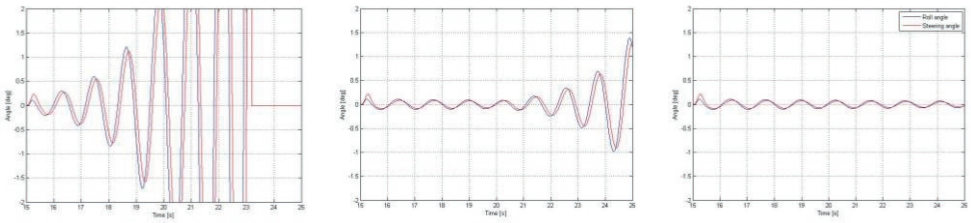

Figure 7.4. *Effect of Two motor system on the roll and steering angle during a simulation of an uncontrolled straight-running simulation at v = 7 m/s.* ***a.*** *without the two motor torque,* ***b.*** *the two motors were turned off at t = 20 s.* ***c.*** *the two motor system turned on (80 Nm).*

Different values of the motor torques were tested and the weave speed was obtained by fitting a state-space model on the time-domain signals. In Figure 7.5 the weave speed was plotted for motor torques up to 100 Nm. The relation between the weave speed and the motor torque was close to a linear relationship. It was shown that by using two motor torques of 100 Nm, the weave speed can decrease by almost 23 %.

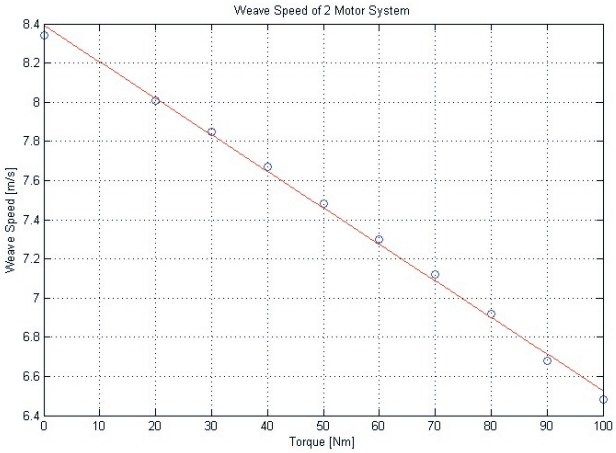

Figure 7.5. *The motor torque of the 2 motor system against the weave speed (speed at which the weave mode stabilizes).*

7.4. Discussion

In this study, an advanced bicycle-cyclist model was used to predict the effect of using electrical bicycle hub motors on the self-stability of the bicycle-cyclist system. It was shown that this model can be used for design purposes and to predict behaviour of add-ons on

electric bicycles that improve safety aspects. The following two issues were analysed with the use of an advanced bicycle-cyclist multi-body dynamic model: - to scientifically prove that using a rear wheel hub motor is better than using a front wheel hub motor regarding bicycle stability, - to show that with using two hub motors simultaneously the bicycle stability can be improved.

The model and the linear analysis method that were used in this study were previously validated [121]. Next to that, non-linear simulations were performed during a cornering movement. In these simulations, some control of the cyclist was considered. However, more work should be done to improve and validate the cyclist control model. Likewise, the biomechanical cyclist model needs validation. However, the presented model can be used to show a proof-of-principle. In this model, the pedalling movement of the cyclist is not taken into account. Addition of this movement of the cyclist in the model could change the behaviour of the system and may affect the control actions of the cyclist.

The weave speed was used as a measure for dynamic stability of the system. At cycling speeds above the weave speed the bicycle-cyclist system was considered dynamically stable. However, this does not necessarily mean that it is safer or feels better for the cyclist cycling on a bicycle that is dynamically more stable. Therefore, elaboration of the model with realistic cyclist control is necessary and furthermore, physical tests are needed to obtain subjective feedback from cyclists.

Some preliminary physical tests with subjects cycling on an electric bicycle with the two-motor system add-on, have already been conducted. The first feedback of the cyclists that tested the bicycle with additional rear motor traction and front motor braking were positive. The bicycle felt more stable than without the two-motor system. One drawback of the system were the high forces on the front fork due to the applied braking torque. These caused a fracture of the front fork. Another drawback was the short battery life due to high energy usage of the two motors.

One solution for the high loss of energy of the two-motor system could be regenerative brakes. The kinetic energy used for braking makes the wheels turn the motor and the motor produces electricity that can be stored in the battery.

The results in this paper scientifically prove that regarding stability, a rear hub motor is better than a front hub motor. It can therefore be expected to be safer, for especially older cyclists, to use a rear hub motor instead of a front hub motor.

Secondly, we showed that the principle of braking with the front motor and simultaneously traction with the rear motor enhances bicycle stability. Using two motors as an electric bicycle add-on, not only provides the benefits of the current electric bicycle, like assistance in pedalling power. It also assists in active bicycle stability control.

When implementing the two-motor system as an electric bicycle add-on for enhancement of safety, a motor controller could be needed. This motor controller should control both motors and calculate the necessary torques to apply them at the right time. Important inputs for this controller could be the forward speed and the roll and steering angle of the bicycle.

7.5. Conclusion

The results of our computer simulations show that a rear wheel hub motor is better than a front hub motor, with respect to the bicycle's lateral stability.

Furthermore, it was shown that the self-stability of a passive bicycle-cyclist system can be improved by using a rear wheel hub motor and a front wheel hub motor simultaneously. The front wheel motor is used for braking, while the rear wheel motor is used for traction. Using two motors as an electric bicycle add-on, not only provides the benefits of the current electric bicycle, like assistance in pedalling power. It also assists in active bicycle stability control and can therefor improve the safety of electric bicycles, especially when considering older cyclists who experience more difficulties with active bicycle stability control.

The simulations conducted in this research were performed in the commercially available software ADAMS. The results indicate that this bicycle-cyclist model could be further used to analyse and predict safety of cyclists in various situations.

Chapter 8

General Discussion

Bicycling stability depends on many different factors, such as the bicycle dynamics which are influenced by bicycle parameters, for instance the wheel radius, mass distribution or head angle. The tire-road contact is the only contact of the bicycle-cyclist system with its environment and therefore influences its behaviour. But most importantly the cyclist's behaviour influences the dynamics of the system. Also, passive biomechanical properties such as arm stiffness and mass influence stability, as well as the posture of the cyclist play a role. The cyclist controls the stability of the system by applying interaction forces to the bicycle at different contact points such as the saddle, handlebars and pedals and by displacement of mass and body parts with respect to the bicycle.

When ageing, physiological changes take place in the human body, loss or deterioration of functions occur that can be associated with balance control. These include a diminishment of vision after the age of fifty which could lead to misjudgements, a diminished accuracy of sensory systems, like the vestibular organ and proprioception systems and a decrease in muscle strength and reaction time [167, 168] . These age-related physiological changes have been related to balance loss in gait and posture [153, 169, 170] and therefore effect bicycling stability too. A previous study associated a higher workload of older cyclists to increased accident risk [113].

There is an increased accident-risk for persons over fifty-five [103]. However, cycling contributes to improved health and quality of life and is therefore encouraged in people of all ages [90]. Therefore, improving the safety of older cyclists is important to enable them to keep cycling.

This thesis contributes to the problem of cycling safety of older cyclists. By improving, testing and validating existing multi-body models, the behaviour of older cyclists was predicted and design guidelines were formed for developing safer bicycles.

8.1. Summary of key findings

In chapter 3 an advanced 3D open-loop bicycle-cyclist multi-body model was presented that was developed in the commercial software ADAMS. The model includes a parametrized bicycle model, a tire-road contact model based on measurements performed by the Motorcycle Dynamics Group of the University of Padova, to identify the mechanical properties of bicycle tires. The cooperation with this research group resulted in a dataset that was used to derive the coefficients needed for the Magic Formula of the Pacejka Model for bicycle tires. The paper presenting these data can be found in [62], furthermore, the

files that can be used to import the derived bicycle tire model in the software ADAMS are available for download.

Simulations with the 3D open-loop bicycle-cyclist multi-body model showed that inflation pressure had a small effect on stability, whereas the tire load had a large effect. Therefore, this load-dependency of the tire parameters is included in the model. Extending simplified models with a realistic tire model leads to a notable decrease in the weave stability and a stabilization of the capsize mode. This effect is mainly caused by the twisting torque.

A sensitivity study of cyclist parameters showed that body stiffness and damping have a small effect on bicycle stability, whereas arm stiffness destabilizes the capsize mode and arm damping destabilizes the weave mode. Tire properties and cyclist properties interacted with each other, therefore it is important to incorporate both in the model.

For the studies presented in chapter 4, 5 and 6 a novel laboratory cycling set-up was developed to apply controlled perturbations. This led to a unique extensive dataset of 15 healthy young and 15 older subjects cycling under normal and perturbed conditions at different cycling speeds. The dataset contains full kinematic data of the bicycle and cyclist and 3D interaction forces at all contact points between the cyclist and bicycle. This data is freely available for other researchers on request, for instance for validating their bicycle-cyclist models.

Time domain analysis showed that older cyclists used more knee movements for balance control compared to younger cyclists and there was increased time delay between roll and steering angles. The frequency analysis revealed more differences between the two age groups; older cyclists needed more effort to counteract high frequency perturbations and younger cyclists used less steering power, but seemed to use more trunk sway. Increased inter-individual variations for older adults indicates that the older participants can be seen as a transition group in terms of physical fitness.

In chapter 5 the complex 3D interaction forces between the bicycle and cyclist were analysed and used in order to validate the cyclist model. It was shown that the cyclist uses more pushing on the handlebars than pulling, while steering and balancing the bicycle. The lateral handlebar forces increased at lower speeds, which can be related to more steering actions and increased co-contraction of upper-arm muscles. The measured bicycle-cyclist interaction forces and measured 3D kinematics were used to validate a bicycle-cyclist interaction computer model. Resultant forces of 8-19% of the maximum force magnitude were used to ensure dynamic consistency of the model. These resultant forces can be

related to inaccuracies of the experimental data and modelling assumptions. Accurately measuring the pedal forces and increased subject-specific modelling could increase the validity of the model.

In chapter 6 a closed-loop cyclist balance control model was developed for young and older cyclists. The steering and upper-body lean control can be modelled with a PD controller with time delay, whereas the outward knee control was limited to low frequencies. The results suggest that the upper body lean control is reflex-like, while the steering control uses visual feedback loops. Differences in the time delays between younger and older cyclists were found. Higher time delays were seen in older cyclists and they also seem to use more knee control. The identified parameters can be used in cyclist control models.

With the use of the developed open-loop bicycle-cyclist multi-body model it was shown in chapter 7 that regarding stability, a rear hub motor is better than a front hub motor. It can therefore be expected to be safer, for especially older cyclists, to use a rear hub motor instead of a front hub motor. Furthermore, it was shown that the principle of braking with the front motor and simultaneous traction with the rear motor enhances bicycle stability. Using two motors as an electric bicycle add-on not only provides the benefits of the current electric bicycle, like assistance in pedalling power, but also assists in active bicycle stability control.

Computer simulations performed with the developed model of this thesis were also used in the development of the SOFIETS, the bicycle developed by the company Indes in cooperation with the project partners of the SOFIE-project (Roessingh R&D and the University of Twente). This bicycle is created to increase the cycling safety of older cyclist, see the Appendix A5 for the brochure of the SOFIETS (made by Indes, in Dutch).

8.2. Bicycle-cyclist models

The contribution of this thesis is partly in the improvement of the tire-road contact model and testing of the effect of tire parameters on the bicycle stability. In motorcycle dynamics, there are already more advanced models compared to bicycle dynamics. This thesis works towards the development of similarly advanced bicycle models. The mechanical properties of the bicycle tires were measured and were used to identify the coefficients of the Pacejka tire model. In previous studies [46], the tire-road contact was also measured, but did not test the effect of tire parameters on bicycle stability. It was also the first time to conduct a sensitivity study of the passive parameters of the cyclist in combination with the tire-road contact model. In the developed model, the three balance control models were identified

that were previously discussed. The differences between older and younger cyclists were successfully modelled, by identifying the difference in control parameters for these two groups. All of these findings can be carried over to even more advanced models of bicycle stability and help to predict the behaviour of older cyclists, thereby giving more insights in this behaviour and ways to improve safety.

Modelling of lumped arms could be included in future models with active muscles to incorporate the lateral forces that were measured on the handlebars. These forces are missing in simplified models that model the arms as a spring-damper system. Muscle tension continuously changes in real-life situations and affects the arm stiffness. The muscle activities in the arms (EMG) were measured during the cycling experiments, which is a step in the direction of future, more advanced models.

Modelling the cyclist's control was one of the most challenging parts in the development of the bicycle-cyclist model. Few studies have been conducted on this topic and there is still much to learn in this area. With the experiments of this study, it was possible to identify a SIMO balance control model that gives more insight into the differences of behaviour between younger and older cyclists. However, this model is a simplified representation of cyclists' behaviour. There was no differentiation between intrinsic dynamics and active control. This can be accomplished by either using a MIMO identification or by doing more EMG measurements of for instance the trunk muscles. This thesis worked towards performing a MIMO identification and have gained datasets with two perturbations which could be used for this. With these datasets, it would be possible to differentiate between heading and balance control. It was difficult to distinguish the two perturbations since the perturbations were very alike and since there was a high correlation between heading and balance. Therefore, identification of a MIMO model is left for future research.

8.3. Effect of aging on bicycling safety

Another research objective was to study the effect of aging on bicycling stability. During the cycling experiments, the limit of the older cyclists' capabilities was not yet found. The older subjects that participated in this experiment were also relatively young. Both of these factors contribute to lessen the findings, which is why greater differences between younger and older subjects can be expected, when even older subjects are used in experiments and when the older subjects can perform even more difficult cycling tasks during the experiments while the subjects' safety and perception of safety stays guaranteed. During the experiments, the greatest difficulty was the fear of falling and perception of safety by the older subjects. The first goal was to include persons of age sixty-five and up for the

older age-group, however this was not possible since the subjects were unable to perform the cycling tasks on the relatively small treadmill. This is why the age-limit had to be dropped to fifty. A bicycle simulator could be used to remedy this problem, because subjects tend to feel safer in a simulator. In order to design a realistic simulator, realistic bicycle models are needed that simulate the bicycle's behaviour. One step in this direction is to include realistic tire-road contact models and 3D bicycle-cyclist interaction forces. Note that this will only be possible if the bicycle dynamical models, tire-road contact models and bicycle-cyclist models are sufficiently validated, in order to develop a realistic bicycle simulator. If this is not the case, the experiments will not accurately show the performance and limitations of older cyclists.

From the results of chapters 4 and 6, already a difference in cycling behaviour between younger and older cyclists can be seen. It was noted that older subjects had more difficulty cycling on the experimental set-up, especially at low speeds. An increased time-delay between roll and steering angles of the older cyclists was found, compared to the younger cyclists. Moore et al. [148] showed that with decreasing speeds more upper-body and lateral knee movements are used by cyclists. This study showed that older cyclists revert to additional balance control actions at a higher speed than younger subjects. This suggests that they were not able anymore to balance the bicycle with only steering actions. At lower speeds, higher control gains are necessary and in combination with an increased reaction time this could lead to balance difficulties. The neural time delays for upper-body lean control movements were much shorter than the neural time delay found for steering. This could explain the need to use these reflexive additional control mechanisms at low speed and difficult cycling situations. Furthermore, older subjects have more difficulty in performing double tasks [171], that also contributes to the perceived difficulty when cycling on the laboratory set-up.

8.4. Design guidelines for improvement of bicycling safety & Practical applications

The goal of developing advanced bicycle-cyclist computer simulation models is to use them to design guidelines for improvement of bicycling safety. Many parameters influence cycling stability and safety, and complex interactions between these parameters exist, as was shown in chapter 3. It is not straightforward to define the parameters that influence stability most, because of these interactions. A 'Design of Experiment' approach, i.e. testing the effects of all parameters could show the most important parameters and interactions of the parameters. In order to perform a design of experiments study, a measure of stability/safety is necessary which is then optimized. The results of this study imply that an

improvement of the stability at low speeds would improve the cycling safety of older cyclists. With the use of the open-loop bicycle-cyclist model of chapter 3 simulations have been performed within the SOFIE project to find a bicycle geometry that decreases the weave speed. This resulted in the adapted geometry of the SOFIE bicycle. The SOFIE bicycle has a larger head angle, short trail, small wheels and short wheelbase. Other improvements were an automatic adjustable saddle height and a drive-off assistance (see Appendix A5). The drive-off assistance helps to decrease the time to reach a stable cycling speed while driving off. The automatic adjustable saddle height is particularly helpful during mounting and dismounting.

The SOFIE bicycle was tested by nine older cyclists. A majority of the subjects experienced the bicycle as supportive and comfortable. Objectively it was found safer during various cycling tasks [172]. The older cyclists showed reduced steering actions and less lateral leg movements while cycling the SOFIE bicycle compared to the conventional bicycle. These results are in accordance with the findings of chapter 4 and 6. The SOFIE-project led to the design of a bicycle that was found successful for its purpose and its target audience.

One of the other solutions that was tested within the SOFIE project was the two-motor solution described in chapter 7. This solution also decreases the weave speed of the bicycle-cyclist system. The computer simulation study shows a proof-of-principle, while preliminary physical tests are also positive. During the SOFIE project a cooperation with the company Jyrobike was started to simulate and test their gyrowheel solution for children's bicycles and scaling this idea up to adult bicycles in order to improve safety of older cyclists.

The conventional bicycle is up for further improvement. The electric bicycle is already an improvement and helps elderly to move more easily and faster when physical fitness decreases. They assist in pedalling power and extent the cycling range of older cyclists. However, the electric bicycle is also associated with an increased injury risk due to a crash [12], so improvement of safety is also needed. This is something that is already possible, but with the design of bicycles we also need to take care of social stigmas. People do not like to ride a bicycle that looks different or 'for the elderly'. Therefor the new designed safer bicycles should look similar to the conventional bicycle, as was accomplished with the design of the SOFIE bicycle and the two-motor system.

With these design guidelines, it was shown in this thesis that computer simulation models are a useful tool to help in bicycle design. Furthermore, it was shown that not always the most complex models are needed to improve cycling safety. Simulations with an open-loop

bicycle-cyclist model were used to improve bicycle stability at low speeds. However, when testing complex situations more complex models are necessary.

8.5. Recommendations for further research

In this thesis, an open-loop bicycle-cyclist dynamical model and a cyclist balance control model have been developed. The next step would be to combine these two models and compare the simulation results of the total model with experimental data. This will be an important step towards validation of bicycle-cyclist models. A design of experiments method can be used to find relations between parameters and to optimize the output.

To further validate the bicycle model with the tire-road contact model, a similar approach as in chapter 4 can be used. Measured interaction forces and motions of the cyclist can be used as an input to the bicycle model, and a tracking agent can be used to estimate the error between the model and experimental data. Next, an optimization of the parameters within a certain boundary could be used to improve the agreement between the model and experiments. Different models with differing complexity could be used to test the needed complexity of the model to ensure good comparison with the experimental data. One important direction will be the development of an active lumped arm model.

The development of a bicycle simulator will be useful to test more extreme cycling situations, which are still safe for older cyclists. In this way, the limits of their cycling capabilities can be reached, which will lead to more insights in the differences and problems of older cyclists.

Machine learning techniques could be used to predict whether a cyclist has an increased risk of injury, when comparing datasets of cyclists' behaviour.

Bibliography

1. Hendriksen, I. and R. van Gijlswijk, *Fietsen is groen, gezond en voordelig.* Leiden: TNO, 2010.
2. voor de Statistiek (CBS), Centraal Bureau, *Mobility dutch population per region for motive and means of transportation*. (2007).
3. Tacken, M., *Mobility of the elderly in time and space in the Netherlands: An analysis of the Dutch National Travel Survey.* Transportation, 1998. **25**(4): p. 379-393.
4. Rejeski, W.J. and S.L. Mihalko, *Physical activity and quality of life in older adults.* The Journals of Gerontology Series A: Biological sciences and medical sciences, 2001. **56**(suppl 2): p. 23-35.
5. Weijermars, W., N. Bos, and H.L. Stipdonk, *Serious road injuries in the Netherlands dissected.* Traffic injury prevention, 2016. **17**(1): p. 73-79.
6. van Loon, I., Broer, K., *Fietsen zo lang het kan (in Dutch)*. 2006.
7. Steffens, U., et al., *Ältere Menschen als Radfahrer.* BERICHTE DER BUNDESANSTALT FUER STRASSENWESEN. UNTERREIHE MENSCH UND SICHERHEIT, 1999(112).
8. BERNHOFT, I., et al., *MORTAL ACCIDENTS WITH CYCLISTS.-MINUTE ANALYSIS OF FREQUENT TYPES OF ACCIDENTS 1986-90.* NOTAT, 1993(4/1993).
9. Scheiman, S., et al., *Bicycle injury events among older adults in Northern Sweden: a 10-year population based study.* Accident Analysis & Prevention, 2010. **42**(2): p. 758-763.
10. Mori, Y. and M. Mizohata, *Characteristics of older road users and their effect on road safety.* Accident Analysis & Prevention, 1995. **27**(3): p. 391-404.
11. W. Ormel, K.K.W., P. den Hertog *Enkelvoudige fietsongevallen (in Dutch)*, C.e. Veiligheid, Editor. 2009, Rijkswaterstaat Dienst Verkeer en Scheepvaart (RWS DVS).
12. Schepers, P., et al., *An international review of the frequency of single-bicycle crashes (SBCs) and their relation to bicycle modal share.* Injury prevention, 2014: p. injuryprev-2013-040964.
13. Ikemoto, Y., W. Yu, and J. Inoue. *A study on balance maintenance strategies during walking-A simulation study*. in *Engineering in Medicine and Biology Society, 2008. EMBS 2008. 30th Annual International Conference of the IEEE*. 2008. IEEE.
14. Iqbal, K. and A. Roy, *A novel theoretical framework for the dynamic stability analysis, movement control, and trajectory generation in a multisegment biomechanical model.* Journal of biomechanical engineering, 2009. **131**(1): p. 011002.
15. van der Kooij, H., E. van Asseldonk, and F.C. van der Helm, *Comparison of different methods to identify and quantify balance control.* Journal of neuroscience methods, 2005. **145**(1): p. 175-203.

16. Peterka, R.J., *Simplifying the complexities of maintaining balance.* IEEE Engineering in Medicine and Biology Magazine, 2003. **22**(2): p. 63-68.
17. Patla, A., J. Frank, and D. Winter, *Assessment of balance control in the elderly: major issues.* Physiotherapy Canada, 1990. **42**(2): p. 89-97.
18. Tinetti, M.E., *Performance-oriented assessment of mobility problems in elderly patients.* Journal of the American Geriatrics Society, 1986. **34**(2): p. 119-126.
19. Chen, C.-K., T.-S. Dao, and C.-K. Yang, *Turning dynamics and equilibrium of two-wheeled vehicles.* Journal of mechanical science and technology, 2005. **19**: p. 377-387.
20. Schwab, A., J. Meijaard, and J. Kooijman. *Some recent developments in bicycle dynamics*. in *Proceedings of the 12th IFToMM World Congress*. 2007.
21. Limebeer, D.J. and R.S. Sharp, *Bicycles, motorcycles, and models.* Control Systems, IEEE, 2006. **26**(5): p. 34-61.
22. Schwab, A., J. Meijaard, and J. Kooijman, *Lateral dynamics of a bicycle with a passive rider model: stability and controllability.* Vehicle system dynamics, 2012. **50**(8): p. 1209-1224.
23. Carvallo, M., *THEORIE DE MOUVEMENT DU MONOCYCLE ET DE LA BYCYCLETTE*. 1901.
24. Whipple, F.J., *The stability of the motion of a bicycle.* Quarterly Journal of Pure and Applied Mathematics, 1899. **30**(120): p. 312-321.
25. Meijaard, J.P., et al., *Linearized dynamics equations for the balance and steer of a bicycle: a benchmark and review.* Proceedings of the Royal Society A: Mathematical, Physical and Engineering Science, 2007. **463**(2084): p. 1955-1982.
26. Schwab, A.L., J.P. Meijaard, and J.M. Papadopoulos, *Benchmark results on the linearized equations of motion of an uncontrolled bicycle.* Journal of mechanical science and technology, 2005. **19**(1): p. 292-304.
27. Kooijman, J., A. Schwab, and J. Meijaard, *Experimental validation of a model of an uncontrolled bicycle.* Multibody System Dynamics, 2008. **19**(1-2): p. 115-132.
28. Kooijman, J., et al., *A bicycle can be self-stable without gyroscopic or caster effects.* Science, 2011. **332**(6027): p. 339-342.
29. Fajans, J., *Steering in bicycles and motorcycles.* American Journal of Physics, 2000. **68**(7): p. 654-659.
30. Jones, D.E., *The stability of the bicycle.* Physics today, 1970. **23**(4): p. 34-40.
31. Åström, K.J., R.E. Klein, and A. Lennartsson, *Bicycle dynamics and control.* IEEE Control Systems Magazine, 2005. **25**(4): p. 26-47.
32. Herfkens, B., *De stabiliteit van het rijwiel ("The stability of the bicycle")*. 1949, Instituut voor Rijwielontwikkeling 's-Gravenhage.
33. Franke, G., W. Suhr, and F. Rieß, *An advanced model of bicycle dynamics.* European Journal of Physics, 1990. **11**(2): p. 116.
34. Tak, T.-O., J.-S. Won, and G.-Y. Baek. *Design sensitivity analysis of bicycle stability and experimental validation*. in *Proceedings, bicycle and motorcycle dynamics 2010 symposium on the dynamics and control of single track vehicles*. 2010.
35. Moore, J. and M. Hubbard, *Parametric study of bicycle stability (P207)*, in *The Engineering of Sport 7*. 2008, Springer. p. 311-318.

36. Papadopoulos, J.M., *Bicycle steering dynamics and self-stability: a summary report on work in progress.* Cornell Bicycle Research Project, Cornell University, 1987: p. 1-23.
37. Basu-Mandal, P., A. Chatterjee, and J.M. Papadopoulos. *Hands-free circular motions of a benchmark bicycle*. in *Proceedings of the Royal Society of London A: Mathematical, Physical and Engineering Sciences*. 2007. The Royal Society.
38. Limebeer, D.J., R. Sharp, and S. Evangelou, *The stability of motorcycles under acceleration and braking.* Proceedings of the Institution of Mechanical Engineers, Part C: Journal of Mechanical Engineering Science, 2001. **215**(9): p. 1095-1109.
39. Sharp, R.S. and D.J. Limebeer, *A motorcycle model for stability and control analysis.* Multibody system dynamics, 2001. **6**(2): p. 123-142.
40. Sharp, R., S. Evangelou, and D.J. Limebeer, *Advances in the modelling of motorcycle dynamics.* Multibody system dynamics, 2004. **12**(3): p. 251-283.
41. Cain, S.M. and N.C. Perkins, *Comparison of experimental data to a model for bicycle steady-state turning.* Vehicle System Dynamics, 2012. **50**(8): p. 1341-1364.
42. McGuan, S.P., *Active human surrogate control of a motorcycle: Stabilizing and de-stabilizing*. 1993, SAE Technical Paper.
43. Cossalter, V., et al. *An advanced multibody model for the analysis of motorcycle dynamics*. in *International conference on mechanical engineering and mechanics, Beijing, China*. 2009.
44. Popov, A., S. Rowell, and J.P. Meijaard, *A review on motorcycle and rider modelling for steering control.* Vehicle System Dynamics, 2010. **48**(6): p. 775-792.
45. Sharma, H.D., S.M. Kale, and N. Umashankar. *Simulation model for studying inherent stability characteristics of autonomous bicycle*. in *Mechatronics and Automation, 2005 IEEE International Conference*. 2005. IEEE.
46. Dressel, A. and A. Rahman, *Measuring sideslip and camber characteristics of bicycle tyres.* Vehicle system dynamics, 2012. **50**(8): p. 1365-1378.
47. Papadopoulos, J.M. *Critique of assumptions underlying bicycle handling research*. in *Bicycle and Motorcycle Dynamics. Symposium on the Dynamics and Control of Single Track Vehicles, TU Delft, the Netherlands*. 2010.
48. Meijaard, J. and A. Schwab. *Linearized equations for an extended bicycle model*. in *III European Conference on Computational Mechanics*. 2006. Springer.
49. de Vries, E. and J. den Brok, *Assessing slip of a rolling disc and the implementation of a tyre model in the benchmark bicycle.* 2010.
50. Koenen, C., *The dynamic behaviour of a motorcycle when running straight ahead and when cornering*. 1983.
51. Cossalter, V., R. Lot, and F. Maggio, *The influence of tire properties on the stability of a motorcycle in straight running and curves*. 2002, SAE Technical Paper.
52. Cossalter, V. and A. Doria, *The relation between contact patch geometry and the mechanical properties of motorcycle tyres.* Vehicle System Dynamics, 2005. **43**(sup1): p. 156-164.
53. Lot, R., *A motorcycle tire model for dynamic simulations: Theoretical and experimental aspects.* Meccanica, 2004. **39**(3): p. 207-220.
54. Sharp, R.S., *On the stability and control of the bicycle.* Applied mechanics reviews, 2008. **61**(6): p. 060803.

55. Da Lio, M., et al. *The influence of tyre characteristics on motorcycle manoeuvrability*. in *European Automotive Congress, Conference II: Vehicle Dynamics and Active Safety*. 1999.
56. Cossalter, V., et al., *Experimental and numerical analysis of the influence of tyres' properties on the straight running stability of a sport-touring motorcycle.* Vehicle System Dynamics, 2012. **50**(3): p. 357-375.
57. Pacejka, H., *Tire and vehicle dynamics*. 2005: Elsevier.
58. Pacejka, H.B. and E. Bakker, *The magic formula tyre model.* Vehicle system dynamics, 1992. **21**(S1): p. 1-18.
59. Pacejka, H., *Lateral dynamics of road vehicles.* Vehicle System Dynamics, 1987. **16**(sup1): p. 75-120.
60. Baslamisli, S.C., I. Polat, and I.E. Kose. *Gain scheduled active steering control based on a parametric bicycle model*. in *Intelligent Vehicles Symposium, 2007 IEEE*. 2007. IEEE.
61. Cossalter, V., et al., *Dynamic properties of motorcycle and scooter tires: Measurement and comparison.* Vehicle System Dynamics, 2003. **39**(5): p. 329-352.
62. Doria, A., et al., *Identification of the mechanical properties of bicycle tyres for modelling of bicycle dynamics.* Vehicle system dynamics, 2013. **51**(3): p. 405-420.
63. Doyle, A.J.R., *The skill of bicycle riding*. 1987, University of Sheffield.
64. Moore, J.K., et al., *Rider motion identification during normal bicycling by means of principal component analysis.* Multibody System Dynamics, 2011. **25**(2): p. 225-244.
65. Kooijman, J., A. Schwab, and J.K. Moore. *Some observations on human control of a bicycle*. in *ASME 2009 International Design Engineering Technical Conferences and Computers and Information in Engineering Conference*. 2009. American Society of Mechanical Engineers.
66. Pick, A. and D. Cole, *Neuromuscular dynamics and the vehicle steering task.* The Dynamics of Vehicles on Roads and on Tracks, 2003. **41**: p. 182-191.
67. Nishimi, T., A. Aoki, and T. Katayama, *Analysis of straight running stability of motorcycles*. 1985, SAE Technical Paper.
68. Doria, A. and M. Tognazzo, *The influence of the dynamic response of the rider's body on the open-loop stability of a bicycle.* Proceedings of the Institution of Mechanical Engineers, Part C: Journal of Mechanical Engineering Science, 2014. **228**(17): p. 3116-3132.
69. Doria, A., M. Formentini, and M. Tognazzo, *Experimental and numerical analysis of rider motion in weave conditions.* Vehicle system dynamics, 2012. **50**(8): p. 1247-1260.
70. Doria, A. and M. Tognazzo. *Identification of the biomechanical parameters of the riders of two-wheeled vehicles by means of vibration testing*. in *ASME 2012 International Design Engineering Technical Conferences and Computers and Information in Engineering Conference*. 2012. American Society of Mechanical Engineers.
71. Cossalter, V., et al., *The effect of rider's passive steering impedance on motorcycle stability: identification and analysis.* Meccanica, 2011. **46**(2): p. 279-292.

72. Cossalter, V., et al. *Measurement and identification of the vibration characteristics of motorcycle riders*. in *Proceedings of ISMA*. 2006.
73. Doria, A., M. Tognazzo, and V. Cossalter, *The response of the rider's body to roll oscillations of two wheeled vehicles; experimental tests and biomechanical models.* Proceedings of the Institution of Mechanical Engineers, Part D: Journal of Automobile Engineering, 2013. **227**(4): p. 561-576.
74. Moore, J.K., et al. *A method for estimating physical properties of a combined bicycle and rider*. in *ASME 2009 International Design Engineering Technical Conferences and Computers and Information in Engineering Conference*. 2009. American Society of Mechanical Engineers.
75. Keppler, V. and B. Solutions. *Analysis of the biomechanical interaction between rider and motorcycle by means of an active rider model*. in *Proceedings, Bicycle and Motorcycle Dynamics 2010 Symposium on the Dynamics and Control of Single Track Vehicles, 20–22 October 2010, Delft, The Netherlands*. 2010.
76. Cossalter, V., A. Bellati, and V. Cafaggi. *Exploratory study of the dynamic behaviour of motorcycle-rider during incipient fall events*. in *In the 19th International Technical Conference on the Enhanced Safety of Vehicles Conference (ESV) in Washington, DC*. 2005.
77. Cangley, P., et al., *A model for performance enhancement in competitive cycling.* Movement & Sport Sciences, 2012(1): p. 59-71.
78. Van den Ouden, J., *Inventory of bicycle motion for the design of a bicycle simulator*. 2011, TU Delft, Delft University of Technology.
79. Peterson, D.L., et al., *Low-power, modular, wireless dynamic measurement of bicycle motion.* Procedia Engineering, 2010. **2**(2): p. 2949-2954.
80. Van Lunteren, A. and H. Stassen. *On the variance of the bicycle rider's behavior*. in *Proceedings of the 6th annual conference on manual control*. 1970.
81. Weir, D.H. and J.W. Zellner, *Lateral-directional motorcycle dynamics and rider control*. 1978, SAE Technical Paper.
82. Nagai, M., *Analysis of rider and single-track-vehicle system; its application to computer-controlled bicycles.* Automatica, 1983. **19**(6): p. 737-740.
83. Chen, C.-K. and T.-S. Dao, *Fuzzy control for equilibrium and roll-angle tracking of an unmanned bicycle.* Multibody system dynamics, 2006. **15**(4): p. 321-346.
84. Cain, S.M., D.A. Ulrich, and N.C. Perkins. *Using measured bicycle kinematics to quantify increased skill as a rider learns to ride a bicycle*. in *ASME 2012 5th Annual Dynamic Systems and Control Conference joint with the JSME 2012 11th Motion and Vibration Conference*. 2012. American Society of Mechanical Engineers.
85. Cain, S.M., *An experimental investigation of human/bicycle dynamics and rider skill in children and adults*. 2013, University of Michigan.
86. Moore, J.K., *Human control of a bicycle*. 2012, University of California Davis.
87. Hess, R., J.K. Moore, and M. Hubbard, *Modeling the manually controlled bicycle.* IEEE Transactions on Systems, Man, and Cybernetics-Part A: Systems and Humans, 2012. **42**(3): p. 545-557.
88. Hess, R.A., *Simplified approach for modelling pilot pursuit control behaviour in multi-loop flight control tasks.* Proceedings of the Institution of Mechanical Engineers, Part G: Journal of Aerospace Engineering, 2006. **220**(2): p. 85-102.

89. Schwab, A., et al., *Rider control identification in bicycling using lateral force perturbation tests.* Proceedings of the Institution of Mechanical Engineers, Part K: Journal of Multi-body Dynamics, 2013. **227**(4): p. 390-406.
90. Pucher, J., J. Dill, and S. Handy, *Infrastructure, programs, and policies to increase bicycling: an international review.* Preventive medicine, 2010. **50**: p. S106-S125.
91. Plöchl, M., et al., *On the wobble mode of a bicycle.* Vehicle System Dynamics, 2012. **50**(3): p. 415-429.
92. Doria, A. and M. Tognazzo, *The influence of the dynamic response of the rider's body on the open loop stability of a bicycle.* Proceedings of the Institution of Mechanical Engineers, Part C: Journal of Mechanical Engineering Science, 2014: p. 0954406214527073.
93. Klinger, F., et al., *Wobble of a racing bicycle with a rider hands on and hands off the handlebar.* Vehicle System Dynamics, 2014. **52**(sup1): p. 51-68.
94. Cossalter, V., R. Lot, and M. Massaro, *An advanced multibody code for handling and stability analysis of motorcycles.* Meccanica, 2011. **46**(5): p. 943-958.
95. De Vries, E.d. and H. Pacejka, *Motorcycle tyre measurements and models.* Vehicle System Dynamics, 1998. **29**(S1): p. 280-298.
96. Chandler, R. and C. Clauser, *Investigation of inertial properties of the human body.* Us Department of Transportation, Report# DOT HS-801 430 Washington DC, 1975.
97. Koopman, H.F.J.M., *The three-dimensional analysis and prediction of human walking*. 1989.
98. Clark, S.K., *Mechanics of pneumatic tires*. 1981: US Department of Transportation, National Highway Traffic Safety Administration.
99. Cossalter, V., *Motorcycle dynamics*. 2006: Lulu. com.
100. Evangelou, S., *Control and Stability Analysis of Two-wheeled Road Vehicles*. 2004, University of London.
101. Massaro, M., V. Cossalter, and G. Cusimano, *The effect of the inflation pressure on the tyre properties and the motorcycle stability.* Proceedings of the Institution of Mechanical Engineers, Part D: Journal of automobile engineering, 2013. **227**(10): p. 1480-1488.
102. Statistiek, C.B.v.d., *Mobility of the Dutch population per region for motive and means of transport [Mobiliteit Nederlandse bevolking per regio naar motief en vervoerwijze]*. 2008, Statistics Netherlands: Voorburg/Heerlen.
103. Veiligheid, C.e., *Single-sided bicycle accidents with 55+*. 2010, Consumer & Safety Netherlands.
104. Ormel, W., K. Klein Wolt, and P. den Hertog, *Enkelvoudige fietsongevallen. Een LIS-vervolgstudie.* 2009, Rijkswaterstaat Dienst Verkeer en Scheepvaart.
105. Schwab, A. and J. Meijaard, *A review on bicycle dynamics and rider control.* Vehicle System Dynamics, 2013. **51**(7): p. 1059-1090.
106. Weir, D., *Motorcycle Handling Dynamics and Rider Control andthe Effect of Design Configurationson Response and Performance*. 1972, PhD Thesis, university ofCalifornia, LA.
107. Cain, S., *An experimental investigation of human/bicycle dynamics and rider skill in children and adults*, in *Biomedical Engineering*. 2013, University of Michigan: Ann Arbor, Michigan, United States.

108. Sharp, R.S., *Stability, control and steering responses of motorcycles.* Vehicle system dynamics, 2001. **35**(4-5): p. 291-318.
109. Dubbeldam, R., J. Buurke, and J. Rietman. *to bike or not to bike? Physical strength and short term memory influence on cycling kinematics.* in *International Cycling Safety Conference*. 2014. Goteborg, Sweden.
110. Mitchell, W.K., et al., *Sarcopenia, dynapenia, and the impact of advancing age on human skeletal muscle size and strength; a quantitative review.* Frontiers in physiology, 2012. **3**.
111. Klitgaard, H., et al., *Function, morphology and protein expression of ageing skeletal muscle: a cross-sectional study of elderly men with different training backgrounds.* Acta Physiologica Scandinavica, 1990. **140**(1): p. 41-54.
112. Collins, J.J., et al., *Age-related changes in open-loop and closed-loop postural control mechanisms.* Experimental Brain Research, 1995. **104**(3): p. 480-492.
113. Vlakveld, W., et al., *Speed choice and mental workload of elderly cyclists on e-bikes in simple and complex traffic situations: A field experiment.* Accident Analysis & Prevention, 2015. **74**: p. 97-106.
114. Kiewiet, H., et al. *A Novel Experimental Setup to Apply Controlled Disturbances to Bicycle Dynamics in a Safe Environment*. in *ASME 2014 International Design Engineering Technical Conferences and Computers and Information in Engineering Conference*. 2014. American Society of Mechanical Engineers.
115. Allum, J., et al., *Age-dependent variations in the directional sensitivity of balance corrections and compensatory arm movements in man.* The Journal of physiology, 2002. **542**(2): p. 643-663.
116. Harrington, M., et al., *Prediction of the hip joint centre in adults, children, and patients with cerebral palsy based on magnetic resonance imaging.* Journal of biomechanics, 2007. **40**(3): p. 595-602.
117. Mauchly, J.W., *Significance test for sphericity of a normal n-variate distribution.* The Annals of Mathematical Statistics, 1940. **11**(2): p. 204-209.
118. Seidler, R.D., et al., *Motor control and aging: links to age-related brain structural, functional, and biochemical effects.* Neuroscience & Biobehavioral Reviews, 2010. **34**(5): p. 721-733.
119. Moore, J., et al., *Rider motion identification during normal bicycling by means of principal component analysis.* Multibody System Dynamics, 2011. **25**(2): p. 225-244.
120. Dubbeldam, R., et al. *SOFIE, a bicycle that supports older cyclists?* in *International Cycling Safety Conference*. 2015. Hannover, Germany.
121. Bulsink, V.E., et al., *The effect of tyre and rider properties on the stability of a bicycle.* Advances in Mechanical Engineering, 2015. **7**(12): p. 1687814015622596.
122. Cangley, P., *Aspects of modelling performance in competitive cycling*. 2012, University of Brighton.
123. Wang, P. and J. Yi. *Dynamic stability of a rider-bicycle system: Analysis and experiments*. in *American Control Conference (ACC), 2015*. 2015. IEEE.
124. Cain, S. and N. Perkins. *Comparison of a bicycle steady-state turning model to experimental data*. in *Bicycle and Motorcycle Dynamics 2010 Symposium on the Dynamics and Control of Single Track Vehicles. Delft, Netherlands*. 2010.

125. Capitani, R., et al., *Handling analysis of a two-wheeled vehicle using MSC. ADAMS/motorcycle.* Vehicle System Dynamics, 2006. **44**(sup1): p. 698-707.
126. Cossalter, V., A. Bellati, and V. Cafaggi. *Exploratory study of the dynamic behaviour of motorcycle-rider during incipient fall events*. in *The 19th international technical conference on the enhanced safety of vehicles conference (ESV)*. 2005.
127. Schmitt, T., D. Zimmer, and F.E. Cellier. *A virtual motorcycle rider based on automatic controller design*. in *Proc. 7th Modelica Conf*. 2009.
128. Bulsink, V.E., et al., *Cycling strategies of young and older cyclists.* Human movement science, 2016. **46**: p. 184-195.
129. Connors, B. and M. Hubbard, *Modelling and Stability Analysis of a Recumbent Bicycle with Oscillating Leg Masses (P131)*, in *The Engineering of Sport 7*. 2008, Springer Paris. p. 677-685.
130. Horn, B.K., *Closed-form solution of absolute orientation using unit quaternions.* JOSA A, 1987. **4**(4): p. 629-642.
131. Moore, J.K., et al. *Accurate measurement of bicycle parameters*. in *Proceedings, Bicycle and Motorcycle Dynamics 2010 Symposium on the Dynamics and Control of Single Track Vehicles, 20Ű22 October 2010, Delft, The Netherlands*. 2010. Citeseer.
132. Davis, R. and M. Hull, *Measurement of pedal loading in bicycling: II. Analysis and results.* Journal of biomechanics, 1981. **14**(12): p. 857-872.
133. Kiewiet, H., et al., *The co-contraction index of the upper limb for young and old adult cyclists.* Accident Analysis & Prevention, 2016.
134. Hull, M. and M. Jorge, *A method for biomechanical analysis of bicycle pedalling.* Journal of biomechanics, 1985. **18**(9): p. 631-644.
135. Kautz, S. and M. Hull, *A theoretical basis for interpreting the force applied to the pedal in cycling.* Journal of biomechanics, 1993. **26**(2): p. 155-165.
136. Chiari, L., et al., *Human movement analysis using stereophotogrammetry: Part 2: Instrumental errors.* Gait & posture, 2005. **21**(2): p. 197-211.
137. Leardini, A., et al., *Human movement analysis using stereophotogrammetry: Part 3. Soft tissue artifact assessment and compensation.* Gait & posture, 2005. **21**(2): p. 212-225.
138. Della Croce, U., et al., *Human movement analysis using stereophotogrammetry: Part 4: assessment of anatomical landmark misplacement and its effects on joint kinematics.* Gait & posture, 2005. **21**(2): p. 226-237.
139. Neptune, R. and M. Hull, *Accuracy assessment of methods for determining hip movement in seated cycling.* Journal of biomechanics, 1995. **28**(4): p. 423-437.
140. Hicks, J.L., et al., *Is my model good enough? Best practices for verification and validation of musculoskeletal models and simulations of movement.* Journal of biomechanical engineering, 2015. **137**(2): p. 020905.
141. DiGioia, J., et al., *Safety impacts of bicycle infrastructure: a critical review.* Journal of safety research, 2017. **61**: p. 105-119.
142. Stelling-Konczak, A., et al., *Mobile phone conversations, listening to music and quiet (electric) cars: are traffic sounds important for safe cycling?* Accident Analysis & Prevention, 2017. **106**: p. 10-22.

143. Twisk, D., S. Platteel, and G. Lovegrove, *An experiment on rider stability while mounting: comparing middle-aged and elderly cyclists on pedelecs and conventional bicycles.* Accident Analysis & Prevention, 2017.
144. Dubbeldam, R., et al., *The different ways to get on and off a bicycle for young and old.* Safety science, 2017. **92**: p. 318-329.
145. Bella, F. and M. Silvestri, *Interaction driver–bicyclist on rural roads: Effects of cross-sections and road geometric elements.* Accident Analysis & Prevention, 2017. **102**: p. 191-201.
146. Billot-Grasset, A., E. Amoros, and M. Hours, *How cyclist behavior affects bicycle accident configurations?* Transportation research part F: traffic psychology and behaviour, 2016. **41**: p. 261-276.
147. Stevens, D., *Stability and handling characteristics of bicycles.* Bachelor thesis, University of New Sout Wales, Dept. of Mechanical and Manufacturing Engineering, 2009.
148. Moore, J.K., et al., *Statistics of bicycle rider motion.* Procedia Engineering, 2010. **2**(2): p. 2937-2942.
149. Cain, S.M., J.A. Ashton-Miller, and N.C. Perkins, *On the skill of balancing while riding a bicycle.* PLoS one, 2016. **11**(2): p. e0149340.
150. Peterson, D.L. and M. Hubbard. *Yaw rate and velocity tracking control of a hands-free bicycle*. in *International Mechanical Engineering Congress and Exposition, Boston*. 2008.
151. Engelhart, D., et al., *Assessment of multi-joint coordination and adaptation in standing balance: a novel device and system identification technique.* IEEE transactions on neural systems and rehabilitation engineering, 2015. **23**(6): p. 973-982.
152. Boonstra, T.A., A.C. Schouten, and H. Van der Kooij, *Identification of the contribution of the ankle and hip joints to multi-segmental balance control.* Journal of neuroengineering and rehabilitation, 2013. **10**(1): p. 23.
153. Engelhart, D., et al., *Adaptation of multijoint coordination during standing balance in healthy young and healthy old individuals.* Journal of neurophysiology, 2016. **115**(3): p. 1422-1435.
154. Jones, T., L. Harms, and E. Heinen, *Motives, perceptions and experiences of electric bicycle owners and implications for health, wellbeing and mobility.* Journal of Transport Geography, 2016. **53**: p. 41-49.
155. Kovácsová, N., et al., *Riding performance on a conventional bicycle and a pedelec in low speed exercises: Objective and subjective evaluation of middle-aged and older persons.* Transportation Research Part F: Traffic Psychology and Behaviour, 2016.
156. Du, W., D. Zhang, and X. Zhao. *Dynamic modelling and simulation of electric bicycle ride comfort*. in *2009 International Conference on Mechatronics and Automation*. 2009. IEEE.
157. Abagnale, C., et al. *Derivation and Validation of a Mathematical Model for a Novel Electric Bicycle*. in *Proceedings of the World Congress on Engineering*. 2015.

158. Maier, O., M. Pfeiffer, and J. Wrede, *Development of a Braking Dynamics Assistance System for Electric Bicycles: Design, Implementation, and Evaluation of Road Tests.* IEEE/ASME Transactions on Mechatronics, 2016. **21**(3): p. 1671-1679.
159. Iuchi, K., H. Niki, and T. Murakami. *Attitude control of bicycle motion by steering angle and variable COG control*. in *31st Annual Conference of IEEE Industrial Electronics Society, 2005. IECON 2005.* 2005. IEEE.
160. Tanaka, Y. and T. Murakami, *A study on straight-line tracking and posture control in electric bicycle.* IEEE Transactions on Industrial Electronics, 2009. **56**(1): p. 159-168.
161. Liu, Y., C. Jia, and J. Han. *Dynamics modeling of an unmanned bicycle with parallel mechanism adjusting stability*. in *2009 International Conference on Mechatronics and Automation*. 2009. IEEE.
162. Lee, S. and W. Ham. *Self stabilizing strategy in tracking control of unmanned electric bicycle with mass balance*. in *Intelligent Robots and Systems, 2002. IEEE/RSJ International Conference on*. 2002. IEEE.
163. Karogal, I. and B. Ayalew, *Independent torque distribution strategies for vehicle stability control*. 2009, SAE Technical Paper.
164. Christini, S.J., et al., *Two wheel drive bicycle with a shock-absorbing front fork*. 2001, Google Patents.
165. Massaro, M., et al., *Numerical and experimental investigation of passive rider effects on motorcycle weave.* Vehicle System Dynamics, 2012. **50**(sup1): p. 215-227.
166. Tak, T.-O., J.-S. Won, and G.-Y. Baek. *Design sensitivity analysis of bicycle stability and experimental validation*.
167. Sturnieks, D.L., R. St George, and S.R. Lord, *Balance disorders in the elderly.* Neurophysiologie Clinique/Clinical Neurophysiology, 2008. **38**(6): p. 467-478.
168. Fozard, J.L., et al., *Age differences and changes in reaction time: the Baltimore Longitudinal Study of Aging.* Journal of gerontology, 1994. **49**(4): p. P179-P189.
169. Laughton, C.A., et al., *Aging, muscle activity, and balance control: physiologic changes associated with balance impairment.* Gait & posture, 2003. **18**(2): p. 101-108.
170. Shkuratova, N., M.E. Morris, and F. Huxham, *Effects of age on balance control during walking.* Archives of physical medicine and rehabilitation, 2004. **85**(4): p. 582-588.
171. Silsupadol, P., et al., *Training-related changes in dual-task walking performance of elderly persons with balance impairment: a double-blind, randomized controlled trial.* Gait & posture, 2009. **29**(4): p. 634-639.
172. Dubbeldam, R., et al., *SOFIE, a bicycle that supports older cyclists?* Accident Analysis & Prevention, 2017. **105**: p. 117-123.
173. Mitiguy, P.C. and K. Reckdahl, *The definition of product of inertia.* Working Model Technical Paper, 1998.
174. Arora, S.G.K., *Study of Significance of Total Pelvic Height and Pelvic Width in Sex Determination of Human Innominate Bone in Gujarat Region.*

Acknowledgments

Nu mijn proefschrift zo goed als klaar is om te printen, staat er nog maar 1 taak op mijn to-do lijstje: namelijk het schrijven van het dankwoord. Als ik zo terugkijk naar de afgelopen jaren, dan zijn er heel wat mensen op mijn pad gekomen die een steentje hebben bijgedragen aan het totstandkomen van het boekje dat hier nu bijna ligt. Deze bijdragen waren natuurlijk vaak inhoudelijk, maar waren ook vaak ondersteunend of als mentale support. Een ding is zeker: zonder de bijdrage van al deze mensen had ik nooit zover kunnen komen.

Om het kort te houden heb ik iedereen die ik graag zou willen bedanken, ondergebracht in onderstaande typografische afbeelding van een fiets (gebaseerd op de Bicycle Typogram van Aaron Kuehn).

Omdat dit toch wel erg kort door de bocht is, zou ik er toch nog iets dieper op in willen gaan ;)

Als eerste wil ik graag Bart bedanken voor alle begeleiding door de afgelopen jaren heen. Je gaf mij de kans om aan het SOFIE-project te beginnen als PhD student en gaf mij altijd het vertrouwen dat we dit project tot een succesvol einde zouden brengen. Ook gaf je het vertrouwen dat ik mijn promotie zou kunnen afronden, wat ik zelf op sommige momenten niet meer zag gebeuren. Met je biomechanische inzicht leek geen enkel probleem je te lastig af. Bedankt voor alle goede tips, die ook gewoon doorgingen nadat mijn contract bij de UT afgelopen was.

Marc, jij hebt me vanaf dag 1 op weg geholpen in de werkzaamheden van een PhD student. Bedankt voor al je goede tips en de leuke samenwerking!

Dorien, jij hebt altijd enthousiast de taak van begeleider overgenomen en was altijd bereid mijn geschreven teksten door te nemen en mee te denken over bepaalde problemen waar ik op vast liep. Heel erg bedankt voor al je input in de papers en het vrijmaken van tijd voor het doorlezen van mijn teksten in je drukke schema.

Maarten, jij was van het begin af aan al betrokken bij het SOFIE-project. Tijdens de projectoverleggen had je vaak zinnige bijdragen en ideeën. Pas later ben je meer betrokken geraakt bij mijn promotietraject. Met name in de eindfase heb ik veel gehad aan al je suggesties, betrokkenheid en tips.

Adrian, samen met jou, begon ik als PhD student binnen hetzelfde project. Bedankt voor de fijne samenwerking en gezelligheid ook buiten het project om. Ik heb veel geleerd van je kennis op het gebied van software engineering en heb altijd veel respect gehad voor je keuze om je hart te volgen naar Amsterdam.

Verder zou ik graag alle projectleden van het SOFIE-project willen bedanken voor de fijne samenwerking. Ik ben erg blij met het resultaat dat we uiteindelijk samen bereikt hebben. Tijdens de tweewekelijkse overleggen was het interessant om te zien hoe de dagelijkse bezigheden van het RRD, Indes en de UT samenkwamen. Rosemary en Wilfred, jullie waren altijd bereid mee te denken en gaven vaak nuttige input tijdens onze afspraken. Rosemary, binnen het RRD heb je een grote bijdrage geleverd aan het totstandkomen van de Sofiets, met het uitvoeren van de validatiestudie en de vele fiets experimenten, bedankt ook voor al je behulpzaamheid. Wilfred, jij hield altijd het eindproduct en de toepassing in het vizier, wat we vanuit een onderzoekspositie nog wel eens kunnen vergeten. Maurice, aan het einde van het project hebben we veel samengewerkt aan het optimaliseren van de geometrie van de fiets en het project met JyroBike. Uiteindelijk heb je samen met je collega's bij Indes ervoor gezorgd dat er een mooi eindproduct stond!

Jaap en Hans, bedankt voor jullie bijdrage en feedback tijdens de projectoverleggen vanuit RRD en Hans bedankt dat je ook in mijn promotiecommissie plaats wilt nemen.

Chris Verheul, bedankt voor je behulpzaamheid als het ging over vragen over de software Adams en het aanleveren van de motion tracking software. Ik heb erg veel gehad aan al je kennis over multi-body dynamica en modelleren. Ook zou ik graag Marcel Ellenbroek willen

bedanken voor de samenwerking in het ontwikkelen van het band-weg contact model in Adams.

Alberto Doria, thank you (and your colleagues at the Motorcycle Dynamics Group) very much for your hospitality and showing us around in your lab in Padua, making it possible to perform the measurements on the bicycle tires and working together on two papers. I always liked to work together with you, as you were always able to provide some useful feedback within short times. We have been in contact once in awhile about the ASME conference and I am happy that we will be meeting again, with you as a member of my graduation committee.

Arend Schwab, in het begin van het project heb je ons goed op weg kunnen helpen en wegwijs gemaakt in de wereld van de fietsdynamica. De bezoeken aan de TU Delft waren erg leerzaam en ik bewonder al je werk dat je hebt verricht in dit mooie vakgebied. Bedankt voor je inbreng en het deelnemen aan de commissie.

Ronald Aarts, zonder al jouw kennis over systeem identificatie zouden de laatste loodjes van mijn promotie een stuk zwaarder geweest zijn. Heel erg bedankt voor je hulp en de samenwerking in mijn laatste paper.

Verder zou ik alle studenten die een bijdrage geleverd hebben in de vorm van een bachelor, stage of master opdracht willen bedanken voor hun werk, dat uiteenliep van het opzetten van de pilot experimenten in het lab tot het ontwikkelen van het band-weg contact en uitvoeren van computer simulaties.

Zonder alle proefpersonen die deelgenomen hebben aan het fiets experiment, zou deze studie niet mogelijk zijn. Ik zou iedereen heel erg willen bedanken die de tijd genomen heeft om mee te doen aan het onderzoek en het heeft aangedurfd om te fietsen op een smalle loopband, waar wij ook nog eens verstoringen op aan brachten. Gelukkig is (bijna) iedereen er heel vanaf gekomen..

En dan waren er de mensen van de vakgroep. Door de leuke werkomgeving ging ik nooit met tegenzin naar de UT, ook al zat het onderzoek wel eens tegen. Ondertussen is mijn tijd op de BW vakgroep alweer een tijdje geleden, maar ik denk nog steeds met veel plezier terug. Ik zou graag iedereen willen bedanken voor de leuke tijd, de koffie en lunch pauzes, voor de leuke activiteiten zoals het wielrennen na het werk, zeilweekendjes, etentjes, vakgroepuitjes en niet te vergeten het zaalvoetballen met het BW team! Hoewel we niet

altijd even goed waren, zag ik naar het einde toe toch een flinke verbetering, wat niet geheel toevallig, samenging met het toenemen van het aantal vrouwelijke voetballers.

In het bijzonder, heb ik goede herinneringen aan HR W-216, waar we soms met de voetjes hoog op de verwarming zaten, er af en toe gevoetbald werd en er een basketbalnetje aanwezig was voor de propjes ;). Denise, we begonnen tegelijk aan ons onderzoek, en zijn helaas niet gelijk geëindigd ;), maar het was altijd gezellig en ik ben blij dat we samen de 4 jaar doorgemaakt hebben, bedankt dat ik alle phd-perikelen samen met je kon delen! Hielke, met jou was het altijd gezellig om samen te werken, we hebben heel wat uurtjes samen doorgebracht in het lab om de fiets experimenten voor elkaar te krijgen, super! Bedankt voor al je bijdrage in het onderzoek en dat je ook het laatste stukje erbij bent als paranimf. Claudia en Mark, jullie ook bedankt voor de leuke tijd in HR W-216! Mark, je hebt me bijna ingehaald, maar net niet ;), alvast heel veel succes volgende week! En Claudia, jou zal ik nog vaak genoeg zien als bijna-buren ;)

René en Vincenzo, ik begon bij jullie op de kamer en merkte al snel dat dat erg grappig kon zijn. Bedankt voor de leuke tijd, ook tijdens de congressen en de super roadtrip door Brazilië. Vincenzo, Ho un appuntamento, finalmente!

Lianne, Wouter en Nicolai, zonder jullie zou de vakgroep niet functioneren. Bedankt voor jullie hulp op organisatorisch gebied, in de werkplaats en in het lab!

Verder zou ik iedereen die de afgelopen jaren gezorgd heeft voor de nodige leuke afleiding willen bedanken. Naast het werken aan dit onderzoek was het altijd fijn om even te kunnen ontspannen bijv tijdens (en na) een voetbaltraining of drankje in de stad. Bedankt voor alle gezellige etentjes, snowboard trips, weekendjes weg, festivals, terrasjes, mountainbike tochtjes, feestjes, kroegentocht, bankhang chill sessies, etc… Ik hoop dat jullie er ook allemaal bij kunnen zijn om het behalen van mijn PhD samen te vieren :)

Jaap, als Twins hebben we zo'n beetje alles samen meegemaakt. Tegenwoordig hebben we allebei ons eigen leven, en daarom lijkt het me leuk om weer eens een gelegenheid samen mee te maken, met jij als mijn paranimf. (en geen pootje haken als we de trap af lopen he ;))

Pap en mam, jullie hebben mij altijd het vertrouwen gegeven dat ik mijn promotie tot een goed einde kon brengen, ook op de momenten dat ik het zelf nauwelijks nog zag gebeuren.. En het is gelukt! :) Bedankt voor al jullie steun en het onvoorwaardelijke vertrouwen in mijn

kunnen. Ik kijk er erg naar uit om het samen nog een keer te vieren op een warm eiland, dat nog een topje op de ijsberg is van jullie bijdrage (of hoe ging dat gezegde ook alweer).

Inés, zonder jou waren de laatste loodjes een stuk zwaarder geweest. We waren pas samen sinds het einde van mijn tijd op de UT, maar jouw steun en hulp hebben ervoor gezorgd dat ik op de juiste momenten kon relaxen. Ik ken niemand die zo behulpzaam en lief is als jij! Je hebt soms heel wat moeten verdragen van mijn gestress, heel erg bedankt dat je altijd positief bent gebleven en me bent blijven steunen. Ik kijk uit naar alle leuke dingen die we nog samen gaan doen :) <3

About the Author

Vera Bulsink was born in Utrecht, the Netherlands, on the 25th of August 1985 and grew up in Aalten, the Netherlands. In 2003 she started the bachelor Biomedical Engineering at the University of Twente, which she finished in 2006 with the bachelor thesis 'Mechanics of normal walking – kinetic data and muscle activities'. Afterwards she continued with the master program Biomedical Engineering at the University of Twente and visited the Center for Sensory & Motor Interaction of Aalborg University in Denmark during her internship. She became particularly interested in sports technology and helped set up experiments to study the biomechanical effects of slipping during turning movements in sports. In 2009 she received the MSc. degree in Biomechanical Engineering of the University of Twente, Enschede, the Netherlands. During her master assignment she developed skills in finite element modeling and studied the effects of bone remodeling on the mechanics of the aging spine, using computer models.

In 2010 she worked as a research engineer at the Bioengineering Institute of Auckland University, New Zealand. She continued working on the development of finite element models of the spine that were used in an orthopedic research project. Furthermore, she worked on generating patient-specific computer models of hip prostheses.

In 2011 she started a PhD project at the laboratory of Biomechanical Engineering of the University of Twente, within the project SOFIE (Slimme Ondersteunende FIEts/Smart Assistive Bicycle). The goal of the project was to improve bicycling stability for older cyclists. She developed multi-body dynamic computer models of the bicycle dynamics, the cyclist biomechanics and control and the tire-road contact. A laboratory cycling set-up was used to generate an extensive cycling dataset of young and older cyclist in order to compare their cycling strategies, validate computer models and identify balance control models.

At the end of the PhD project she worked also part time as lab manager of the movement laboratory and worked as a trainee at Innosport Papendal of NOC*NSF, Arnhem, the Netherlands to scientifically support elite athletes and their coaches at the national sports training center.

Journal Contributions

Doria, A., Tognazzo, M., Cusimano, G., **Bulsink, V.E.**, Cooke, A., & Koopman, H.F.J.M. (2013). Identification of the mechanical properties of bicycle tyres for modelling of bicycle dynamics. *Vehicle system dynamics*, *51*(3), 405-420.

Bulsink, V. E., Doria, A., van de Belt, D., & Koopman, H.F.J.M (2015). The effect of tyre and rider properties on the stability of a bicycle. *Advances in mechanical engineering*, *7*(12), 1687814015622596.

Bulsink, V. E., Kiewiet, H., van de Belt, D., Bonnema, G. M., & Koopman, B. (2016). Cycling strategies of young and older cyclists. *Human movement science*, *46*, 184-195.

Kiewiet, H., **Bulsink, V. E.**, Beugels, F., & Koopman, H.F.J.M. (2016). The co-contraction index of the upper limb for young and old adult cyclists. *Accident Analysis & Prevention*.

Bulsink, V.E., van de Belt, D., Bonnema, G.M., Koopman, H.F.J.M, (2017). Validation of a Biomechanical Model of a Cyclist Using Bicycle Interaction Forces, *submitted to Transactions of Biomedical Engineering*

Bulsink, V.E., Aarts, R.G.K.M, Kiewiet, H., van de Belt, D., Bonnema, G.M., Koopman, H.F.J.M, (2017). Identification of a Cyclist Balance Control Model, *submitted to Journal of Biomechanics*

Conference Contributions

Bulsink, V.E., Dubbeldam, R., Beusenberg, C.M., Koopman, H.F.J.M. (2012), Prolonged mobility and health of elderly: the human aspects of engineering stability during cycling. *International Conference on Aging, Mobility and Quality of Life, University of Michigan, Ann Arbor, USA, 24-26 June 2012*

Bulsink, V.E., Dubbeldam, R., Beusenberg, C.M. & Koopman, H.F.J.M. (2012). Ouderen langer mobiel en gezond: de mens als sturend systeem voor stabiliteit bij fietsen. In *Nationaal Verkeersveiligheidscongres NVVC - papers 2012*, Rotterdam (pp. 1-5). *Rotterdam, the Netherlands*

Bulsink, V. E., Beusenberg, C. M., & Koopman, H.F.J.M. (2013). Cornering in bicycling: computer model simulations. *XXIV Congress of the international society of biomechanics, Natal, Brazil, August 4-9, 2013*

Bulsink, V.E. and Beusenberg, C.M. and Koopman, H.F.J.M. (2013) *Advanced Multi-body model to assess bicycle and rider stability.* In: *14th International Symposium on Computer Simulation in Biomechanics, Natal, Brazil, August 1-3, 2013 (pp. 15 - 16).*

Cooke, A., Beusenberg, M., Bonnema, M., Poelman, W., **Bulsink, V.E.**, Koopman, H.F.J.M., & Dubbeldam, R. (2012, October). Methods to assess the stability of a bicycle rider system. In *ASME 2012 5th Annual Dynamic Systems and Control Conference joint with the JSME 2012 11th Motion and Vibration Conference* (pp. 189-193). American Society of Mechanical Engineers.

Bulsink, V.E., Beusenberg, C.M., Bonnema, G.M. & Koopman, H.F.J.M. (2013). Validation of a bicycle/rider model to assess stability. *4th Dutch Bio-Medical Engineering Conference: Egmond aan Zee, The Netherlands, January 24-25, 2013.*

Kiewiet, H., **Bulsink, V. E.**, van de Belt, D., & Koopman, H.F.J.M. (2014, August). A novel experimental setup to apply controlled disturbances to bicycle dynamics in a safe environment. In *ASME 2014 International Design Engineering Technical Conferences and Computers and Information in Engineering Conference* (pp. V003T01A034-V003T01A034). American Society of Mechanical Engineers.

Bulsink, V.E., Bonnema, G.M., van de Belt, D., Koopman, H.F.J.M. (2016). Electrical bicycle hub motors & stability. Why a rear motor is better than a front motor & Two motors are better than One. *International Cycling Safety Conference 2016, Bologna, Italy, November 3-4 2016*

Appendix

A.1. Bicycle-rider model

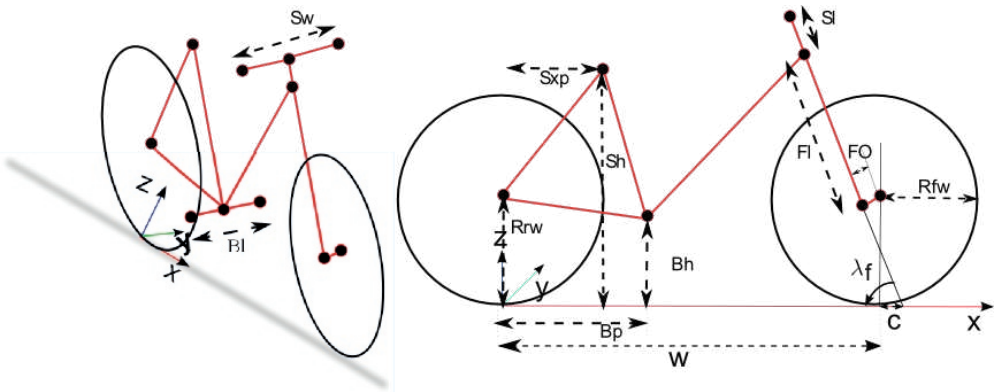

Figure A.1*. Parameters of the bicycle model. The origin of the global coordinate system is defined in the contact point of the rear wheel with the ground, the orientation is according the right-handed rule, with the x-axis pointing in forward direction and the z-axis pointing upwards.*

Table A.1. *Input variables for the passive bicycle-rider model.*

Variable	**Symbol**	**Value (Bicycle 1)**	**Value (Bicycle 2)**
Head angle	λ_f	1.21 rad	1.18 rad
Fork offset	*FO*	0.086 m	0.029 m
Fork length	*Fl*	0.500 m	0.500 m
Wheelbase	*w*	1.150 m	1.125 m
Trail	*c*	0.041 m	0.112 m
Radius Rear wheel	R_{rw}	0.350 m	0.350 m
Radius Front wheel	R_{fw}	0.350 m	0.350 m
Saddle x-position	*Sxp*	0.230 m	0.230 m (variabel per subject)

Saddle Height	*Sh*	0.700 m	0.70 m (variabel per subject)
Bracket x-position	*Bxp*	0.575 m	0.465 m
Bracket Height	*Bh*	0.250 m	0.250 m
Bracket length	*Bl*	0.300 m	0.200 m
Steer length	*Sl*	0.238 m	0.238 m
Steer width	*Sw*	0.176 m	0.176 m
Back angle	*BA*	0.35 rad	Variable
Vertical stiffness & damping of the tire	K_z & B_z	108970 N/m 5448 N·s/m	Variable
Torsional stiffness & damping around the line connecting the hip and the ankle	K_l & B_l	1000 N·m/rad & 50 N·m·s/rad	Variable
Torsional stiffness & damping at the L4-L5 joint (around the sagittal axis)	K_r & B_r	1000 N·m/rad & 50 N·m·s/rad	Variable
Torsional stiffness & damping at the L4-L5 joint (around the longitudinal axis)	K_w & B_w	75 N·m/rad 5 N·m·s/rad	Variable
Torsional stiffness & damping at the L4-L5 joint (around the frontal axis)	Kp & Bp	1000 N·m/rad & 50 N·m·s/rad	Variable
Linear arm stiffness & damping	Ka & Ba	525 N/m & 100 N/m·s	Variable
Torsional arm stiffness & damping	Kat & Bat	5.0 N·m/rad & 0.9 N·m·s/rad	Variable
Mass of the rear frame	Mrf	8.30 kg	8.62 kg
Mass of the front fork	Mff	2.42 kg	3.72 kg
Mass of the rear wheel	M_{rw}	4.01 kg	4.22 kg

Mass of the front wheel	M_{fw}	3.34 kg	3.72 kg
Mass moments of inertia of the rear frame*	$\begin{bmatrix} I_{rfxx} & 0 & -I_{rfzx} \\ 0 & I_{rfyy} & 0 \\ -I_{rfxz} & 0 & I_{rfzz} \end{bmatrix}$	$\begin{bmatrix} 0.694 & 0 & -0.103 \\ 0 & 1.105 & 0 \\ -0.103 & 0 & 0.509 \end{bmatrix}$ kg·m^2	$\begin{bmatrix} 0.506 & 0 & -0 \\ 0 & 0.214 & \\ -0.117 & 0 & 0.(\end{bmatrix}$ kg·m^2
Mass moments of inertia of the front fork*	$\begin{bmatrix} I_{ffxx} & 0 & -I_{ffzx} \\ 0 & I_{ffyy} & 0 \\ -I_{ffxz} & 0 & I_{ffzz} \end{bmatrix}$	$\begin{bmatrix} 0.168 & 0 & 0.067 \\ 0 & 0.158 & 0 \\ 0.067 & 0 & 0.046 \end{bmatrix} kg{\cdot}m^2$	$\begin{bmatrix} 0.272 & 0 & 0.14(\\ 0 & 0.214 & 0 \\ 0.146 & 0 & 0.17(\end{bmatrix}$ g·m^2
Centre of mass of the rear frame	[x_{rf}, y_{rf}, z_{rf}]	[0.320, 0, 0.590] m	[0.334, 0, 0.466] m
Centre of mass of the front fork	[x_{ff}, y_{ff}, z_{ff}]	[0.980, 0, 0.720] m	[0.907, 0, 0.808] m
Centre of mass of the rear wheel	[x_{rw}, y_{rw}, z_{rw}]	[0, 0, 0.350] m	[0, 0, 0.350] m
Centre of mass of the front wheel	[x_{fw}, y_{fw}, z_{fw}]	[1.150, 0, 0.350] m	[1.125, 0, 0.350]
Rider length	L_r	1.800 m	Variable
Rider mass	M_r	80.0 kg	Variable
Mass moments of inertia of the rider*	$\begin{bmatrix} I_{rxx} & 0 & -I_{rzx} \\ 0 & I_{ryy} & 0 \\ -I_{rxz} & 0 & I_{rzz} \end{bmatrix}$	$\begin{bmatrix} 10.4737 & 0 & 0.10307 \\ 0 & 10.9094 & 0 \\ 0.10307 & 0 & 2.17315 \end{bmatrix}$ kg·m^2	Variable
Centre of mass of the rider	[x_r, y_r, z_r]	[0.39, 0, 1.06] m	Variable
Mass of the lower arms + hands	Ma	3.82 kg	Variable
Centre of mass of the front fork + lower arms and hands	[x_a, y_a, z_a]	[0.815, 0, 0.955] m	Variable
Mass moments of inertia of the front fork + lower arms and hands*	$\begin{bmatrix} I_{axx} & 0 & -I_{azx} \\ 0 & I_{ayy} & 0 \\ -I_{axz} & 0 & I_{azz} \end{bmatrix}$	$\begin{bmatrix} 10.36598 & 0 & 0.05944 \\ 0 & 0.33823 & 0 \\ 0.05944 & 0 & 0.12625 \end{bmatrix}$ kg·m^2	Variable

* the definition of the product of inertia in Adams is a positive summation: $-I_{xz} = \int xz \cdot dm$ [173]

A.2. Tire model

The Magic Formula fitting formulas and coefficients of the tire model are listed here. Equations are written in the x_w y_w z_w coordinate system of ADAMS (Fig A.2).

The normalized vertical load increment $dfz = \frac{Fz - F_{z0}}{F_{z0}}$ is used to scale the parameters to the vertical load applied during a dynamic simulation. F_z is the vertical load on the tire at a certain point during the simulation. F_{z0} is the vertical load on the tire during the measurement of the tire parameters (the nominal load).

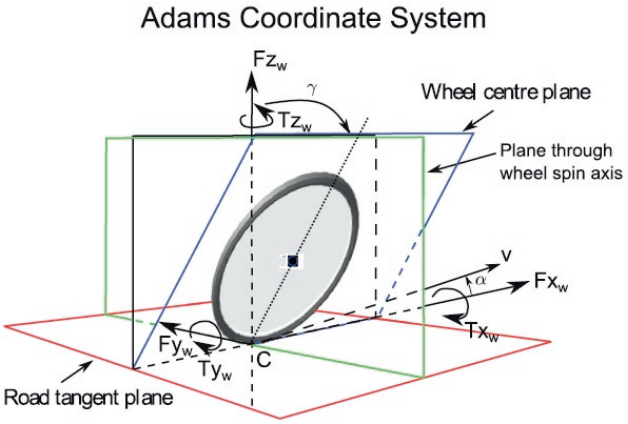

Figure A.2. *The equations for the tire model are written in the x_w y_w z_w coordinate system of ADAMS.*

Longitudinal force

The Magic Formula fitting formula for the longitudinal force is given by:

$$F_x(\kappa) = D_x \cdot \sin[C_x \cdot \arctan\{B_x \cdot \kappa\}] \quad \text{(A2.1)}$$

with $D_x = \mu_x F_z$

And the longitudinal slip stiffness K_κ by:

$$K_\kappa = B_x \cdot C_x \cdot D_x \quad \text{(A2.2)}$$

Lateral force

$$F_y(\alpha, \gamma) = D_y \cdot \sin\big(f(\alpha) + g(\gamma)\big) \quad \text{(A2.3)}$$

whereby $f(\alpha)$ en $g(\gamma)$ are the simplified Magic Formula's with sideslip angle (α) and camber angle (γ) as input values (equation (A2.4) and (A2.5)); the same D-coefficient is used in both relations (*Dy*). D_{y1} is the lateral friction coefficient and the load-dependency of the lateral friction coefficient can be controlled with D_{y2} [57].

$$f(\alpha) = \sin(C_\alpha \cdot arctan(B_\alpha \cdot \alpha)) \quad \text{(A2.4)}$$
$$g(\gamma) = \sin(C_\gamma \cdot arctan(B_\gamma \cdot \gamma)) \quad \text{(A2.5)}$$

$$\mathrm{D_y} = \mu_\mathrm{y} \cdot \mathrm{F_z} \quad \text{(A2.6)}$$

$$\mu_\mathrm{y} = \mathrm{D_{y1}} \cdot e^{D_{y2} \cdot \mathrm{dfz}} \quad \text{(A2.7)}$$

The dependency of the cornering stiffness on the vertical force is non-linear and controlled by the parameters $K_{\alpha_{max}}$ (the maximum value of the dimensionless cornering stiffness) and $K_{\alpha_{peak}}$(the peak stiffness factor):

$$K_\alpha = K_{\alpha_{max}} \cdot F_{z0} \cdot \sin(\mathrm{atan}(\frac{F_z}{K_{\alpha_{peak}} \cdot F_{z0}})) \quad \text{(A2.8)}$$

$$B_\alpha = \frac{K_\alpha}{C_\alpha \cdot D_y} \quad \text{(A2.9)}$$

The load-dependency of the camber stiffness is linear:

$$K_\gamma = F_z \cdot (K_{\gamma 1} + K_{\gamma 2} \cdot dfz) \quad \text{(A2.10)}$$

$$B_\gamma = \frac{K_\gamma}{C_\gamma \cdot D_y} \quad \text{(A2.11)}$$

Self-aligning torque

The self-aligning torque is a multiplication of the lateral force with the pneumatic trail t. A cosine version of the Magic Formula is used to fit the pneumatic trail $t(\alpha)$:

$$T_z(\alpha) = -t(\alpha) \cdot F_y(\alpha) \quad \text{(A2.12)}$$

$$t(\alpha) = D_t \cdot \cos(C_t \cdot \mathrm{atan}(B_t \cdot \alpha)) \cdot \cos(\alpha) \quad \text{(A2.13)}$$

$$B_t = (B_{t1} + B_{t2} \cdot dfz) \quad \text{(A2.14)}$$

$$D_t = \frac{F_z \cdot r_f}{F_{z0}} (D_{t1} + D_{t2} \cdot dfz) \quad \text{(A2.15)}$$

In which r_f is tire radius.

Twisting torque

The twisting torque is measured as a function of camber angle γ. This relation is linear, therefore the following equation is used to fit this data, with r_f being the wheel radius:

$$T_z(\gamma) = F_Z \cdot r_f \cdot D_{tt} \cdot \gamma \quad \text{(A2.16)}$$

$$D_{tt} = D_{tt1} + D_{tt2} \cdot dfz \quad \text{(A2.17)}$$

Rolling resistance torque

The rolling resistance torque depends on the vertical force F_z, the radius of the wheel r_f and the rolling resistance coefficient D_{Ty}.

$$T_y = -r_f \cdot F_Z \cdot D_{Ty} \quad \text{(A2.18)}$$

Table A2. *Mean rolling resistance torque (Nm) and standard deviation (inside brackets).*

Load	***400 N***	***400 N***	***400 N***	***400 N***
Pressure	**2 bar**	**3 bar**	**4 bar**	**5 bar**
Tire 1	1.029 (0.335)	-	0.865 (0.291)	-
Tire 2	1.319 (0.683)	1.046 (0.389)	1.116 (0.290)	1.007 (0.452)
Tire 3	-	-	1.114 (0.262)	-
Tire 4	-	-	1.202 (0.395)	-

Overturning torque

The overturning torque is a function of camber angle γ, radius of the tire cross section r_c and the vertical force F_z.

$$T_x(\gamma) = -F_z \cdot r_c \cdot \gamma \quad \text{(A2.19)}$$

In Adams the parameter QSX2 is used: $QSX2 = \frac{r_c}{r_f}$

Fitting coefficients of the tire model

Table A3. *Fitting coefficients of the tire model.*

Coefficient name	**Name used in the tire property file**	**Explanation**	**Value**
$\boldsymbol{C_x}$	PCX1	Shape factor for longitudinal force	1.000 [-]
$\boldsymbol{D_x}$	PDX1	Longitudinal friction μ_x at *Fz0*	1.642 [N]
$\boldsymbol{K_x}$	PKX1	Longitudinal slip stiffness at *Fz0*	12.00 [N]
$\boldsymbol{C_\alpha}$	PCY1	Shape factor for sideslip force	0.990 [-]

C_γ	PCY2	Shape factor for camber force	1.000 [-]
D_{y1}	PDY1	Lateral friction μ_y at *Fz0*	1.642 [-]
D_{y2}	PDY2	Exponent lateral friction μ_y	-0.017 [-]
$K_{\alpha_{max}}$	PKY1	Maximum value of cornering stiffness $\frac{K_\alpha}{F_{z0}}$	-16.07 [rad^{-1}]
$K_{\alpha_{peak}}$	PKY3	Peak cornering stiffness factor $\frac{K_\alpha}{F_{z0}}$	1.011 [rad^{-1}]
$K_{\gamma 1}$	PKY6	Camber stiffness factor K_γ	-1.444 [rad^{-1}]
$K_{\gamma 2}$	PKY7	Vertical load dependency of camber stiffness K_γ	-0.510 [rad^{-1}]
B_{t1}	QBZ1	Trail slope factor for trail B_t at Fz0	73.49 [-]
B_{t2}	QBZ2	Variation of slope B_t with load	-87.36 [-]
C_t	QCZ1	Shape factor C_t for pneumatic trail	1.000 [-]
D_{t1}	QDZ1	Peak trail D_t	0.054 [-]
D_{t2}	QDZ2	Variation of peak trail D_t with load	-0.043 [-]
D_{TT1}	QDZ8	Linear dependency of twisting torque on camber	-0.134 [-]
D_{TT2}	QDZ9	Variation of the twisting torque with load	0.084 [-]
D_{Ty}	QSY1	Rolling resistance torque coefficient	0.008 [-]
D_{Tx}	QSX2	Overturning torque coefficient	0.053 [-]

A.3. Cyclist Parameters

The dimensions of body parts were determined from marker position of the static human trial, as is given in Table A4.

The definition of the positions of the Hip Joint Center's (HJC) are based on [116]. The position of the right hip joint (in mm) with respect to the LRF of the pelvis (as was given in Table 5.2) is given as:

$$\begin{matrix} x \\ y \\ z \end{matrix} = \begin{bmatrix} 0.24 \cdot PD + 9.9 \\ 0.33 \cdot PW + 7.3 \\ -0.30 \cdot PW - 10.9 \end{bmatrix}$$

The location of the L4L5 joint in the LRF of the pelvis is given as:

$$\begin{matrix} x \\ y \\ z \end{matrix} = \begin{bmatrix} 0 \\ 0 \\ 0.828 * HW \end{bmatrix}$$

(HW is the hip width)

The positions of the Center of Mass of the body parts are given below. They are given with respect to the local reference frames as given in Table 4.2.

- Pelvis: x = 0.333d1, z = 0.5 d2, y = 0.0 (d1 = x-distance between pelvis and L4L5 joint, d2 = z-distance)
- Upper leg: x = -0.025d3, z = 0.607d3, y = 0.037d3 (d3 = length femur)
- Lower leg: x = -0.011d4, z = 0.581d4, y = 0.026d4 (d4 = length lower leg)
- Foot: x = 0.037Lt, z = -0.745d5+0.007, y =0.0 (d5 = height ankle joint)
- Torso: x = 0.0, y = 0.0, z = ⅔d6 (d6 = torso length)
- Head: x = 0.0, y = 0.0, z = 0.0 (midpoint)

A3.1 Mass properties

The mass of the cyclist body parts of the multi-body model are estimated using the following regression equations, based on the total mass (M_t) of the subject (in gm) [96].

- Head: 0.032 M_t+1.906
- Upper body: 0.532 M_t -706
- Upper arm: 0.016 M_t +809
- Lower arm: 0.020 M_t -218
- Hand: 0.007 M_t -30
- Upper leg: 0.126 M_t -1688
- Lower leg: 0.038 M_t +179
- Foot: 0.008 M_t +343
- Pelvis: 0.0662 M_t
- Total_leg: 0.127 M_t -1166
- HAT: 0.58 M_t +2009
- Lower arm+Hand: 0.027 M_t -248

The moment of inertia (in kg*m^2) of the cyclist's body parts are estimated using the following regression equations, based on the total mass (M_t) of the subject (in gm) [96]. The moment of inertia is given at the location of the CoM of the body part in the local reference frames.

- Head
  - I_{xx} = 2.129 M_t +32.030
  - I_{yy} = 1.676 M_t +54.918
  - I_{zz} = 3.186 M_t -6.846
- Upper body
  - I_{xx} = 269.9 M_t -3156034
  - I_{yy} = 284.493 M_t -7664880
  - I_{zz} = 102.507 M_t - 2895524
- Upper arm
  - I_{xx} = 0.535 M_t +98150
  - I_{yy} = 0.661 M_t +89662
  - I_{zz} = 0.400 M_t -4018
- Lower arm
  - I_{xx} = 1.508 M_t -31431
  - I_{yy} = 1.397 M_t -26562
  - I_{zz} = 0.313 M_t - 11645
- Hand
  - I_{xx} = 0.129 M_t -850
  - I_{yy} = 0.134 M_t -2599
  - I_{zz} = 0.085 M_t -3401
- Upper leg
  - I_{xx} = 24.102 M_t -233522
  - I_{yy} = 21.186 M_t -222796
  - I_{zz} = 9.262 M_t -378738
- Lower leg
  - I_{xx} = 5.434 M_t +37127
  - I_{yy} = 5.341 M_t +44749
  - I_{zz} = 0.949 M_t -32220
- Foot
  - I_{xx} = 0.433 M_t +5371
  - I_{yy} = 0.355 M_t +7296
  - I_{zz} = 0.153 M_t -2989
- Pelvis
  - I_{xx} = 6.3*10^-4 M_t
  - I_{yy} = 2.40*10^-4 M_t
  - I_{zz} = 5.17*10^-4 M_t

Table A4. *Dimensions of the cyclist model with their definitions.*

Dimension	Definition
Pelvic Depth (PD)	distance between Mid ASIS and Mid PSIS
Pelvic Width (PW	distance between LASIS and RASIS
Pelvic Height (PH)	0.7*pelvic width (male) 0.74*pelvic width (female) [174]
Upper leg length	distance between ASIS and Knee joint
Lower leg length	distance between Knee joint and ankle joint
Upper body length	distance L4l5 and mid Shoulders
Upper arm length	distance between shoulder and elbow
Lower arm length	distance between elbow and wrist
Ankle height	distance between ankle and ground
Shoulder width	distance between left and right shoulder

A.4 Pedal angles

Table A5 gives the estimated left and right pedal angles.

Table A5. *Estimated left and right pedal angles, with here indicated: A - the amplitude, B - the shift and C - the offset, of the estimated left pedal angle.*

Subject	Cycling Speed	Right pedal angle			Left pedal angle		
		A: Amplitude (m)	**B: Shift (°)**	**C: Offset (m)**	**A: Amplitude (m)**	**B: Shift (°)**	**C: Offset (m)**
1	7	47	15	-23	51	-27	45
	4	47	15	-23	44	-16	36
	3	47	3	-27	45	-11	33
	2	22	42	-16	28	-24	20
2	7	49	12	-25	50	-20	32
	4	37	34	-0.4	27	-12	9
	3	42	53	-3	31	-45	10
	2	37	33	-8	26	-25	6
3	7	55	12	-24	53	-23	25

4	54	9	-26	47	-15	26
3	55	-9	-22	52	7	16
2	42	28	0.0	37	-20	-3

A.5. Brochure SOFIE Bicycle

INDES

E-mobility

Human Care

Medical Cure

contact: info@indes.eu

INDES

Project SOFIE ontwerpdoelstellingen

Een fiets creëren waarmee ouderen zich veilig voelen en op hoge leeftijd blijven doorfietsen

- Voorkomen van vallen tijdens op- en afstappen
- Stabiel stuurgedrag, voorkomen grote slingerbewegingen

Low-tech ipv high-tech

- Realistisch
- Short time to market
- Betaalbaar

Het moet een fiets zijn die je wilt hebben!

- Eigentijds design
- Niet stigmatiserend
- Makkelijk in gebruik

CREATING PRODUCTS PEOPLE RELY ON

Kenmerken

- Aangepast frame
- Steile stuurpen
- Kleine wielen en korte wielbasis
- Lage instap
- Automatisch zadel
- Directe en vloeiende wegrijhulp

Voordelen

- Makkelijk en veilig op- en afstappen
- Stilstaan met beide voeten op de grond
- Makkelijk sturen
- Bij lage snelheid al stabiel
- Passende elektrische ondersteuning
- Compact

Gebruikerservaringen

- Positief tot zeer positief
- Minder slingeren
- Minder balanscorrectie met benen
- Makkelijker uitwijken
- Stabiele opstappositie